High-gain observer-based motion control and stability analysis of a towed underwater vehicle

Doctoral Dissertation

HIGH-GAIN OBSERVER-BASED MOTION CONTROL AND STABILITY ANALYSIS OF A TOWED UNDERWATER VEHICLE

March 2018

Graduate School of Marine Science and Technology
Tokyo University of Marine Science and Technology
Doctoral Course of Applied Marine Environmental Studies

MINOWA ASUMA

Contents

List of Figures

List of Tables

1 Introduction

This introductory chapter first premises the background and outline of the underwater vehicles, which have been becoming requisite devices in oceanic research. Next, focusing on towed underwater vehicles (TUVs), related previous works are introduced and reviewed briefly. Based on them, some important viewpoints to address control problems of TUVs are located and the objectives of this work are explained. Finally, the organization of the dissertation is presented.

1.1 Background

Over the last several decades, underwater vehicles have been one of the most powerful and effective tools for marine sciences. They can be equipped with various kinds of instruments, which are indispensable to oceanic researches, thus scientists and researchers are increasingly depending on them [1], [2]. For instance, sonars are essential for benthic mapping and almost the only one measure to perceive the deep ocean over a wide view. While cameras provide another visual resource with a relatively narrow range of scope, which are necessary for undersea operation, detailed resource mapping, organism collection, and so on. Since physical, chemical and biological data are always the fundamentals of investigations, a large variety of sensors, such as the conductivity temperature depth profiler (CTD) and acoustic doppler current profiler (ADCP), are also important devices for scientific measurements [3], [4].

Hence, according to the variety of research objectives, some types of underwater vehicles and control methods for them have been developed. For example, remotely operated vehicles (ROVs) have been employed since it was put into practice in 1960s, which are generally composed of an umbilical cable and underwater body [5]-[13]. Autonomous underwater vehicles (AUVs) or unmanned undersea vehicles (UUVs) are now the main targets of investigations of underwater vehicles [14]-[18]. They are often used as a towing platform for a towfish as well as a simple probe [19]-[25], and various approaches to control AUVs have been pursued in accordance with versatile surveys [26]-[38]. Further, motion control of vehicle-manipulator systems have also been studied, e.g., [39]-[41], where its application range

extends to even the exploration of other heavenly bodies [42].

Among such vehicles, towed underwater vehicles (TUVs) may seem to be less capable because they have to be towed by a mothership to be in motion like a kite flying in the air. However, the great advantages of the TUVs compared to other vehicles originate from the following points; the lack of thrusters or propulsions enables ones to reduce the cost for the development and to avoid the apprehension for the power supply [43]. This trait also retains the mobility of the mothership and the easiness in practical operations. Moreover, towing type apparatuses are suitable for wide-region explorations, so that they also play important roles in scientific investigations [2], [44]. Thus, TUVs have been convenient and useful for oceanographical, geological, biological, environmental and more other research situations in no way inferior to AUVs and ROVs.

1.2 Previous Works

First of all, previous works related to TUVs can be classified roughly into two groups according to the towing arrangements; that is, single-stage towing arrangements [44]-[57] and two-stage towing arrangements [58]-[92]. The configuration of the former case is similar to that of ROVs, while the latter includes gravitational depressors or launcher systems and secondary towing cable, which is neutrally buoyant and connected to the vehicle. Obviously, such an arrangement can alleviate the influence of the dynamics of the primal towing cable, but is rather complicated to deal with and requires higher cost in practice. Of course, it depends on the purpose and priority of each research that which towing arrangement is suitable; nevertheless, more simple settings are focused on in this study and only the single-stage towing arrangement will be considered.

Second, a lot of efforts toward motion control problems of TUVs are able to be divided into some groups in view of a control design method. For instance, the simplest examples come from a controller based on proportional-integral-derivative (PID) control [45], [61], [62], [64], [65]. This method does not have to consider a model dynamics in detail and hence is relatively easy to apply. The linear-quadratic (LQ) and linear-quadratic-integral (LQI) optimal frameworks have been utilized in many studies, particularly in Japanese researches [44], [53], [54], [56], [58]. The integral operation in-

cluded in the LQI control framework is expected to achieve robust servo control performance. Note that all of these studies have constructed controllers with full or reduced order linear observers. The linear H_∞ control theory [47], [57] and the linear parameter varying (LPV) control methodology [49] have been employed to obatin respective robust controllers, and a comparison between an LQI-based controller and a linear H_∞-based controller has been conducted [55], where both controllers have been gain-scheduled and the superiority of the H_∞-based controller has been demonstrated. In addition, the control configured vehicle (CCV) technique and the fuzzy logic have been utilized to control the attitude of the vehicle [50], [51]; particularly, the former has conducted the water tank experiment and derived the set of physical parameters, which is necessary for computations.

Despite that these investigations have offered a certain amount of satisfactory results, most of the TUVs in practice are still used passively and even is not equipped with any control devices. One of the explanations for this gap may be given by considering the cardinal characteristics of motion control problems of TUVs; some complex nonlinear dynamics. The typical principal problem is highly-nonlinear hydrodynamic forces, which have to be dealt with more or less in every kind of underwater systems. How to treat the dynamics of a towing cable is the other important issue, because the flexible cable leads to an infinite-dimensional problem. For example, the cable can be treated as a series of elastic elements with the mass-lumped node to model its physical characteristics [45], [46] or as a long thin circular cylinder to analyze the motion of the cable and forces on towfish [69], [70]. In fact, a marine cable and/or underwater towed system have been a challenging subject in ocean engineering, e.g., cable dynamics such as hydrodynamic response and transient behavior [71]-[78], towed array systems mainly for acoustic researches [79]-[84], and with underwater vehicles or other towed systems [85]-[94]. On the other hand, their fundamental methods were similarly depending on finite-element approaches. The most conventional and fundamental approximation is based on a lumped-mass method [95], where the towing cable is regarded as some concatenated rigid segments. Additionally, the cable dynamics cause difficulty in adopting a full state-feedback controller practically. Owing to this, an output-feedback controller needs to be designed.

According to these factors, the nonlinear dynamics seem to be a key to better motion control of TUVs; however, only few previous works have addressed control problems of TUVs by considering their nonlinearities directly. One of the interesting exceptions is a Lyaponov-based nonlinear adaptive controller presented in [66], [67], [68], where the controlled system demonstrates preferable performance by simulations. But the model is based on the two-stage towing arrangement, hence the method is not available for the target in this study immediately. Therefore, it can be said that there is a room for improvement and amelioration in control systems of TUVs via direct consideration of the nonlinear dynamics.

Antecedently, our group has presented a theoretic analysis of a control system structure of TUVs with single-stage towing arrangement, which possesses two pairs of movable wings at the center (the main wing) and rear (the tail wing) to control its depth and attitude [96]. Based on it, a control design method employing a high-gain observer has been proposed and its regulation performances has been evaluated with simple simulations [97], [98]. A high-gain observer is one kind of nonlinear design technique [99], which is known to be able to estimate the state of the system considering the nonlinearity thoroughly. Based on an initial value theorem in [100], the study [101] has presented the design of robust feedback controller with a high-gain observer for fully-linearizable systems and the stability analysis utilizing the singular perturbation method. This achievement has triggered a chain of researches; for example, [102]-[104], and see [105]-[107] for more detailed history, recent development and references. But this versatile control design method and stability analysis have not been applied to motion control problems of TUVs before our study.

Consequently, the main motivation of our work is application of the high-gain observer-based approach to consider the nonlinear dynamics of the TUV system. In addition to this, robustness of the control system also has to be taken into account to obtain better control performance, since model variations and uncertainties are unavoidable. Evaluations from such a viewpoint have not been performed yet in [97] and [98]. Note that external disturbances such as tide and wave are always present in practical situations but in this study excludes the problem to avoid excessive complications.

1.3 Objectives and Contents of the Dissertation

This dissertation presents a high-gain observer-based motion control method and stability analysis of the TUV to show the effectiveness and importance of the direct consideration of nonlinear dynamics. The control law utilized in this study is based on LQ and LQI optimal control methods, which have never been combined with a nonlinear observer to our best knowledge, although their applications have already been investigated as reviewed above. Thus robust performance of the LQI-control-based approach would be expected to improve and, in order to confirm this, the proposed controller will be compared to a conventional linear observer-based controller by some types of simulations. The most remarkable feature and originality of the work are the detailed stability analysis referring to [101] for the LQ-control-based approach, where the region of attraction is estimated as well as the proof of the asymptotic stability. It should be emphasized that the conventional estimates are improved by devising a "state-space scaling method", and this method can be applied not only for problems of underwater vehicles but also other control systems extensively.

The other crucial point of view of the research is the relationship between the orders of the system and controller. Generally, the system order is required to be as high as possible, in case that the higher degree of the model leads to the more realistic model. By contrast, a lower-order controller is desirable with respect to the complexity of controller design, the number of parameters to be tuned, calculation cost, and so on. Consequently, the ideal situation is that a lower-order controller is enough robust to be able to control higher-order systems. In particular for TUVs, this viewpoint is inevitable because strictly speaking the model is expressed by a partial differential equation and becomes an infinite-order system. If that is the case, the order of the system on which the controller is based must be taken into consideration studiously.

As mentioned above, finite-element approaches were taken in most of contributions for treating the dynamics of marine cables. This study also chooses the conventional lumped-mass approach to approximate the cable due to the requirement of simplicity and validity of the model, so that a partial differential equation and an infinite-dimensional problem can be avoided. Hence, the order of the TUV system increases according to the

number of the cable segments, i.e., a degree of the approximation, and the lowest-order model of the TUV is adopted to design control systems in this study. The obtained controllers will be evaluated by simulations to confirm whether they can be available for higher-order, i.e., more realistic, systems or not.

The chapters of this dissertation are organized as follows.

- Chapter 2 provides the problem setting including some essential assumptions, on which the study will depend. The dynamical models corresponding to different conditions are formulated in a common state-space representation.

- Chapter 3 describes the control design method of the LQ-control-based approach with the high-gain observer. Not only a regulator around one equilibrium point but also a method of switching controllers for depth tracking is developed with the lowest-order model.

- Chapter 4 presents the results of the stability analysis of the controllers designed in Chapter 3 based on the singular perturbation method, which consists of the proof of the asymptotic stability and estimation of the region of attraction. An improving method for the estimation is also presented and its efficacy will be confirmed by comparing with the results of conventional one.

- Chapter 5 demonstrates evaluations on the controllers designed in Chapter 3 by simulations. Two types of control problems are considered; regulation with various initial deviations of the equilibrium states, which includes comparison with the results of the analysis in Chapter 4, and depth tracking via switching controllers.

- Chapter 6 describes the expansion of the control strategy so as to enhance the robustness against model uncertainties. The control design method of the LQI-control-based approach is presented and a linear Kalman filter-based output-feedback controller is also introduced for the purpose of comparison.

- Chapter 7 demonstrates evaluations on the controllers designed in Chapter 6. Simulations with some model uncertainties are conducted

to show the superiority of the proposed control system, and the applicability for the higher-order systems and depth tracking performance will be investigated.

- Chapter 8 provides conclusions on what have been found from this work and a summary of the tasks left behind.

2 Problem Setting and Dynamical Model

This chapter presents the problem definition and dynamical model formulation of a TUV. Some important assumptions and coordinate systems for the problem, which will be common throughout the study, are introduced. These settings enable us to formulate the equations of motion of the TUV and to derive a state-space representation. Further, the system is rewritten into the form based on the *input-output linearization* scheme for the control system design in Chapter 3.

2.1 Problem Definition

A TUV with two pairs of movable wings is considered throughout this study, and motions of which are restricted to the vertical plane to concentrate on the most important problem in a practical situation. The "main wings" is at the center of the vehicle and the "tail wings" is a pair of the rear ones, which are intended to control the depth and attitude of the vehicle. Note that most of existing TUVs does not have such movable wings.

A schematic diagram of the TUV and coordinate frames employed in this study are depicted in Fig. 2.1, where all the angles are defined to be positive in the counterclockwise sense. A streamline-shaped body is considered, so that the drag force on the body can be neglected. The inertia frame $O_0X_0Z_0$ is the global coordinates attached to the towing point on the mothership, whose Z axis is collimated with the direction of gravity. The frame on each cable segment is denoted by $O_iX_iZ_i(1 \leq i \leq n)$ and the angle of the ith cable segment is denoted by x_i. The frame attached to the center of the vehicle O_{n+1} and attitude of the vehicle are $O_{n+1}X_{n+1}Z_{n+1}$ and x_{n+1}, respectively. The input angles of the main and tail wings are denoted by u_1 and u_2. The distance from O_n to O_{n+1} is $L_v = 0.205$ m and the distance from O_{n+1} to O_t, the center of the tail wing, is $L_t = 0.7$ m. The length of the vehicle is 2 m and height is 0.41 m, that is, the size of the vehicle in Fig. 2.1 is deformed for convenience of exposition. Table. 2.1 summarizes each notation in Fig. 2.1.

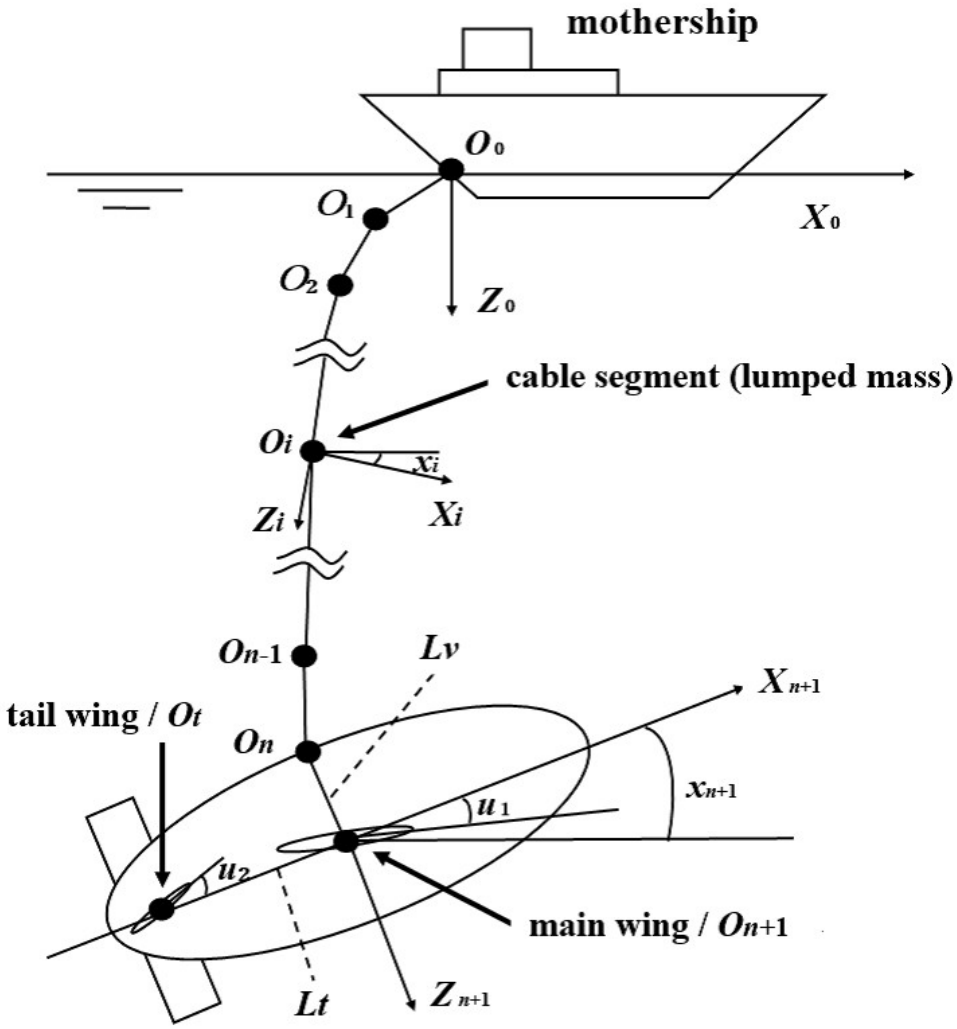

Figure 2.1. Schematic diagram of the TUV and configuration of the problem.

Table 2.1. Notations in Fig. 2.1

$O_0X_0Z_0$	frame attached to the towing point on the mothership
$O_iX_iZ_i$	frame attached to the ith cable segment
$O_{n+1}X_{n+1}Z_{n+1}$	frame attached to the center of the vehicle
$O_tX_tZ_t$	frame attached to the center of tail wings
x_i	angle of the ith cable segment
x_{n+1}	the attitude of the vehicle
u_1	input angle for the main wings
u_2	input angle for the tail wings
L_v	distance from O_1 to O_2
L_t	distance from O_2 to O_t

Here, the following assumptions are made in addressing motion control problems of TUVs;

A1 the mothership advances in the horizontal direction with constant velocity v_0 and its dynamics will be ignored;

A2 the dynamics of the wing actuators and environmental water current will be ignored;

A3 the control inputs for the main and tail wings are set bounds within $\pm 30^\circ$;

A4 if the control system performs such that the attitude of the vehicle is restricted within $\pm 45^\circ$, the control process is regarded successful; and

A5 the towing cable is approximated by a finite number of rigid segments with its mass concentrated at the end point and all forces for each cable segment are assumed to be applied to the point of mass.

A1 and A2 are the simplifications from the viewpoint of control system design and analysis, and due to the stage of the study. However, the robust controller in the later chapter has a potential to deal with these disturbing factors and simulation results with changing v_0 will be shown in Chapter 7. A3 and A4 are necessary in order to make simulations more valid by taking into account the *dynamic stall* approximately; strictly speaking, bounds for the angles of attack have to be set to model the phenomenon more

precisely. The saturation of the control inputs not only has restrictive effect but also alleviates a baneful influence of peaking phenomena of the high-gain observer as shown in Chapter 5.

As mentioned in Section 1.3, the order of the control system is one of the important factors in control system design of TUVs and A5 implies that the number of the cable segments n rules the order of the system. Hence, due to the intention of this study, the lowest-order $n = 1$ model is constructed to design and evaluate controllers as in [97] and [98]. Moreover, total six cases of the TUV model are prepared to compare the results as shown in Table. 2.2. The difference between the models C1 to C4 is only the towing cable length L; C1 with 30 m, C2 with 100 m, C3 with 200 m and C4 with 300 m. C5 and C6 include some modifications for C3 and C4, where the values of the towing speed v_0 and the square measure of the main and tail wings are set twice as large as the nominal one so as to consider other physical design specification cases of the vehicle. These cases will show the steady effectiveness of the proposed control system in later chapters. Note that the doubled wings area of C5 and C6 are implemented to increase the hydrodynamic forces related to the wings. Finally, C2, the cable length $L = 100$ m model, will be basically employed as a standard model to explain the control system design and the results of the analysis and simulations throughout the study.

Table 2.2. Models for the problem

Case	Cable length L (m)	v_0 (m/s)	Wings area
C1	30	4	nominal
C2	100	4	nominal
C3	200	4	nominal
C4	300	4	nominal
C5	200	8	doubled
C6	300	8	doubled

2.2 Dynamical Model

The dynamical model of the TUV can be described without considering redundant state variables by the Lagrange approach as follows:

$$E(x)\ddot{x} + F(x) = \tau_{bg}(x) + \tau_h(x, u), \tag{2.1}$$

where $x = [x_1, \ldots, x_{n+1}, \dot{x}_1, \ldots, \dot{x}_{n+1}]^T = [x_1, \ldots, x_{2(n+1)}]^T \in \Re^{2(n+1)}$ denotes the state-vector and $u = [u_1, u_2]^T \in \Re^2$ is the input vector; $E(x) \in \Re^{(n+1)\times(n+1)}$ is the symmetric inertia matrix, $F(x) \in \Re^{(n+1)}$ represents the Coriolis and centripetal force vector, $\tau_{bg}(x) \in \Re^{(n+1)}$ is the buoyancy and gravity, and $\tau_h(x, u) \in \Re^{(n+1)}$ represents the hydrodynamic forces, respectively.

Explicit expressions for each term are given by (2.2)-(2.6) with the abbreviations $s(\cdot)$ and $c(\cdot)$ of $\sin(\cdot)$ and $\cos(\cdot)$.

$$\begin{aligned}
E(x) &= \begin{bmatrix} E_{11} & \cdots & E_{1,n+1} \\ E_{21} & \cdots & E_{2,n+1} \\ \vdots & \ddots & \vdots \\ E_{n+1,1} & \cdots & E_{n+1,n+1} \end{bmatrix} \\
E_{ij} &= E_{ji} \\
&= \frac{1}{2}\left(\frac{L}{n}\right)^2 \{(M_{11} + M_{22} + 2k_{ij}ma_c)c(x_i - x_j) \\
&\quad + (M_{11} - M_{22})c(x_i + x_j - 2x_{n+1})\} \\
&\quad (\text{for } i, j \in \underline{n}) \\
E_{i,n+1} &= E_{n+1,i} \\
&= \frac{L}{n}\{(M_{13} + L_v M_{11})c(x_i - x_{n+1}) - M_{23}s(x_i - x_{n+1})\} \\
&\quad (\text{for } i \in \underline{n}) \\
E_{n+1,n+1} &= M_{33} + L_v(L_v M_{11} + 2M_{13}),
\end{aligned} \tag{2.2}$$

where the inertia matrix of the vehicle M consists of the element M_{ij} as

$$M = \begin{bmatrix} m_v + a_{v11} & 0 & m_v z_g + a_{v13} \\ 0 & m_v + a_{v22} & -m_v x_g + a_{v23} \\ m_v z_g + a_{v13} & -m_v x_g + a_{v23} & J_v + a_{v33} \end{bmatrix}$$

and k_{ij} denotes the element of the $n \times n$ matrix

$$k = \begin{bmatrix} n & n-1 & n-2 & \dots & 1 \\ n-1 & n-1 & n-2 & \dots & 1 \\ n-2 & n-2 & n-2 & \dots & 1 \\ \vdots & \vdots & \vdots & \ddots & \vdots \\ 1 & 1 & 1 & \dots & 1 \end{bmatrix}.$$

J_v denotes the inertia moment and (x_g, z_g) denotes the coordinates of the center of gravity of the vehicle in $O_{n+1}X_{n+1}Z_{n+1}$.

$$\begin{aligned}
F(x) &= [F_1, \dots, F_{n+1}]^T \\
F_i &= \sum_{j=1}^{n} [\frac{1}{2}\left(\frac{L}{n}\right)^2 \{(M_{11} + M_{22} + 2k_{ij}ma_c)s(x_i - x_j) \\
&\quad - (M_{11} - M_{22})s(x_i + x_j - 2x_{n+1})\}\dot{x}_j \\
&\quad + \left(\frac{L}{n}\right)^2 (M_{11} - M_{22})s(x_i + x_j - 2x_{n+1})\dot{x}_j\dot{x}_{n+1}] \\
&\quad + \frac{L}{n}\{M_{23}c(x_i - x_{n+1}) + (M_{13} + L_vM_{11})s(x_i - x_{n+1})\}\dot{x}_{n+1}^2 \\
&\quad + \frac{L}{n}(M_{11} - M_{22})s(x_i - 2x_{n+1})v_0\dot{x}_{n+1} \\
&\quad + \frac{1}{2}\left(\frac{L}{n}\right)\{(M_{11} - M_{22})c(x_i - 2x_{n+1}) \\
&\quad + (M_{11} + M_{22} + 2k_{1i}ma_c)c(x_i)\}\dot{v}_0 \\
&\quad (\text{for } i \in \underline{n}) \\
F_{n+1} &= \sum_{i=1}^{n} [\sum_{j=1}^{n} \{-\frac{1}{2}\left(\frac{L}{n}\right)^2 \cdot (M_{11} - M_{22})s(x_i + x_j - 2x_{n+1})\dot{x}_i\dot{x}_j\} \\
&\quad - \frac{L}{n}\{M_{23}c(x_i - x_{n+1}) + (M_{13} + L_vM_{11})s(x_i - x_{n+1})\}\dot{x}_i^2 \\
&\quad - \frac{L}{n}(M_{11} - M_{22})s(x_i - 2x_{n+1})v_0\dot{x}_i] \\
&\quad + \frac{1}{2}(M_{11} - M_{22})s(2x_{n+1})v_0^2 \\
&\quad + \{M_{23}s(x_{n+1}) + (M_{13} + L_vM_{11})c(x_{n+1})\}\dot{v}_0. \qquad (2.3)
\end{aligned}$$

$$
\begin{aligned}
\tau_{bg}(x) =& [\tau_{bg1}, \ldots, \tau_{bgn+1}]^T \\
\tau_{bgi} =& \frac{L}{n}\{\frac{Lk_{1i}}{n}(B_c - m_c g) + B_v - m_v g\}s(x_i) \\
& (\text{for } i \in \underline{n}) \\
\tau_{bgn+1} =& \{B_v L_v - m_v g(L_v + z_g)\}s(x_{n+1}) + (B_v x_b - m_v g x_g)c(x_{n+1}), \quad (2.4)
\end{aligned}
$$

where B_c and B_v represent the buoyancy of the cable per unit length and the buoyancy of the vehicle, $(x_b, 0)$ denotes the coordinates of the center of buoyancy of the vehicle in $O_{n+1}X_{n+1}Z_{n+1}$ and g is the gravitational acceleration.

$$
\begin{aligned}
\tau(x,u) =& [\tau_{h1}, \ldots, \tau_{hn+1}]^T \\
\tau_{hi} =& -\sum_{j=i}^{n} h_{cj} c(\alpha_j + x_i - x_j) \\
& + \frac{L}{n}\{-h_{mD} c(\alpha_{n+1} + x_i - x_{n+1}) - h_{tD} c(\alpha_t + x_i - x_{n+1}) \\
& + (h_{vL} + h_{mL}) s(\alpha_{n+1} + x_i - x_{n+1}) + h_{tL} s(\alpha_t + x_i - x_{n+1})\} \\
& (\text{for } i \in \underline{n}) \\
\tau_{hn+1} =& h_{vL} L_v s(\alpha_{n+1}) + CM + h_{mL} L_v s(\alpha_{n+1}) - h_{mD} L_v c(\alpha_{n+1}) \\
& + (h_{tL} L_v - h_{tD} L_t) s(\alpha_t) - (h_{tD} L_v + h_{tL} L_t) c(\alpha_t), \quad (2.5)
\end{aligned}
$$

where $(-L_t, 0)$ denotes the coordinates of the center of hydrodynamic force on the tail wings in $O_{n+1}X_{n+1}Z_{n+1}$ and CM represents a constant parameter with respect to hydrodynamic moment. The angle of attack is defined by $\alpha_i = \tan^{-1}(v_{iz}/v_{ix})\,(v_{ix} \neq 0)$, where $v_i = [v_{ix}, v_{iz}]^T$ as the velocity vector of O_i associated with $O_i X_i Z_i$. h_* represents each hydrodynamic force as in the following;

$$
\begin{aligned}
h_{ci} =& \frac{L}{n}(CD_{c1}\alpha_i^2 + CD_{c2})\|v_i\|^2 \\
h_{mD} =& \{CD_{m1}(\alpha_{n+1} + u_1 + CL_{m2})^2 + CD_{m2}\}\|v_{n+1}\|^2 \\
h_{mL} =& CL_{m1}(\alpha_{n+1} + u_1 + CL_{m2})\|v_{n+1}\|^2 \\
h_{tD} =& \{CD_{t1}(\alpha_t + u_2)^2 + CD_{t2}\}\|v_t\|^2 \\
h_{tL} =& CL_{t1}(\alpha_t + u_2)\|v_t\|^2 \\
h_{vL} =& CL_{v1}\alpha_{n+1}\|v_{n+1}\|^2, \quad (2.6)
\end{aligned}
$$

where h_{ci} represents the drag on the ith cable segment and CD_* and CL_* denote the drag and the lift coefficients. The suffixes D and L denote drag and lift, and m, t and v denote the main wing, the tail wing and the body of the vehicle, respectively. The physical parameters for computation are adopted from [50], which are shown in Table 2.3.

Table 2.3. Physical parameters for computation

Sign	Value	Unit
a_c	$1.76715\rho \times 10^{-4}$	kg/m
a_{v11}	0.010ρ	kg
a_{v13}	0	kgm
a_{v22}	0.539ρ	kg
a_{v23}	0.032ρ	kgm
a_{v33}	0.039ρ	kgm^2
B_c	0.69g	N/m
B_v	0.162ρg	kg
CD_{c1}	$-1.23075\rho \times 10^{-3}$	$\mathrm{Ns}^2/\mathrm{m}^3$
CD_{c2}	$3.975\rho \times 10^{-3}$	$\mathrm{Ns}^2/\mathrm{m}^3$
CD_{m1}	0.60835ρ	$\mathrm{Ns}^2/\mathrm{m}^2$
CD_{m2}	0.00274506ρ	$\mathrm{Ns}^2/\mathrm{m}^2$
CD_{t1}	0.0335183ρ	$\mathrm{Ns}^2/\mathrm{m}^2$
CD_{t2}	$7.22347\rho \times 10^{-4}$	$\mathrm{Ns}^2/\mathrm{m}^2$
CL_{m1}	1.72595ρ	$\mathrm{Ns}^2/\mathrm{m}^2$
CL_{m2}	-0.141372	rad
CL_{t1}	0.202770ρ	$\mathrm{Ns}^2/\mathrm{m}^2$
CL_{v1}	0.0766708ρ	$\mathrm{Ns}^2/\mathrm{m}^2$
CM	1.17268	m
g	9.8	$\mathrm{m/s}^2$
J_v	26.078	kgm^2
L_t	0.7	m
L_v	0.205	m
m_c	0.95	kg/m
m_v	182.687	kg
x_b	0.017	m
x_g	0.017	m
z_g	0.02	m
ρ	1025	$\mathrm{kg/m}^3$

2.3 State-Space Formulation and Transformed System

Consequently, a state-space representation of Eq. (2.1) is derived as

$$\dot{x} = f(x) + g(x, u), \tag{2.7}$$

where

$$f(x) = \begin{bmatrix} \dot{x}_i \\ E(x)^{-1}\{-F(x) + \tau_{bg}(x)\} \end{bmatrix}, \tag{2.8}$$

$$g(x, u) = \begin{bmatrix} 0 \\ E(x)^{-1}\tau_h(x, u) \end{bmatrix}. \tag{2.9}$$

The measured outputs, depth and attitude of the vehicle, can be also represented in

$$\begin{aligned} y &= [y_1, y_2]^T \\ &= \begin{bmatrix} \frac{L}{n}\sum_{i=1}^{n} c\ (x_i) + L_v c\ (x_{n+1}) \\ x_{n+1} \end{bmatrix}. \end{aligned} \tag{2.10}$$

The system represented by (2.7) and (2.10) is the target of our control design.

Next, to utilize a high-gain observer-based approach with the lowest-order model in Chapter 3, the coordinates of the system (2.7) need to be transformed according to the scheme used in *input-output linearization*, e.g., see [99] and [101]. The derivatives of the output (2.10) with $n = 1$ are calculated as

$$\begin{aligned} \dot{y} &= \begin{bmatrix} -L\dot{x}_1 s(x_1) - L_v \dot{x}_2 s(x_2) \\ \dot{x}_2 \end{bmatrix} \\ \ddot{y} &= H(x) + G(x, u), \end{aligned} \tag{2.11}$$

where $H(x) = L_f^2 y$ and $G(x, u) = L_g L_f y$. The *Lie derivatives* with respect to f and g are represented by $L_f(\cdot)$ and $L_g(\cdot)$, respectively. Then, the control system (2.7) and (2.10) can be rewritten as

$$\begin{aligned} \dot{z} &= A_z z + B_z \phi(z, u) \\ y &= C_z z, \end{aligned} \tag{2.12}$$

where $z = [z_1^T, z_2^T]^T = [y^T, \dot{y}^T]^T = T(x)$ is the transformation and

$$A_z = \begin{bmatrix} 0 & I_2 \\ 0 & 0 \end{bmatrix}$$
$$B_z = \begin{bmatrix} 0 \\ I_2 \end{bmatrix}$$
$$C_z = \begin{bmatrix} I_2 & 0 \end{bmatrix} \tag{2.13}$$

are the constant matrices. Note that this transformation bundles the nonlinear terms into $\phi(z, u) = H(T^{-1}(z)) + G(T^{-1}(z), u)$ so that the observer based on the system (2.12) can consider the nonlinear dynamics of the original system completely.

3 Motion Control Design Using an LQ-Control-Based Approach

This chapter presents an LQ-control-based approach with a high-gain observer. Employing a high-gain observer by [99], an output-feedback controller is designed based on a state-feedback controller derived from the linearization around an equilibrium point. In addition, a depth tracking control system by switching controllers is constructed.

3.1 Equilibrium Point and Linearization

In order to design a control system, an equilibrium point of the system (2.7) has to be obtained, which satisfies $f(x^*) + g(x^*, u^*) = 0$. The lowest-order model has four states, $x = [x_1, x_2, \dot{x}_1, \dot{x}_2]^T$ (deg, deg, deg/s, deg/s), then the equilibrium input $u^* = [u_1^*, u_2^*]^T$ (deg, deg) is calculated providing $x^* = [-60.0, 0, 0, 0]$ so that the equilibrium depth of the vehicle is equivalent to the half length of the cable. The equilibriums resulting from these settings will be referred to as "Central Equilibrium Point" (CEP) in this study and Table. 3.1 shows the CEP for each model. Then the approximate linearized system around the equilibrium point is derived as

$$\begin{aligned} \dot{w} &= Aw + Bv \\ p &= Cw, \end{aligned} \tag{3.1}$$

where A, B, C denote each coefficient matrix and $w = x - x^* = [x_1 - x_1^*, x_2 - x_2^*, \dot{x}_1 - \dot{x}_1^*, \dot{x}_2 - \dot{x}_2^*]^T = [w_1, w_2, w_3, w_4]^T$, $v = u - u^* = [u_1 - u_1^*, u_2 - u_2^*]^T$.

Table 3.1. Equilibriums for each model

Case	u_1 (deg)	u_2 (deg)	Depth (m)
C1	7.0456	−0.3735	15.205
C2	3.8573	−0.6319	50.205
C3	−0.7660	−1.5637	100.205
C4	−5.4630	−3.1833	150.205
C5	11.2648	−0.6689	100.205
C6	8.7584	−1.1457	150.205

3.2 Controller Using an LQ State-Feedback Gain

3.2.1 State-Feedback Controller

Based on the linearized system (3.1), an LQ feedback gain K is computed as

$$K = R^{-1}B^{T}S, \tag{3.2}$$

where S denotes the positive-definite solution of the Riccati equation

$$A^{T}S + SA - SBR^{-1}B^{T}S + Q = 0. \tag{3.3}$$

Q and R denotes the weighting matrices, which are chosen as the identity matrix I_4 and I_2, respectively. The resulting gain (3.2) minimizes the cost function

$$J = \int_0^{\infty} (w^{T}Qw + v^{T}Rv)dt. \tag{3.4}$$

Hence, the control input of this state-feedback controller is given by

$$v = -Kw. \tag{3.5}$$

Each gain (3.2) with coefficient matrices is listed (A.1)-(A.6) in Appendix A.

3.2.2 Output-Feedback Controller with a High-Gain Observer

The transformed system (2.12) yields a high-gain observer with the observer gain Γ as

$$\dot{\hat{z}} = A_z\hat{z} + B_z\phi(\hat{z}, u) + \Gamma(y - C_z\hat{z}), \tag{3.6}$$

$$\Gamma = \begin{bmatrix} \alpha_1/\epsilon & 0 \\ 0 & \alpha_1/\epsilon \\ \alpha_2/\epsilon^2 & 0 \\ 0 & \alpha_2/\epsilon^2 \end{bmatrix}. \tag{3.7}$$

$\hat{z}$ denotes the estimate of z and a design parameter ϵ predominates the whole estimation performance; the smaller ϵ becomes, the better the observer works theoretically. The positive constant $\alpha_i (i = 1, 2)$ is set as $\alpha_1 = 1.4, \alpha_2 = 1$ to be the same as in [97] and [98] so that $s^2 + \alpha_1 s + \alpha_2 = 0$ has stable roots. While $\epsilon = 0.01$ is adopted in this study instead of

$\epsilon = 0.001$, which has been concluded the best value in [97] and [98]. This modification is necessary for abating the effect of the peaking and managing the wide range of the cable length. Consequently, the control input of this output-feedback controller is expressed as

$$v = -K\hat{w}, \tag{3.8}$$

where $\hat{w} = \hat{x} - x_0^*$. $\hat{x}$ is calculated from $T^{-1}(\hat{z})$, the inverse transformation of $T(x)$ in Section 2.3.

4 Stability Analysis via Singular Perturbation Method

This chapter presents a stability analysis of the proposed LQ-control-based approach. Employing the singular perturbation method, Theorem 1 and Lemma 1 are utilized to consider not only an asymptotic stability of the system but also its estimate of the region of attraction as in [101]. Moreover, a state-space scaling method of Theorem 2 is devised so that less conservative estimates are obtained. Note that all the specific values in this chapter correspond to C2, i.e., the model with $L = 100$ m, unless otherwise specified.

4.1 Singularly Perturbed System

First, introducing the original estimation error $\bar{e} = z - \hat{z}$ and the scaled estimation error

$$\begin{aligned} e &= N^{-1}(\epsilon)\bar{e} \\ N(\epsilon) &= \begin{bmatrix} \epsilon I_2 & 0 \\ 0 & I_2 \end{bmatrix}, \end{aligned} \tag{4.1}$$

the system (2.7) can be rewritten as

$$\dot{w} = f_c(w) + \tilde{f}(w, N(\epsilon)e) \tag{4.2}$$

using w in (3.1). $f_c(w)$ denotes the closed-loop system (2.7) under the state-feedback control (3.5) and the second term $\tilde{f}(w, N(\epsilon)e) = f_c'(w, N(\epsilon)e) - f_c(w)$ represents the difference between $f_c(w)$ and $f_c'(w, N(\epsilon)e)$, the system with the output-feedback control (3.6) and (3.8). Note that $f_c(0) = 0$ and $\tilde{f}(w, 0) = 0$.

Second, the observer (3.6) is transformed using the derivative of $\bar{e}$ as

$$\dot{\bar{e}} = A_e\bar{e} + B_z\delta(z, \bar{e}) \tag{4.3}$$

with Hurwitz $A_e = A_z - \Gamma C_z$. Note that $\delta(z, \bar{e}) = \phi(z, u(\hat{z})) - \phi(\hat{z}, u(\hat{z}))$ and $N^{-1}(\epsilon)B_z = B_z$. Applying e yields the rewritten observer

$$\epsilon\dot{e} = A_e e + \epsilon\tilde{g}(w, N(\epsilon)e), \tag{4.4}$$

where $A_e = \epsilon N^{-1}(\epsilon)A_e N(\epsilon)$, $\tilde{g} = B_z\delta(T(w + x^*), N(\epsilon)e)$ and $\tilde{g}(0, 0) = 0$.

Third, it is notable that the original estimation error dynamics (4.4) is almost equivalent to the "fast system"

$$\frac{\mathrm{d}e}{\mathrm{d}\tau} = A_e e \tag{4.5}$$

for sufficiently small ϵ, where e converges to 0 quite fast due to A_e and the time $\tau = t/\epsilon$. This implies that the state-space equation (4.2) promptly converges to the "slow system"

$$\dot{w} = f_c(w) \tag{4.6}$$

and then w converges to 0 rather slowly.

Thus, the singularly perturbed system (4.2) and (4.4) can be considered in the following analysis.

4.2 Lyapunov function candidate

Next, a Lyapunov function candidate for the full singularly perturbed system is derived by combining each Lyapunov function of (4.5) and (4.6). The Lyapunov equation $P(A - BK) + (A - BK)^T P = -I_4$ is solved to obtain the positive-definite matrix

$$P = \begin{bmatrix} 21.008 & -0.8838 & 0.6107 & -0.0100 \\ -0.8838 & 1.1662 & 2.0254 & 0.0374 \\ 0.6107 & 2.0254 & 35.649 & 0.4945 \\ -0.0100 & 0.0374 & 0.4945 & 0.0151 \end{bmatrix} \tag{4.7}$$

and a Lyapunov function $W(w) = w^T P w$ of (3.1) with C2 is constructed for the slow system (4.6), which satisfies

$$\beta_1 \|w\|^2 \leq W(w) \leq \beta_2 \|w\|^2 \tag{4.8}$$

$$\dot{W}(w) \leq -\beta_3 \|w\|^2 \tag{4.9}$$

$$\|\frac{\partial W}{\partial w}\| \leq \beta_4 \|w\| \tag{4.10}$$

for all $w \in D_1 \subset \Re^4$. D_1 containing the origin is a domain to be estimated and positive constants β_1 to β_4 are calculated from the eigenvalues λ's of P as in Table 4.1, where $\lambda_{\min}(\cdot)$ and $\lambda_{\max}(\cdot)$ denote the minimal and the

Table 4.1. Positive constant $\beta_i\,(1 \leq i \leq 4)$

β_i	Calculation	Value
β_1	$\lambda_{min}(P)$	0.0081
β_2	$\lambda_{max}(P)$	35.796
β_3	satisfying $\dot{W}/\|w\|^2 \leq -\beta_3$	0.0001
β_4	$2\lambda_{max}(P)$	71.592

maximal eigenvalues, respectively. In this analysis, a "hyper rhombus" with each vertex on one of the state-space coordinate axes is defined as

$$\begin{aligned}&\mathcal{R}h(p_1, p_2, p_3, p_4)\\ &\quad := \{(w_1, w_2, w_3, w_4) | w_i = s_i p_i, \Sigma_i |s_i| \leq 1, s_i \in \Re, i = 1, 2, 3, 4\}\end{aligned} \tag{4.11}$$

to depict estimates of region of attraction, where p_i denotes the coordinate of the vertex on each axis. Applying this representation, an estimate of the region of attraction for the system with the state-feedback controller is obtained

$$D_1 = \mathcal{R}h(28.3, 7.6, 0.4, 28.3) \quad \text{(deg, deg, deg/s, deg/s).} \tag{4.12}$$

While a Lyapunov function for the fast system can be constructed since A_e is Hurwitz. The positive-definite solution

$$P_e = \begin{bmatrix} 5.0 \times 10^7 & 0 & -0.5 \times 10^4 & 0 \\ 0 & 7.0 \times 10^7 & 0 & -0.5 \times 10^4 \\ -0.5 \times 10^4 & 0 & 3.6 \times 10^3 & 0 \\ 0 & -0.5 \times 10^4 & 0 & 0.5 \times 10^4 \end{bmatrix} \tag{4.13}$$

of the Lyapunov equation $P_e A_e + A_e^T P_e = -I_4$ yields $V(e) = e^T P_e e$, and a domain for e containing the origin is also denoted by $D_2 \subset \Re^4$, which is set as

$$D_2 = \mathcal{R}h(2.2 * 10^5, 1.3 * 10^7, 2.2 * 10^5, 1.3 * 10^7) \quad \text{(m, deg, m/s, deg/s).} \tag{4.14}$$

Note that p_i represents the range of e_i and the scaled estimation error (4.1) implies that a region of non-scaled estimation error

$$\bar{D}_2 = \mathcal{R}h(2.2 * 10^3, 1.3 * 10^5, 2.2 * 10^5, 1.3 * 10^7) \quad \text{(m, deg, m/s, deg/s).} \tag{4.15}$$

Hence a Lyapunov function candidate for the full singularly perturbed system results from a weighted sum of those two Lyapunov functions,

$$\nu(w,e) = \frac{W(w)}{\mu_0} + \frac{V(e)}{\sigma_0}, \tag{4.16}$$

where $\mu_0 > 0, \sigma_0 > 0$.

4.3 Stability Analysis

4.3.1 Asymptotic Stability

Now Theorem 1 is introduced referring to the extension in [101] of the Tikhonov's theorem as follows:

Theorem 1 *Suppose in addition to the assumptions* (4.8) − (4.10)*, the system* (4.2) *and* (4.4) *satisfies*

$$\|\tilde{f}(w, N(\epsilon)e)\| \leq \beta_5 \|e\| \tag{4.17}$$

$$\|\tilde{g}(w, N(\epsilon)e)\| \leq \beta_6 \|w\| + \beta_7 \|e\| \tag{4.18}$$

for all $(w,e) \in D_1 \times D_2$*, where* β_5 *to* β_7 *are non-negative constants. Then there exists* $\epsilon^* > 0$ *such that for* $0 < \epsilon < \epsilon^*$*, the origin of* (4.2) *and* (4.4) *is asymptotically stable and a region of attraction is estimated by*

$$\Omega = \{(w,e) \mid \frac{W(w)}{\mu_0} + \frac{V(e)}{\sigma_0} \leq 1\} \subset D_1 \times D_2. \tag{4.19}$$

Let the solution of the slow system be $\bar{w}(t)$ and that of the full singularly perturbed system be $w(t,\epsilon)$. Theorem 1 means that for all initial state in Ω, the limit

$$w(t,\epsilon) \to \bar{w}(t) \tag{4.20}$$

is hold as $\epsilon \to 0$ uniformly in t for all $t \geq 0$. Note that the constants μ_0 and σ_0 are chosen satifying

$$\Omega_1 = \{w | W(w) \leq \mu_0\} \subset D_1, \tag{4.21}$$

$$\Omega_2 = \{e | V(e) \leq \sigma_0\} \subset D_2. \tag{4.22}$$

In order to apply Theorem 1, the assumptions (4.17) and (4.18) have to be confirmed. Assuming $\beta_6 = \beta_7$ reduces the number of constants, and β_5

and β_6 over $D_1 \times D_2$ are calculated by

$$\frac{\|\tilde{f}(w, N(\epsilon)e)\|}{\|e\|} \leq \beta_5, \tag{4.23}$$

$$\frac{\|\tilde{g}(w, N(\epsilon)e)\|}{\|w\| + \|e\|} \leq \beta_6. \tag{4.24}$$

Each range of the variables is divided by ten for searching over $D_1 \times D_2$. To successfully perform the above computation, the argument of $\arccos(\cdot)$ in the inverse transformation $T^{-1}(z)$ is bounded within ± 1, because the estimation error can vary independently of the practical geometric constraints. Consequently, the resulting $\beta_5 = 10$ and $\beta_6 = 10^7$ verifies that the CEP is asymptotically stable.

4.3.2 Estimates of Region of Attraction

Finally, an estimate of the region of attraction is considered. A conventional method, e.g., explained in [99] as in the following lemma is attempted first:

Lemma 1 (estimate of region of attraction) *Consider a simply connected closed set D containing the origin on the Euclidean space $\Re^n$. Then,*

$$r_{w\min} = \min_{w \in \partial D} \|w\| \tag{4.25}$$

$$\sigma_w = \lambda_{\min}(P) r_{w\min}^2 \tag{4.26}$$

$$\Omega_w = \{w \mid w^T P w \leq \sigma_w, w \in \Re^n\}, \tag{4.27}$$

where $\partial(\cdot)$ denotes the boundary of the set and $P \in \Re^{n \times n}$ is a positive-definite matrix, so that $\Omega_w \subseteq D$.

Proof: See Appendix B.1.

Note that compared with products of hyper rhombuses $D_1 \times D_2$ by (4.12) and (4.14), w and e in the coupled form (4.19) are not desirable to grasp the specific region of attraction particularly with higher than three-dimensional space. Therefore, to calculate products of hyper rhombuses independently, $\Omega_1' \times \Omega_2' \subset \Omega$ are defined as

$$\Omega_1' = \{w | W(w) \leq \mu_0 * 0.9\} \subset \Omega_1, \tag{4.28}$$

$$\Omega_2' = \{e | V(e) \leq \sigma_0 * 0.1\} \subset \Omega_2. \tag{4.29}$$

It should be remarked that the region of attraction in our case consists of two parts, the slow system and fast one, which are completely different in the following point. Since the slow system adopts the controller based on the approximate linearized system, the condition (4.9) constrains its closed-loop stability within a vicinity of the origin. Meanwhile, the global stability is ensured for the fast system for sufficiently small ϵ and, as long as D_1 and D_2 are bounded, the coupled conditions (4.17)-(4.18) are satisfied invariably due to the global continuousness in their arguments of the functions $\tilde{f}$ and $\tilde{g}$. Hence, in the prospect of the entire singularly perturbed system, Ω_1' for the slow system can not be extended arbitrarily, but Ω_2' for the fast system is not the case.

Utilizing Lemma 1 and calculation in Chapter 8 of [99], μ_0 and σ_0 are determined as $\mu_0 \leq \lambda_{min}(P) * r_w^2 = 4.0 * 10^{-7}$ and $\sigma_0 \leq \lambda_{min}(P_e) * r_e^2 = 4.4 * 10^{13}$, where $r_w = 0.007 = \|w\|_{min}$ and $r_e = 1.107 * 10^5 = \|e\|_{min}$ on each boundary D_1 and D_2, respectively. Resulting estimates in the form of (4.28)-(4.29) are

$$\mathcal{R}h(0.01, 0.03, 0.01, 0.28) \subset \Omega_1' \quad \text{(deg, deg, deg/s, deg/s)}, \tag{4.30}$$

$$\mathcal{R}h(290, 1.4 * 10^4, 2.9 * 10^5, 1.7 * 10^7) \subset \Omega_2' \quad \text{(m, deg, m/s, deg/s)}, \tag{4.31}$$

which means that original region $\bar{\Omega}_2'$ is

$$\mathcal{R}h(2.9, 140, 2.9 * 10^5, 1.7 * 10^7) \subset \bar{\Omega}_2' \quad \text{(m, deg, m/s, deg/s)}. \tag{4.32}$$

From the viewpoint of practical use, the above result Ω_1' is quite conservative and not available. This is due to the unbalance between the eigenvalues λ, and hence a "state-space scaling method" justified theoretically by the following theorem is devised to improve the estimate in the sense of less conservativeness:

Theorem 2 (state-space scaling method) *Consider the same situation as in Lemma 1 and Eqs. (4.25)–(4.27). Taking the matrix square root $P^{1/2}$ results in a linear map $\mathcal{T}_P : \Re^n \to \Re^n$ defined as*

$$\mathcal{T}_P(w) = P^{1/2} w. \tag{4.33}$$

Then,

$$
\begin{aligned}
D_{w'} &= \mathcal{T}_P(D) && (4.34)\\
r_{w'\min} &= \min_{w' \in \partial D'_w} \|w'\| && (4.35)\\
\sigma_{w'} &= r^2_{w'\min} && (4.36)\\
\Omega_{w'} &= \{w \mid w^T P w \leq \sigma_{w'}, w \in \Re^n\} && (4.37)
\end{aligned}
$$

so as to hold $\sigma_w \leq \sigma_{w'}$ *and* $\Omega_w \subseteq \Omega_{w'} \subseteq D$.

Proof: See Appendix B.2.

Thus the estimate of the region of attraction can be expected to be expanded by this scaling method. The minimum distance from the origin to the boundary of the transformed polytope, r_{min}, is searched to apply Theorem 2 and the new constant $\mu_0 = r^2_{min} = 3.7 * 10^{-4}$ yields

$$
\mathcal{R}h(0.22, 0.97, 0.17, 8.55) \subset \Omega'_1 \quad \text{(deg, deg, deg/s, deg/s)}. \tag{4.38}
$$

According to the scaled results, the value for the vehicle attitude w_2 is larger than that for the cable w_1. This tendency is proper considering the configuration of the TUV and is clarified compared to the conventional result (4.30). The comparison between the conventional estimate and the scaled one is also shown in Fig. 4.1, which is the projections onto the w_1-w_2 plane with $w_3 = w_4 = 0$, and the validity of the proposed scaling method is explicit. Note that the essence of Theorem 2 is to rebalance the minimal and maximal eigenvalues of a positive-definite matrix included in the Lyapunov function, so that the state-space scaling method can be widely employed for other stability analyses.

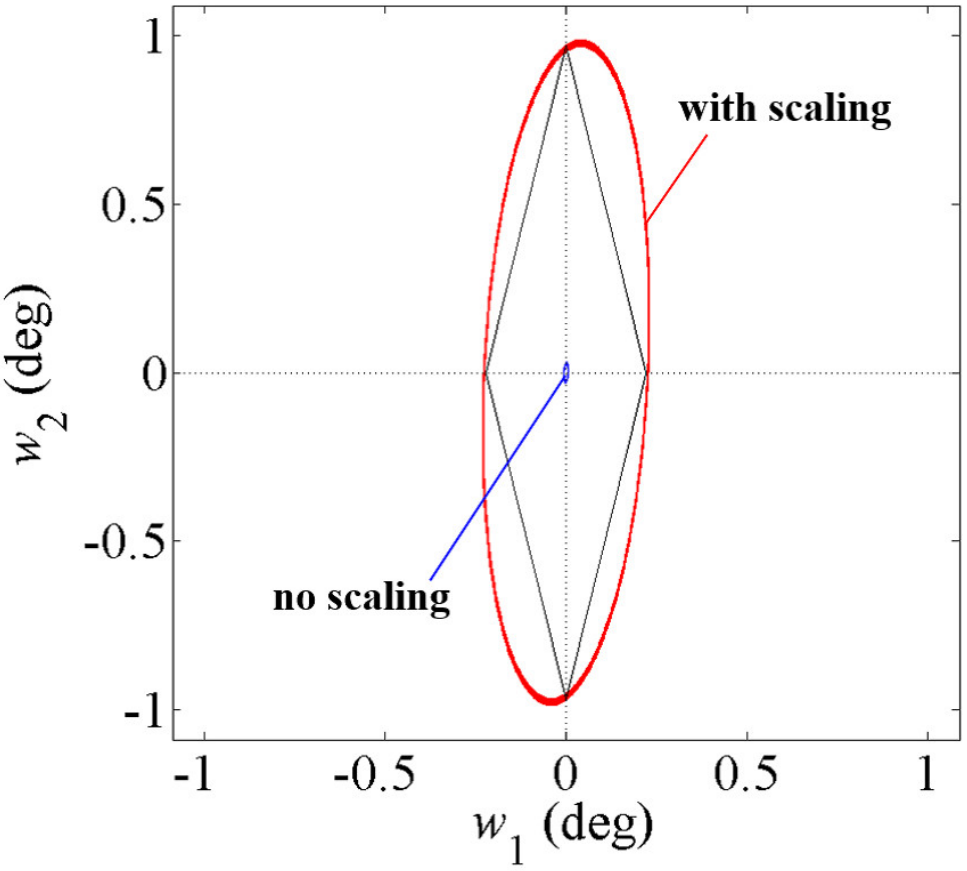

Figure 4.1. Projections of the estimates of region of attraction with $w_3 = w_4 = 0$: $W(w) \leq 4.0 * 10^{-7} * 0.9$ (no scaling) and $W(w) \leq 3.7 * 10^{-4} * 0.9$ (with scaling).

Further, Table 4.2 presents the analysis results for all the cases C1-C6, where D_1, the estimates by the conventional and proposed scaling method are listed by utilizing the same procedure in this chapter. First, the estimates by both methods for C1 show the best results compared to other estimates, which is due to the shortness of the cable length, $L = 30$ m. Second, the results for C2-C4 become worse according to the extension of the cable length. In particular, the values of w_3 in D_1 are the smallest in the deviation w and restrict the results of the estimates. Then the estimates for C5 and C6 are more conservative than those of C3 and C4. This is due to the methodology of choosing the Lyapunov function and there might be some additional linear transformation methods for a positive-definite matrix P so as to improve the analysis result. In any case, it can be concluded the state-space scaling method has improved the estimate of region of attractions compared to the conventional method.

At the end of this chapter, estimates of the region of attractions of C2 by the proposed method for other equilibriums near the CEP are presented in Fig. 4.2, where the obtained estimates as the projections onto the x_1-x_2 plane similar to Fig. 4.1 are depicted. The equilibriums are selected corresponding to the depths (a) 49.7 m, (b) 50.0 m, (c) 50.2 m (CEP), (d) 50.4 m and (e) 50.7 m, respectively. As seen from the figure, not only (c) with red line but also (b) and (d) with blue lines contain the origin of the coordinates, which represents the CEP of C2. In other words, the local regions of attraction indicate overlap and subsume the next equilibriums each other. Such a sequence implies the feasibility of the switching control system for the full operating range by switching multiple controllers in accordance with the respective equilibriums. This analysis reveals that the local regions of attraction relate to the reachable operating range and supplies a highly suggestive perspective on the relationship between them theoretically, although those estimates of the region of attraction are still conservative. Thus, the next question that how many controllers are needed to cover the full operating range in the actual switching control system of C2 will be investigated in Section 5.2 by simulations.

Table 4.2. Results of the analysis

Case	C1
D_1	$\mathcal{R}h(25.3, 7.5, 1.4, 26.8)$
Conventional estimate	$\mathcal{R}h(0.04, 0.10, 0.06, 0.92)$
Scaled estimate	$\mathcal{R}h(0.4, 0.92, 0.56, 8.33)$
Case	C2
D_1	$\mathcal{R}h(28.3, 7.6, 0.4, 28.3)$
Conventional estimate	$\mathcal{R}h(0.01, 0.03, 0.01, 0.28)$
Scaled estimate	$\mathcal{R}h(0.22, 0.97, 0.17, 8.55)$
Case	C3
D_1	$\mathcal{R}h(23.4, 7.4, 0.2, 23.5)$
Conventional estimate	$\mathcal{R}h(0.002, 0.016, 0.001, 0.147)$
Scaled estimate	$\mathcal{R}h(0.15, 0.92, 0.09, 8.20)$
Case	C4
D_1	$\mathcal{R}h(20.2, 7.2, 0.1, 19.3)$
Conventional estimate	$\mathcal{R}h(0.001, 0.008, 0.001, 0.078)$
Scaled estimate	$\mathcal{R}h(0.09, 0.67, 0.05, 6.26)$
Case	C5
D_1	$\mathcal{R}h(100, 16.4, 0.06, 27.0)$
Conventional estimate	$\mathcal{R}h(0.0005, 0.0021, 0.0025, 0.053)$
Scaled estimate	$\mathcal{R}h(0.01, 0.04, 0.05, 1.09)$
Case	C6
D_1	$\mathcal{R}h(96.9, 18.6, 0.03, 27.5)$
Conventional estimate	$\mathcal{R}h(0.0002, 0.0001, 0.0009, 0.027)$
Scaled estimate	$\mathcal{R}h(0.01, 0.03, 0.03, 0.75)$

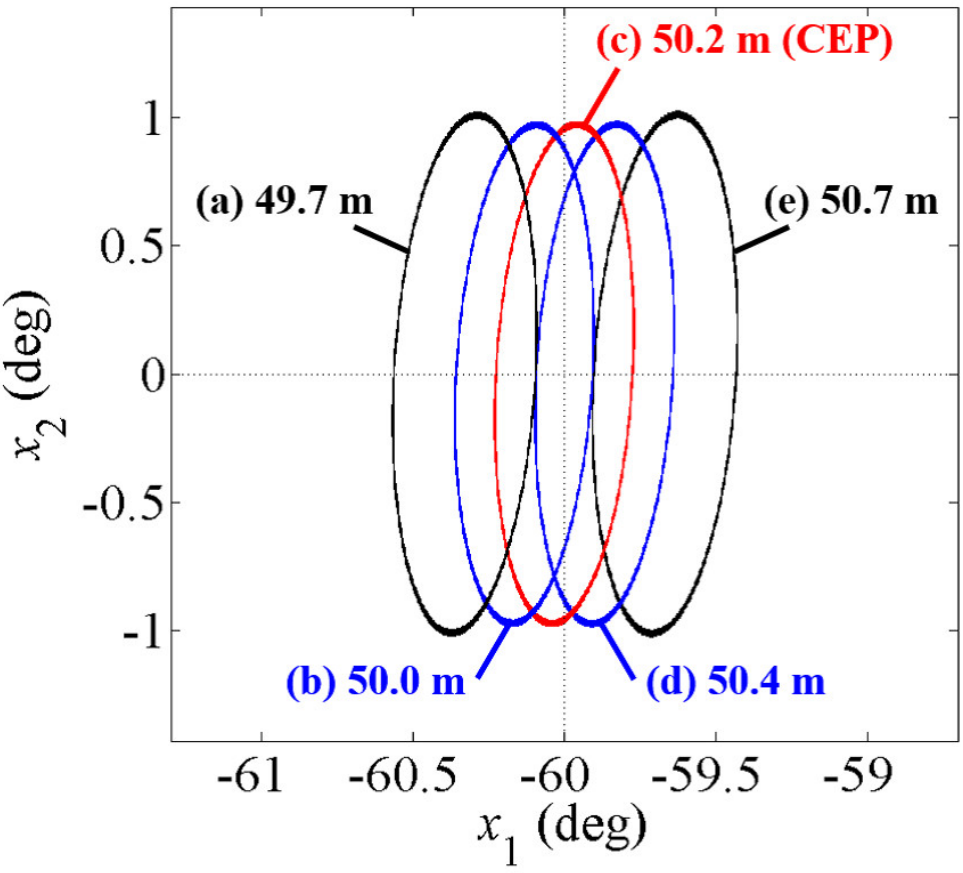

Figure 4.2. Estimates of region of attractions with C2 and $w_3 = w_4 = 0$ for the different equilibriums: the depth corresponding to (a) 49.7 m, (b) 50.0 m, (c) 50.2 m (CEP), (d) 50.4 m and (e) 50.7 m.

5 Simulation Results for the LQ-Control-Based Approach

This chapter presents control performance evaluation simulations on the LQ-control-based approach presented in Chapter 3. Demonstrations of regulation in terms of initial deviations of the state variables are performed for the $n = 1$ model, where the comparison of the results with the stability analysis in Chapter 4 is included. Additionally, depth tracking by switching controllers is investigated to show the full operating range for C2 and to justify the perspective from the stability analysis.

5.1 Depth and Attitude Regulation

5.1.1 Settings

First, an "allowable initial deviation" as the pair (id_1, id_2) is defined to focus on regulation performance with initial deviations of the states, where considering the combinations of the signs, all the simulations with the initial deviation set $w(0) = [\pm id_1, \pm id_1, \pm id_2, \pm id_2]^T$ succeeds in regulating the system to the CEP. In order to evaluate the controllers, id_{1max} and id_{2max} are investigated by following two-step way.

Step1 Set $w = [0.1, 0.1, 0.1, 0.1]^T$ as the initial deviation and simulate with all the signs. According to the simulation results, increase (id_1, id_2) by 0.1° and 0.1°/s, and repeat the procedure to find the maximal allowable value id_{1max} for id_1 and id_2.

Step2 Set id_{1max} for id_1 and id_2 as the initial deviation in order to investigate the maximal allowable value for id_2. By only changing id_2 in a similar manner to the second step, find the maximal allowable value id_{2max} for id_2.

Therefore, a "maximum allowable initial deviation" $id_{max} = (id_{1max}, id_{2max})$ for each case obtained by the procedure can be regarded as a kind of criterion with respect to the region of attraction. Note that id_{max} suggests that $\Omega_1'' = \Phi_1 \times \Phi_2$ might correspond to an estimate of the region of attraction

for the state-feedback controller:

$$\Phi_1 = [-id_{1max}, id_{1max}] \times [-id_{1max}, id_{1max}] \quad (\text{deg}) \times (\text{deg}), \tag{5.1}$$
$$\Phi_2 = [-id_{2max}, id_{2max}] \times [-id_{2max}, id_{2max}] \quad (\text{deg/s}) \times (\text{deg/s}), \tag{5.2}$$

and $\Omega_1'' \times \bar{\Omega}_2''(\bar{\Omega}_2'' = T(\Omega_1''))$ might be also an estimate of that for the output-feedback controller.

5.1.2 Results

Table 5.1 enumerates each maximum allowable initial deviation (id_{1max}, id_{2max}) and corresponding depth range from the CEPs. For example, the result for C2 with the state-feedback controller is (3.0, 3.1); that is, pseudo estimation as Ω_1'' is obtained by

$$\Phi_1 = [-3.0, 3.0] \times [-3.0, 3.0] \quad (\text{deg}) \times (\text{deg}), \tag{5.3}$$
$$\Phi_2 = [-3.1, 3.1] \times [-3.1, 3.1] \quad (\text{deg/s}) \times (\text{deg/s}). \tag{5.4}$$

According to the comparison between the theoretical estimate D_1 (4.12) in Chapter 4.2 and Ω_1'' by (5.3) and (5.4), D_1 almost contains Ω_1'' with respect to both Φ_1 and Φ_2. However, some $w(0)$ exterior of D_1 but interior of (5.3) and (5.4) can be regulated. This fact is due to the trajectory of the Lyapunov function $W(w)$, where $W(w)$ does not decrease monotonically as shown later (see Fig. 5.8). Hence one of the limitations of the theoretical estimate and the necessity of the improvement in obtaining better $W(w)$ are ascertained. Next, the result with the output-feedback controller is (2.3, 2.4), in other words

$$\Phi_1 = [-2.3, 2.3] \times [-2.3, 2.3] \quad (\text{deg}) \times (\text{deg}), \tag{5.5}$$
$$\Phi_2 = [-2.4, 2.4] \times [-2.4, 2.4] \quad (\text{deg/s}) \times (\text{deg/s}), \tag{5.6}$$

which implies that

$$\bar{\Psi}_1 = [-3.6, 3.3] \times [-2.3, 2.3] \quad (\text{m}) \times (\text{deg}), \tag{5.7}$$
$$\Psi_2 = [-3.6, 3.3] \times [-2.4, 2.4] \quad (\text{m/s}) \times (\text{deg/s}), \tag{5.8}$$

for $\bar{\Omega}_2'' = \bar{\Psi}_1 \times \Psi_2$. Comparing Ω_1' by (4.38) and Ω_1'' by (5.5) and (5.6) reveals the conservativeness of the theoretical estimate too.

As seen from the results of C1 to C4 in Table 5.1, id_{max} diminishes along with the elongation of the cable length reasonably. While the results of C5 and C6 are improved, which implies that the modifications for the physical design specifications are valid and the proposed control approach is essentially effectual.

Table 5.1. $id_{max} = (id_{1max}, id_{2max})$ and corresponding depth range from CEP for each model

Case	State-feedback	Corresponding depth range (m)
C1	(28.4, 28.5)	$[-14.187, 10.527]$
C2	(3.0, 3.1)	$[-4.601, 4.464]$
C3	(1.0, 1.0)	$[-3.038, 3.008]$
C4	(0.4, 0.4)	$[-1.817, 1.810]$
C5	(7.7, 7.7)	$[-24.111, 22.304]$
C6	(6.0, 6.0)	$[-27.980, 26.335]$
Case	Output-feedback	Corresponding depth range (m)
C1	(15.0, 15.0)	$[-7.242, 6.206]$
C2	(2.3, 2.4)	$[-3.516, 3.435]$
C3	(0.5, 0.5)	$[-1.515, 1.508]$
C4	(0.1, 0.2)	$[-0.454, 0.453]$
C5	(7.2, 7.2)	$[-22.499, 20.918]$
C6	(5.6, 5.6)	$[-26.070, 24.636]$

Here, in order to investigate the time series data in detail, the demonstration results of the proposed LQ-based controller for C2 are presented in Figs. 5.1, 5.2, 5.3, 5.4, 5.5, 5.6, 5.7 and 5.8. The initial deviation for both controllers is set as $w(0) = x(0) - x^* = [-2.3, 2.3, 2.4, 2.4]^T$, which is corresponding to id_{max} with the output-feedback controller, and the initial estimation for the high-gain observer is set as $\hat{z}(0) = [50.205, 0, 0, 0]^T$, i.e., the CEP.

Figs. 5.1 and 5.2 present the outputs by the state-feedback and output-feedback controller, where both the depth and attitude reveal nearly the same trajectories. This implies that the performance of the state-feedback controller is recovered by the high-gain observer in the output-feedback controller to a certain extent. As illustrated, the attitude y_2 in Fig. 5.2 reaches about 45°, which bounds the id_{max} for the output-feedback controller compared to that for the state-feedback controller in the amount. The difference between the graphs would become more clear by comparing the control inputs as Figs. 5.3 and 5.4, where two time-scale graphs are prepared; the top one is for full time range and the bottom is for the first 1 second of the simulations. It can be seen from the figures that the input of the output-feedback controller shows more abrupt change in a short period of time and the saturation works well. Otherwise, the control input might extend to impractical value as shown in Fig. 5.5, which are the trajectories for the same simulation of the output-feedback controller without the input saturation. Before the convergence, both u_1 and u_2 largely overshoot within almost ±500°. Further, the importance of the input saturation is also confirmed by Figs. 5.6 and 5.7, where the estimation errors for angles and angular velocities are depicted with two time-scale graphs. Although an impulsive response called the "peaking phenomenon" is exhibited in the bottom graphs for the first 0.4 seconds, the top one for full time range seems to converge to 0 promptly. Thus the control input saturation is intrinsically required not only to consider the *dynamic stall* but to mitigate the influence of the peaking phenomenon of the high-gain observer so that the whole proposed control system is stable. In addition, Fig. 5.8 is presented to depict the example of the gap between the theoretical estimate and the original region of attraction. There are the trajectories of the Lyapunov function $W(w)$ for both controllers in two time-scale; the top one is for full

time range and the bottom is for 5 seconds in start point. It is obvious that the initial deviation $w(0) = x(0) - x^* = [-2.3, 2.3, 2.4, 2.4]^T$ is out of D_1 and the time series data for $W(w)$ shows an increment in less than first 1 second.

At the end of the demonstrations of the regulation performance, Fig. 5.9 is presented, which indicates the output with the output-feedback controller and no initial deviation, that is, $x(0) = x^*$ and $w(0) = [0, 0, 0, 0]^T$. However, the towing speed v_0 is set as 6 m/s, which is faster than that of the nominal model. In consequence, the regulation completely fails as seen from the figure. This implies that the proposed controller is not robust enough to model uncertainties, and therefore an LQI-control-based approach will be investigated in Chapter 6 and 7 to enhance the robustness of the proposed controller.

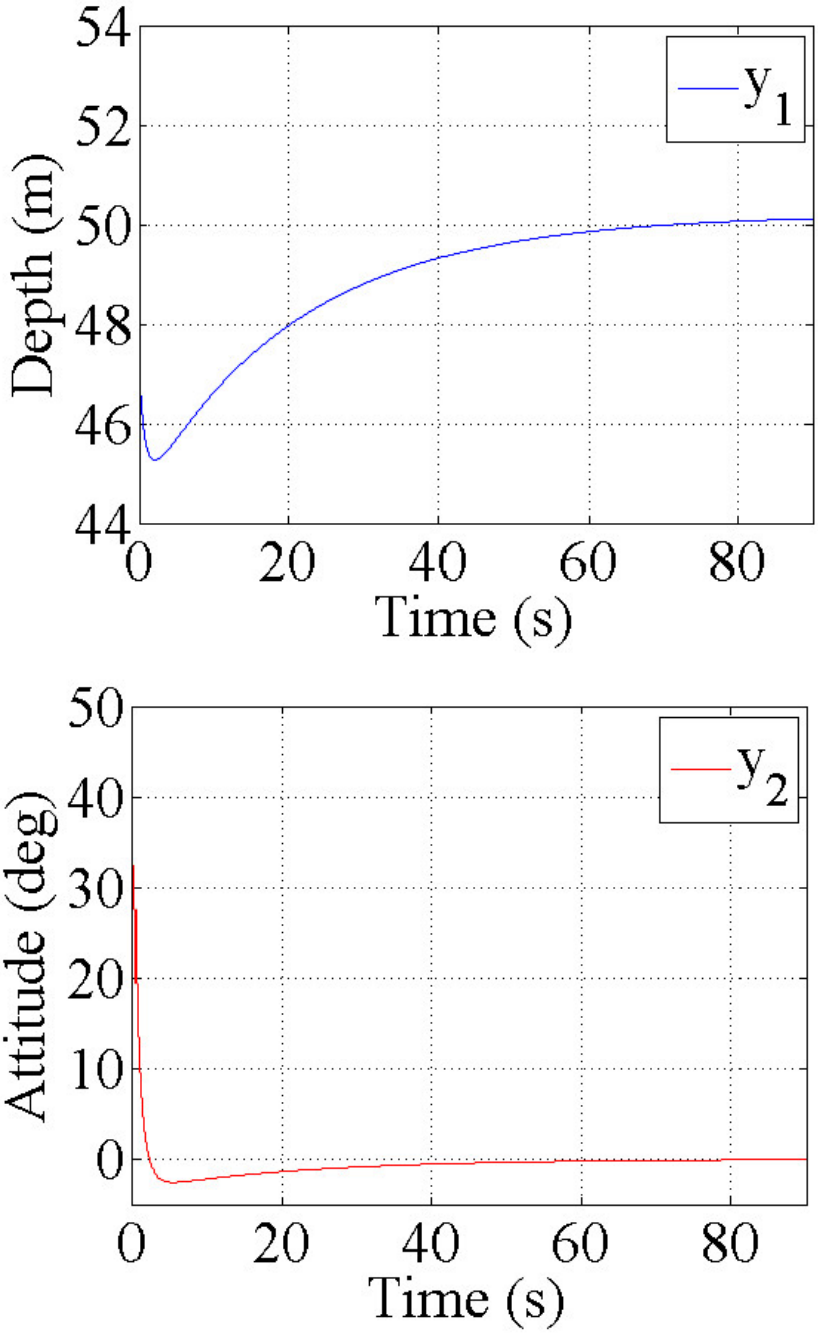

Figure 5.1. Simulation results of depth and attitude regulation with $w(0) = [-2.3, 2.3, 2.4, 2.4]^T$ by the state-feedback controller.

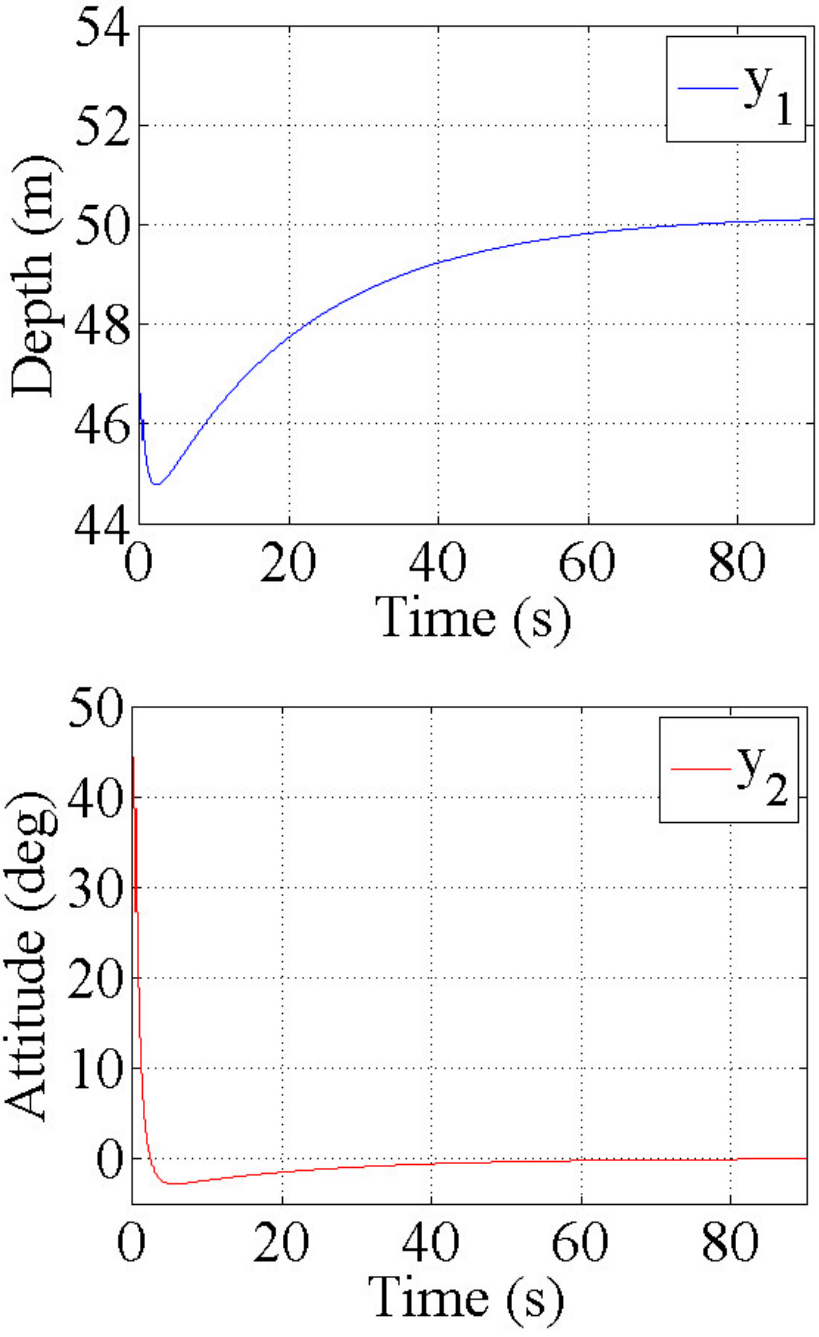

Figure 5.2. Simulation results of depth and attitude regulation with $w(0) = [-2.3, 2.3, 2.4, 2.4]^T$ by the output-feedback controller.

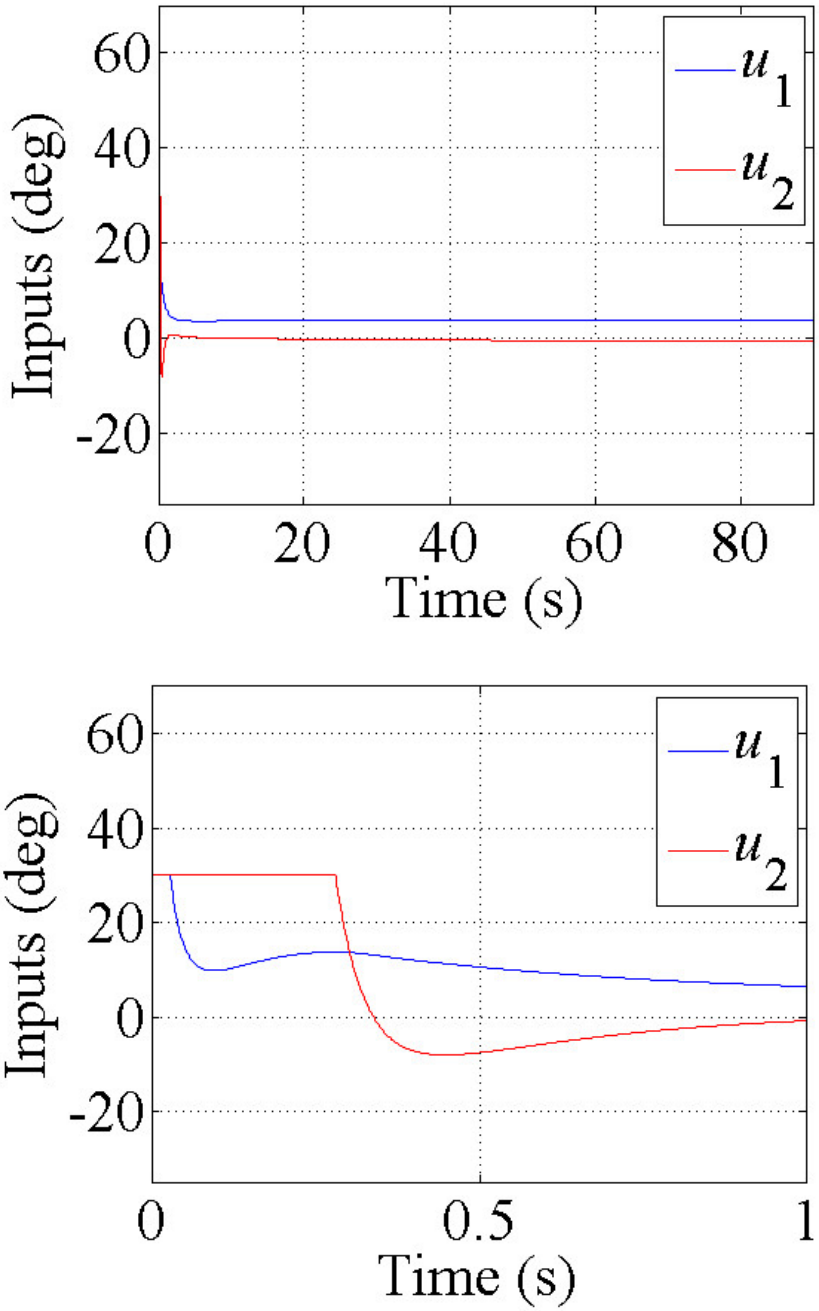

Figure 5.3. Control inputs of depth and attitude regulation with $w(0) = [-2.3, 2.3, 2.4, 2.4]^T$ by the state-feedback controller; *top* full time range, *bottom* in the first 1 second.

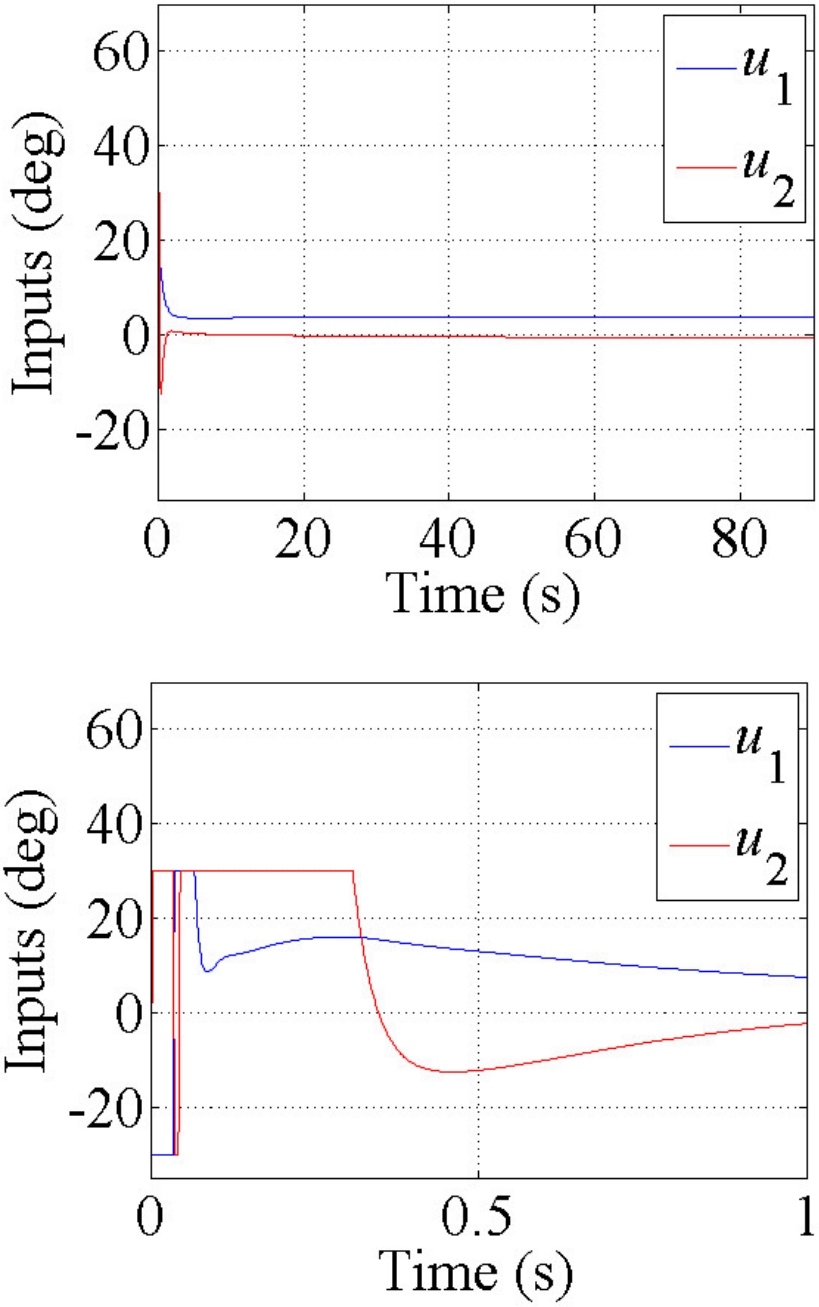

Figure 5.4. Control inputs of depth and attitude regulation with $w(0) = [-2.3, 2.3, 2.4, 2.4]^T$ by the output-feedback controller; *top* full time range, *bottom* in the first 1 second.

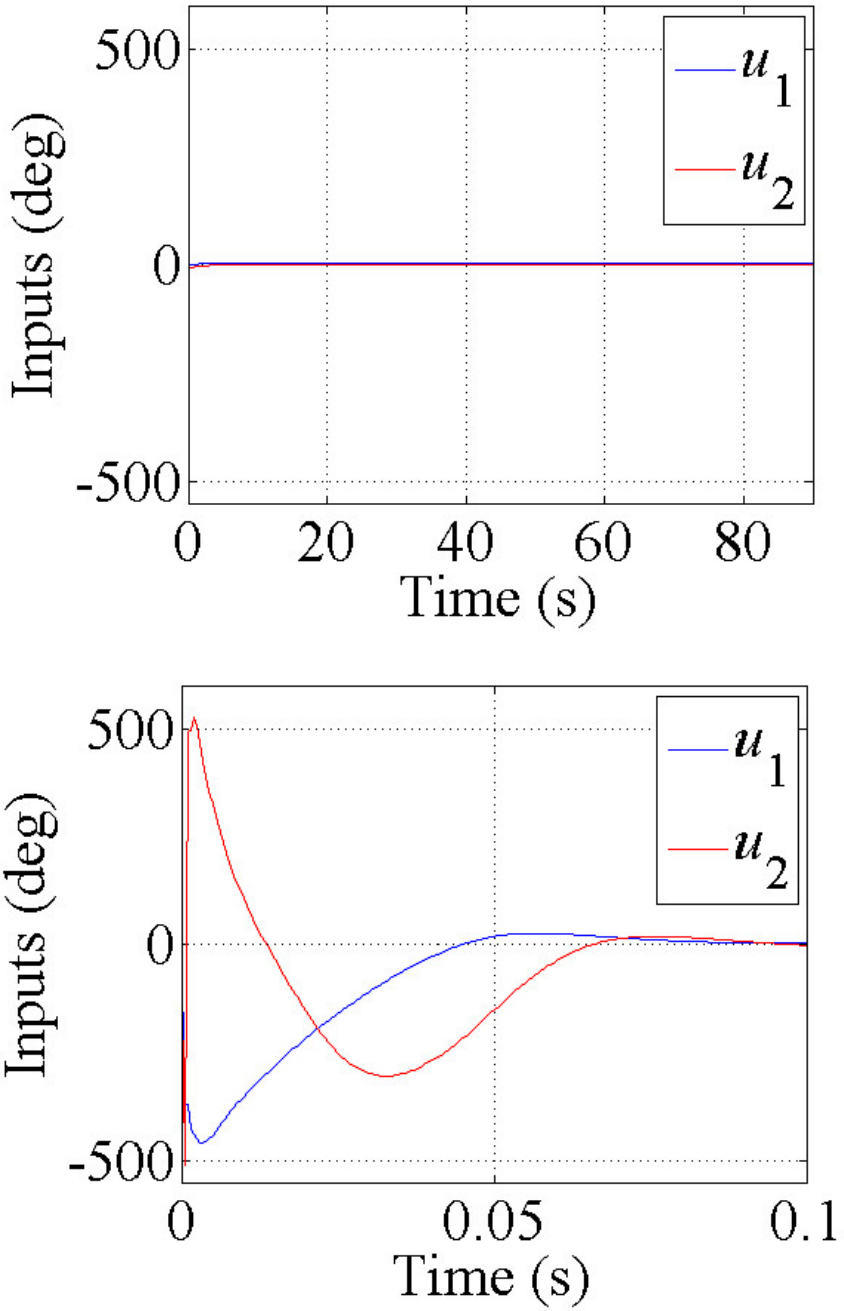

Figure 5.5. Control inputs of depth and attitude regulation with $w(0) = [-2.3, 2.3, 2.4, 2.4]^T$ by the output-feedback controller without saturation; *top* full time range, *bottom* in the first 0.1 seconds.

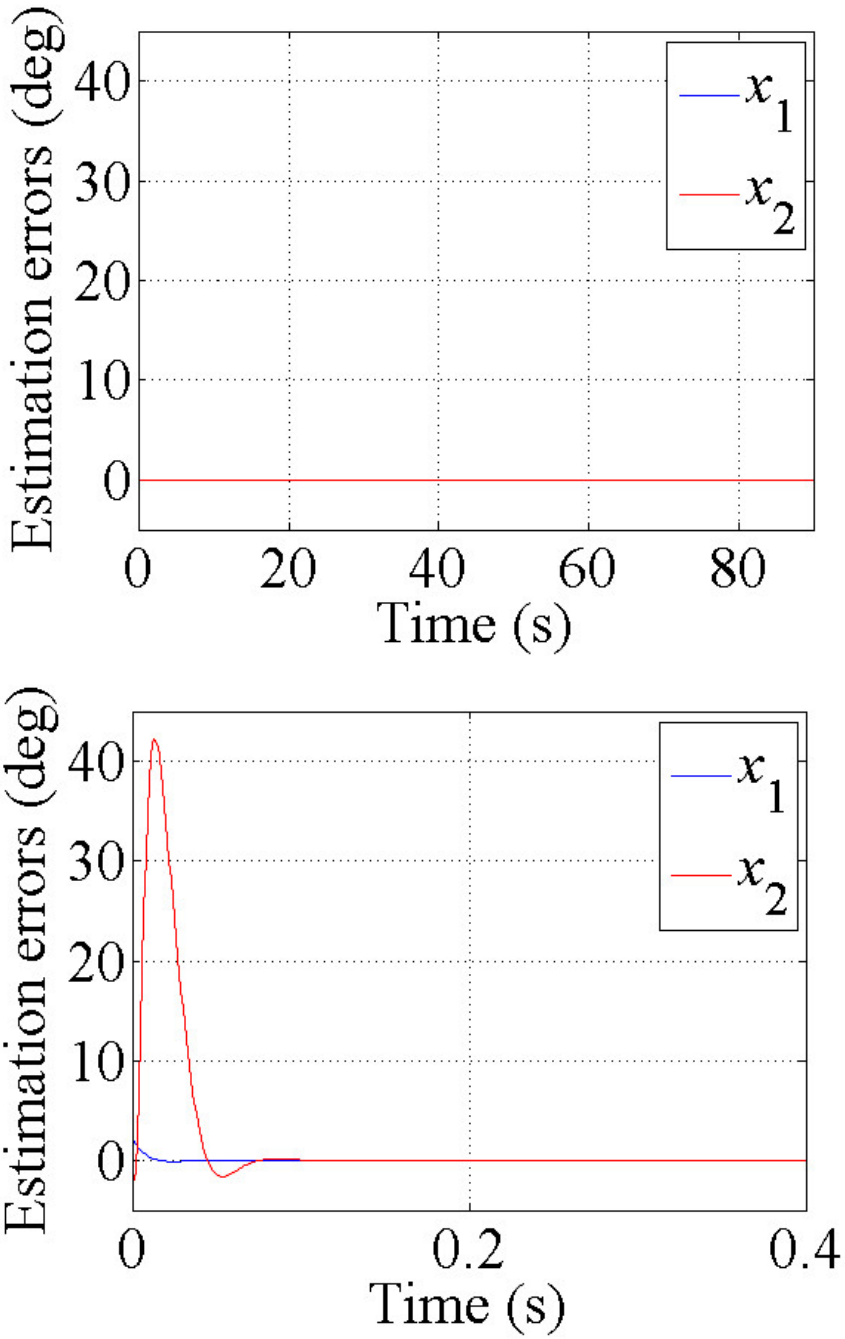

Figure 5.6. Estimation errors for angles of depth and attitude regulation with $w(0) = [-2.3, 2.3, 2.4, 2.4]^T$ by the output-feedback controller; *top* full time range, *bottom* in the first 0.5 seconds.

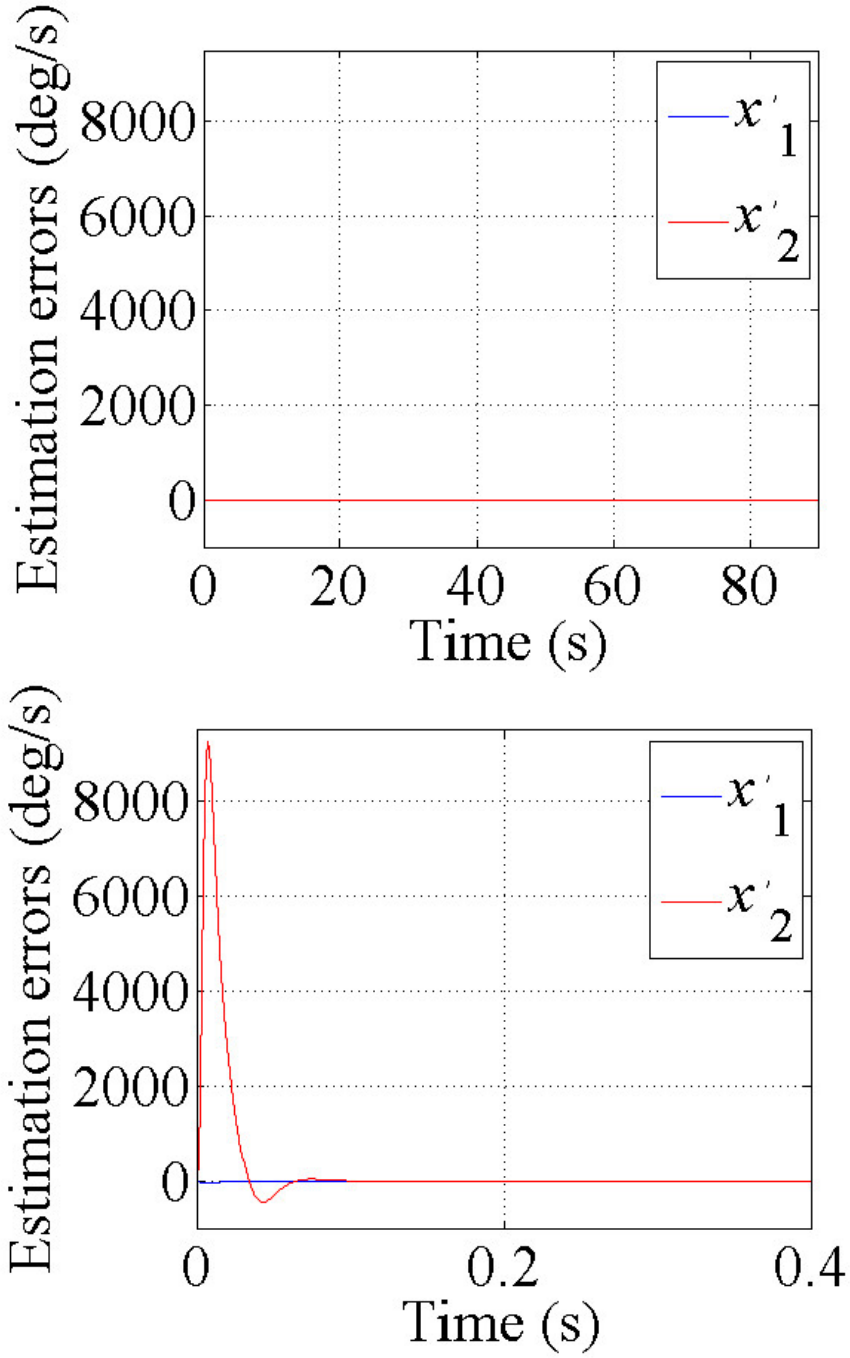

Figure 5.7. Estimation errors for angular velocities of depth and attitude regulation with $w(0) = [-2.3, 2.3, 2.4, 2.4]^T$ by the output-feedback controller; *top* full time range, *bottom* in the first 0.5 seconds.

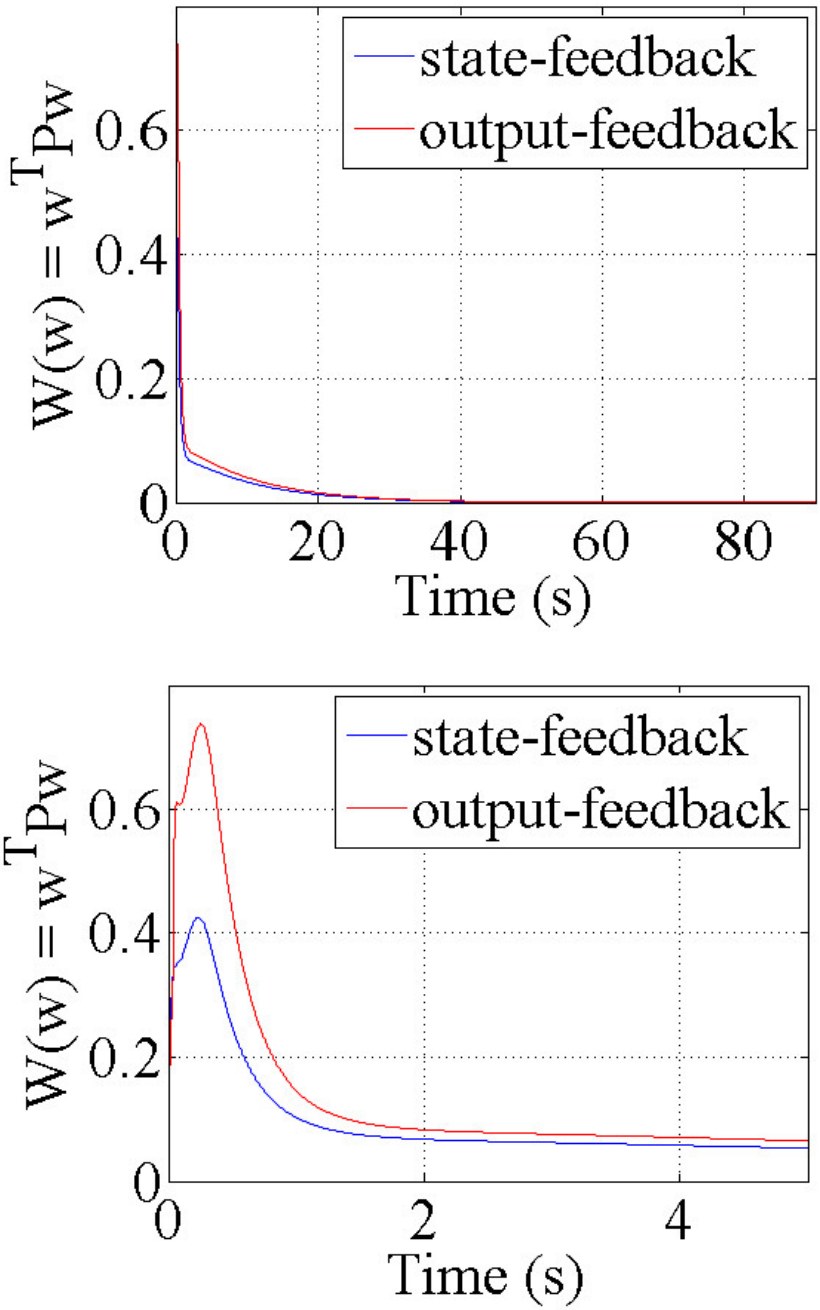

Figure 5.8. Trajectories of the Lyapunov function of depth and attitude regulation with $w(0) = [-2.3, 2.3, 2.4, 2.4]^T$ by each controller; *top* full time range, *bottom* in the first 5 seconds.

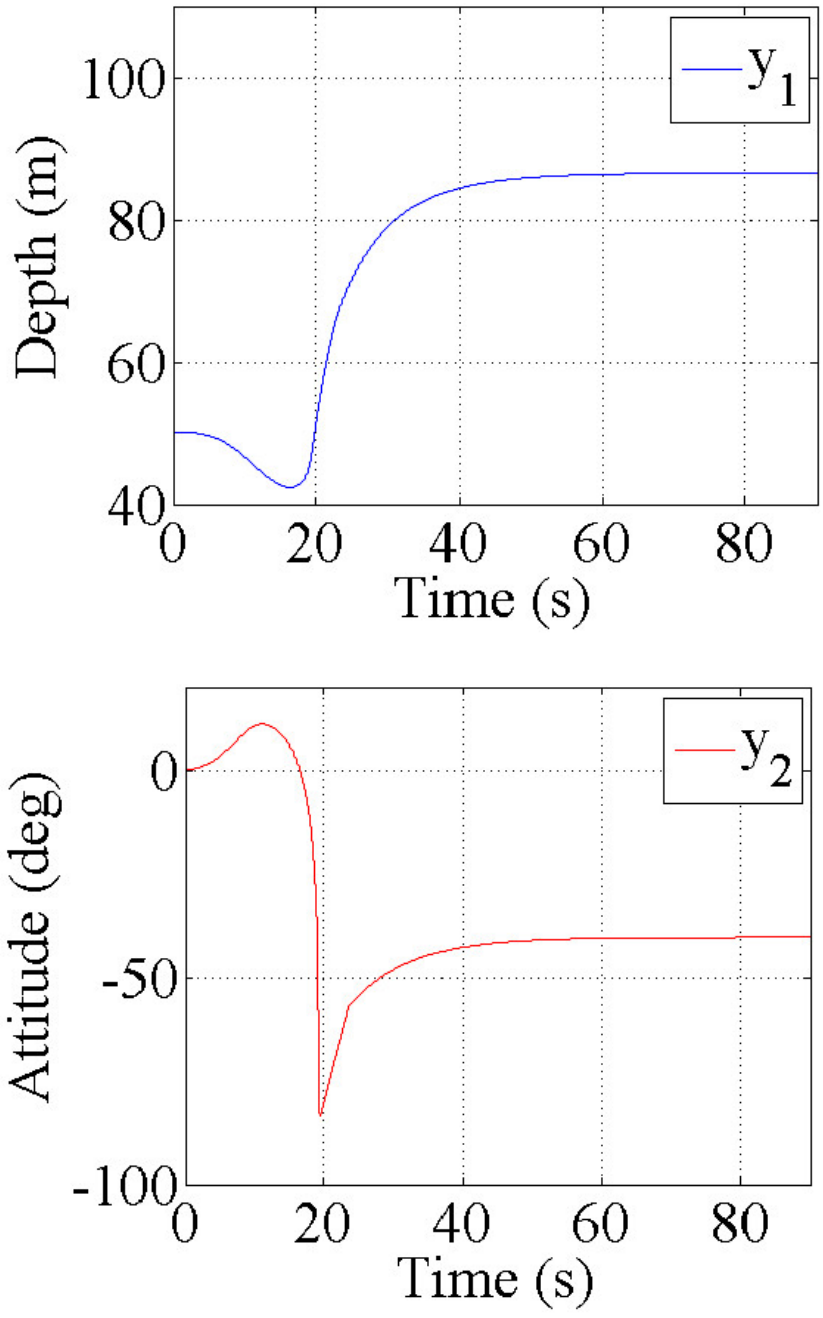

Figure 5.9. Simulation results of depth and attitude regulation with $w(0) = [0, 0, 0, 0]^T$ and towing speed $v_0 = 6$ m/s by the output-feedback controller.

5.2 Depth Tracking via Switching Controllers

5.2.1 Settings

Next, depth tracking control simulations for C2 via switching controllers are demonstrated to evaluate the full operating range. In this study, the procedure described as follows is employed to construct a depth tracking control system:

1. calculating multiple equilibrium points;
2. obtaining the LQ feedback gain K_{y_1} as Eq. (3.2) in Section 3.2 with respect to each equilibrium;
3. connecting each state-feedback with the high-gain observer (3.6);
4. switching K_{y_1} to change the depth of the vehicle y_1.

Note that the suffixes of K_{y_1} denote corresponding depths, e.g., K_{45} is the feedback gain for the equilibrium point of the depth 45.205 m, K_{50} is for the CEP (see (A.2) in Appendix A), K_{55} is for the equilibrium point of 55.205 m, and so on. Total 19 equilibrium points corresponding to the depths by each 5 m, i.e., around 5, 10, $\cdots$, 95 m are targeted.

In Section 4.3, it is demonstrated that the regions of attraction relate to a switching control system inextricably. For example, suppose that the TUV is intended to descend or ascend from the initial depth d_0 to the terminus depth d_1. The depth can be changed by switching the controller with K_{d_0} to that with K_{d_1} directly only when the region of attraction of the controller K_{d_1} with the equilibrium of the depth d_1 includes the equilibrium of the initial depth d_0. Otherwise, some controllers of intermediate depths will be necessary to reach the d_1 from the d_0.

Accordingly, two patterns of depth tracking paths are set to investigate the full operating range of the proposed controller by the simulations. One trajectory begins from the CEP with $d_0 = 50.205$ m and descends to $d_1 = 50.205 + \Delta d$ m ($5 \leq \Delta d \leq 45$) then goes back to d_0. In other words, the trajectory becomes 50.205 m $\rightarrow 50.205 + \Delta d$ m $\rightarrow 50.205$ m (Pattern 1). The other trajectory is the reverse pattern of the former one, that is, 50.205 m $\rightarrow 50.205 - \Delta d$ m $\rightarrow 50.205$ m (Pattern 2). Δd_{max} for each pattern is examined by checking all the tracking control trials successful or not for

$\Delta d = 5, 10, \cdots, \Delta d_{max}$ with no initial deviations. A schedule of switching controllers is arranged as $t = 0$ to 10 s for d_0, $t = 10$ to 200 s for d_1, and $t = 250$ to 400 s for d_2. Besides, the vehicle attitude is also controlled to be horizontal by the controllers during the trials.

5.2.2 Results

The simulation results show that the full operating range of the depth with $L = 100$ m cable is from 5 m to 85 m, i.e., Δd_{max} for Pattern 1 is 35 m and Δd_{max} for Pattern 2 is 45 m for both the state-feedback and output-feedback controllers. Figs. 5.10 and 5.11 show the tracking control results with the output-feedback controllers for Pattern 1 and Pattern 2, respectively. It is clear that the switching control system succeeds in tracking the reference depths smoothly in the both patterns, which means that the full operating range can be covered by only three controllers with maintaining the attitude of the vehicle horizontal. The above graphs, which depict the trajectory of the vehicle depth, also reveal that descending control takes shorter than ascending control to converge.

Based on this outcome, the direct change of the depth between 5 m and 85 m are examined. The controllers are switched so that the vehicle tracks as 50.205 m $\rightarrow$ 85.205 m $\rightarrow$ 5.205 m (Pattern 3) and 50.205 m $\rightarrow$ 5.205 m $\rightarrow$ 85.205 m (Pattern 4), where the schedule of switching the controllers accords with that for Pattern 1 and Pattern 2. Figs. 5.12 and 5.13 depict the results of Pattern 3 and Pattern 4, and elucidate that this tracking control is successful for Pattern 3 but not for Pattern 4. From the theoretical viewpoint, these results imply that the region of attraction of the controller with K_5 contains the equilibrium with K_{85}, but that with K_{85} does not include the equilibrium with K_5. Consequently, the connecting controllers are necessary to conform the vehicle as Pattern 4 and Fig. 5.14 presents such a successful result, where the controller for $d_0 = 50.205$ m are employed again between $t = 200$ to 320 s.

In addition, Figs. 5.15, 5.16, 5.17, 5.18 and 5.19 show the same tracking control pattern results with the state-feedback controllers, which are almost similar to those with the output-feedback controller. Reconfirm that the vehicle attitude never exceeds the limit $\pm 45^\circ$ except in Fig. 5.18. Hence, it can be concluded that the switching control system can transmit the vehicle

between the shallowest and deepest depths and the perspective obtained by the estimate of the region of attraction in Chapter 4 is warranted.

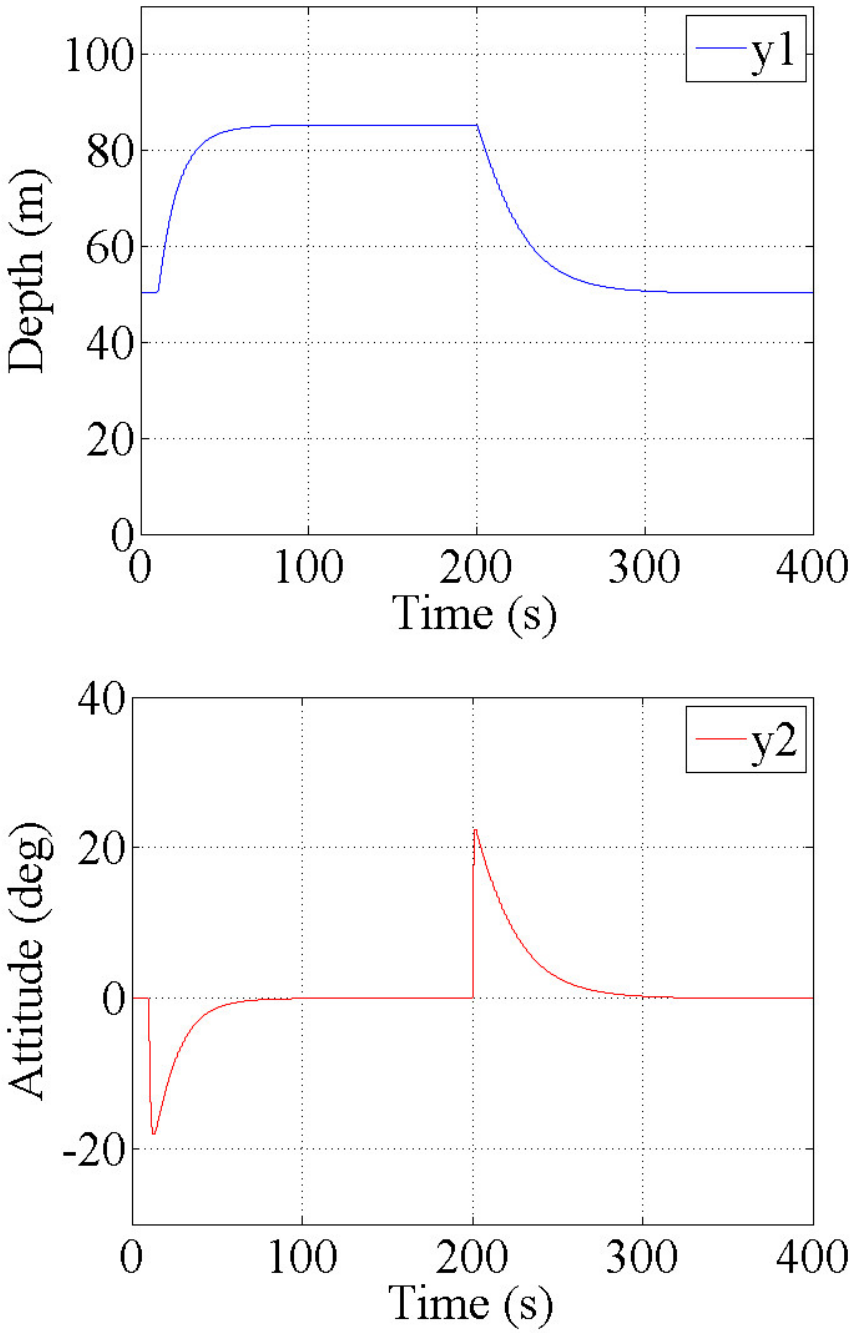

Figure 5.10. Tracking control simulation results of Pattern 1 by the output-feedback controller.

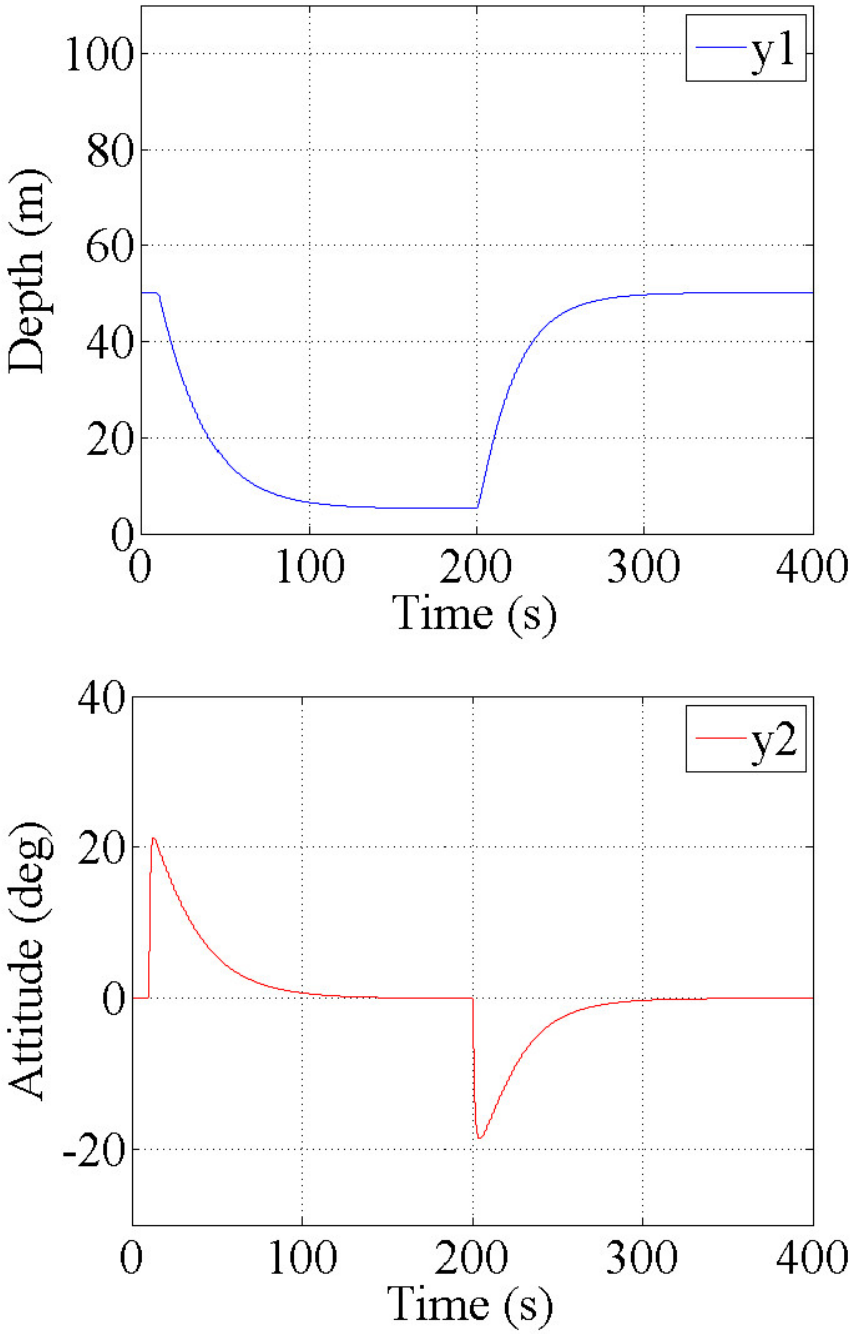

Figure 5.11. Tracking control simulation results of of Pattern 2 by the output-feedback controller.

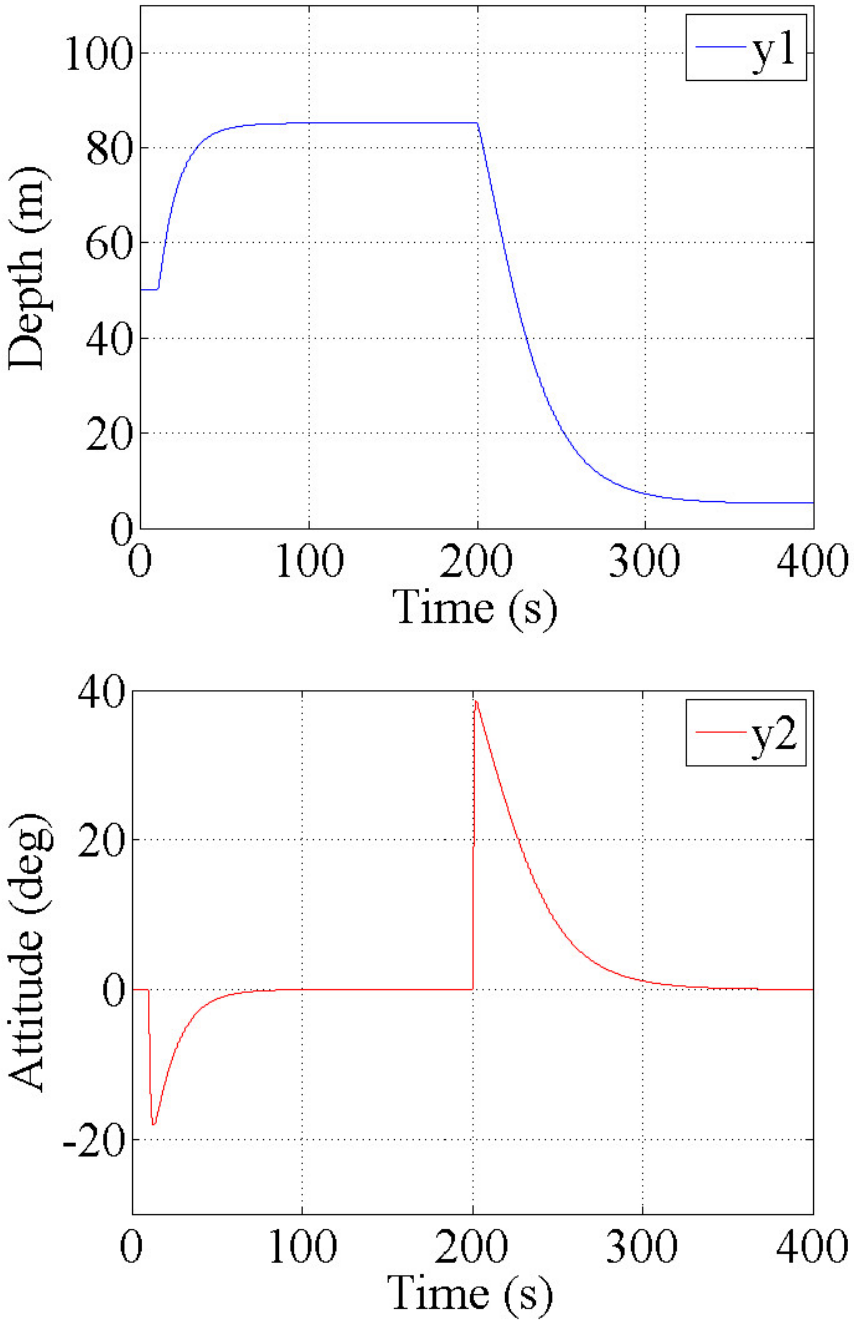

Figure 5.12. Tracking control simulation results of of Pattern 3 by the output-feedback controller.

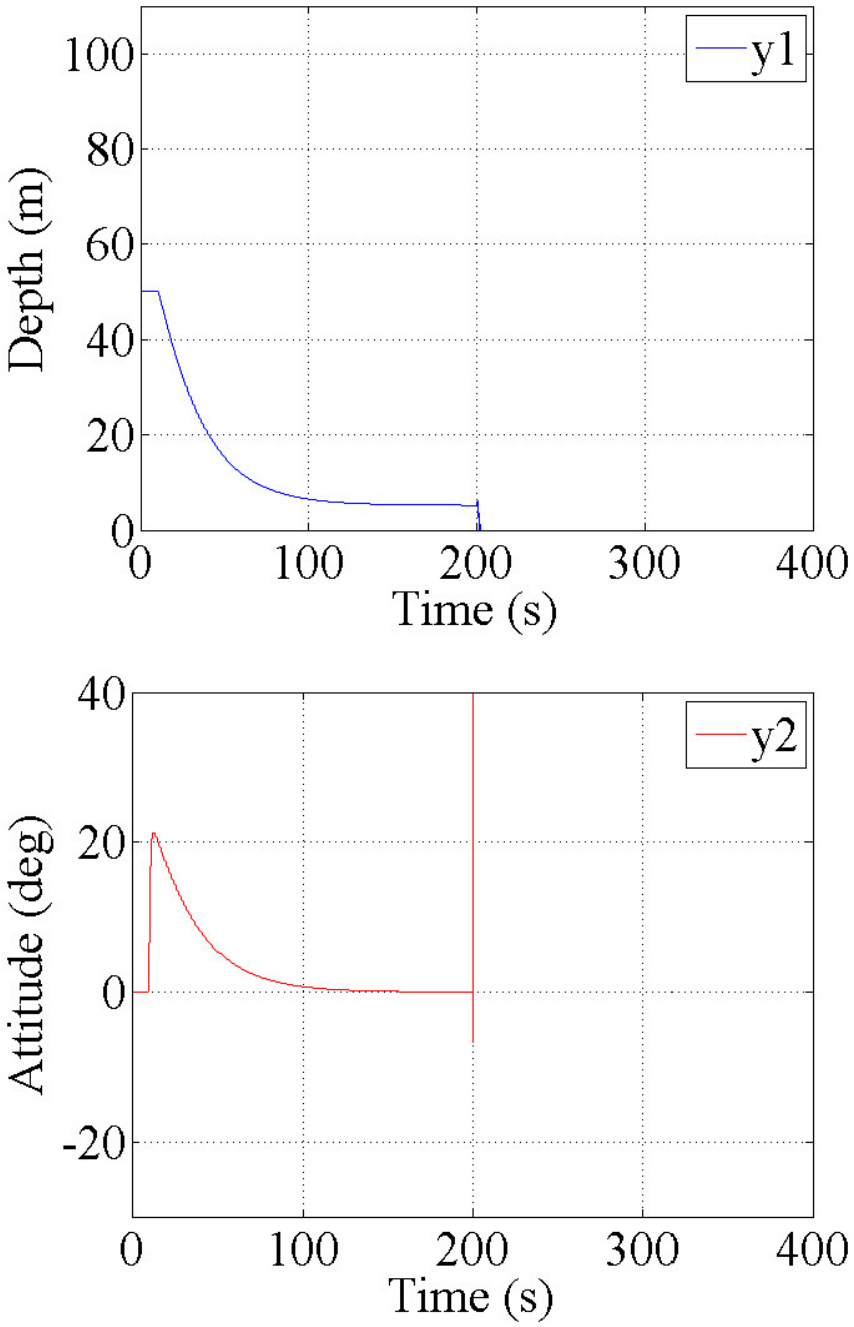

Figure 5.13. Tracking control simulation results of of Pattern 4 by the output-feedback controller.

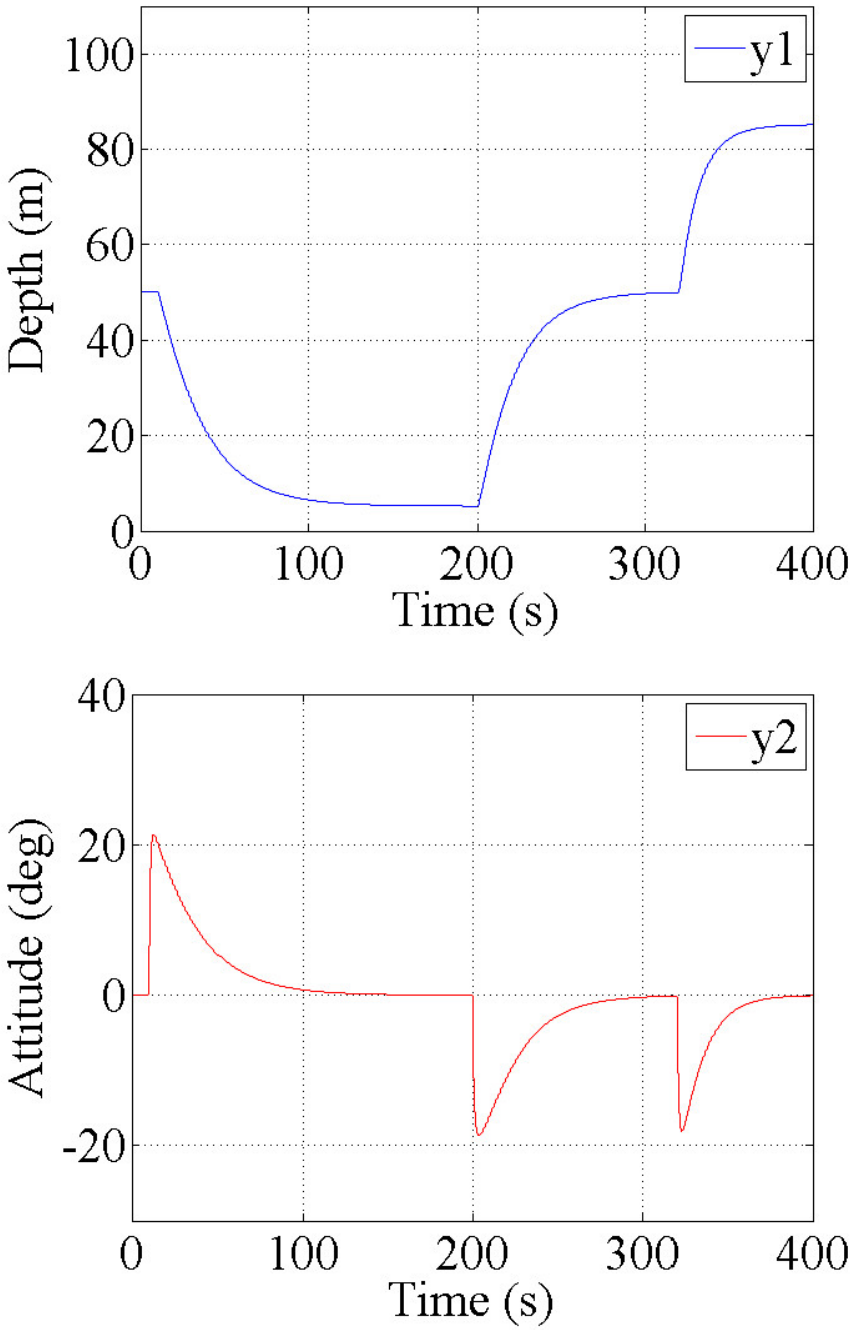

Figure 5.14. Tracking control simulation results of of Pattern 4 with by the output-feedback controller.

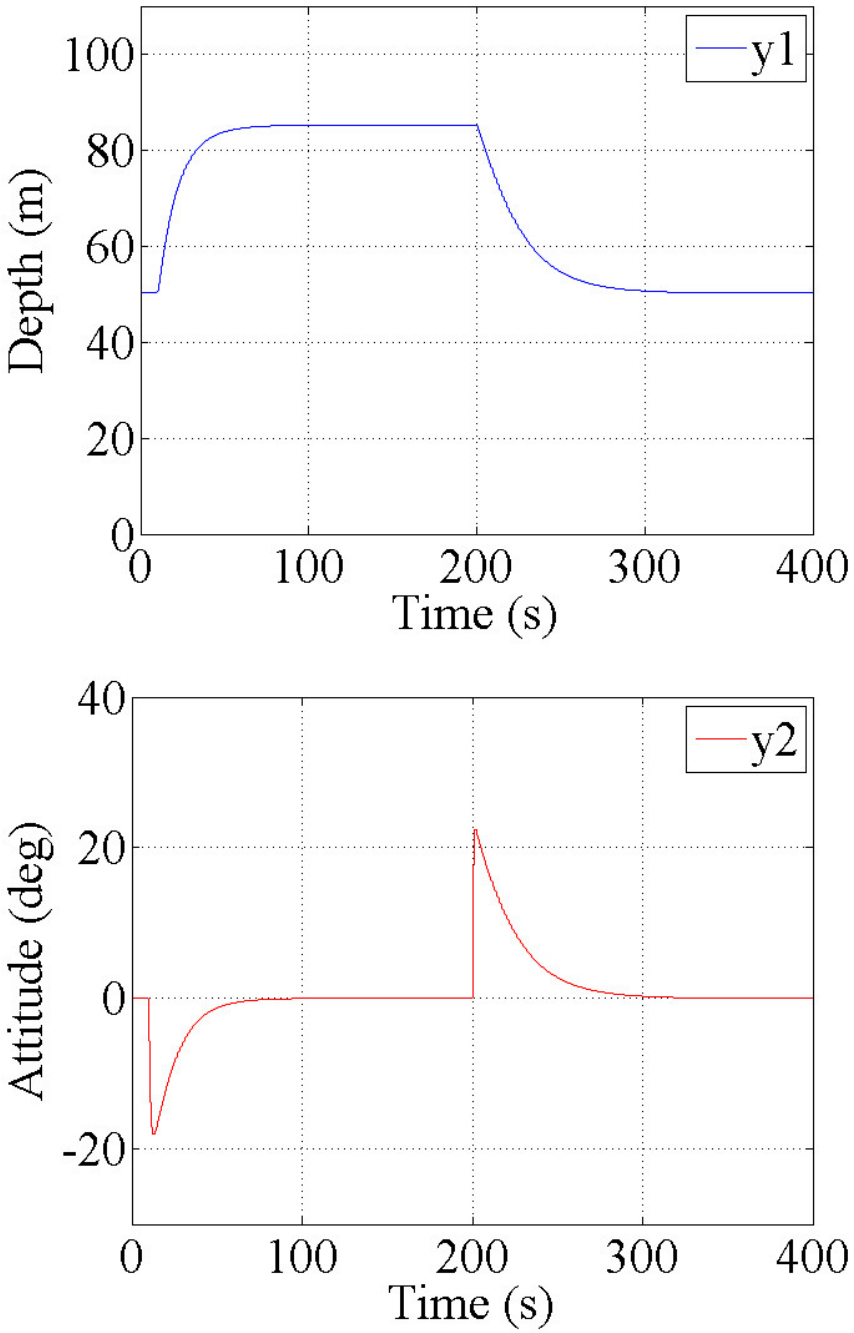

Figure 5.15. Tracking control simulation results of Pattern 1 by the state-feedback controller.

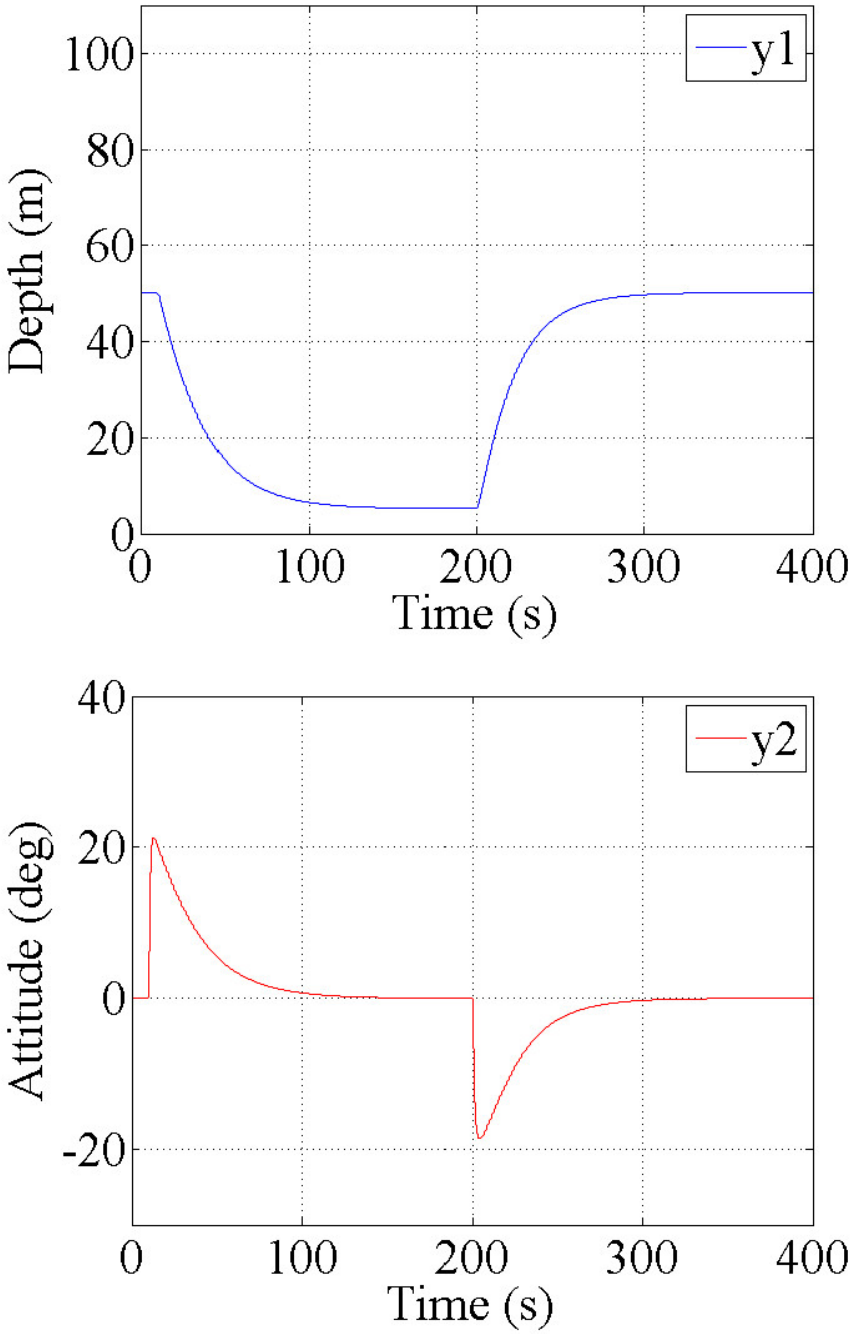

Figure 5.16. Tracking control simulation results of of Pattern 2 by the state-feedback controller.

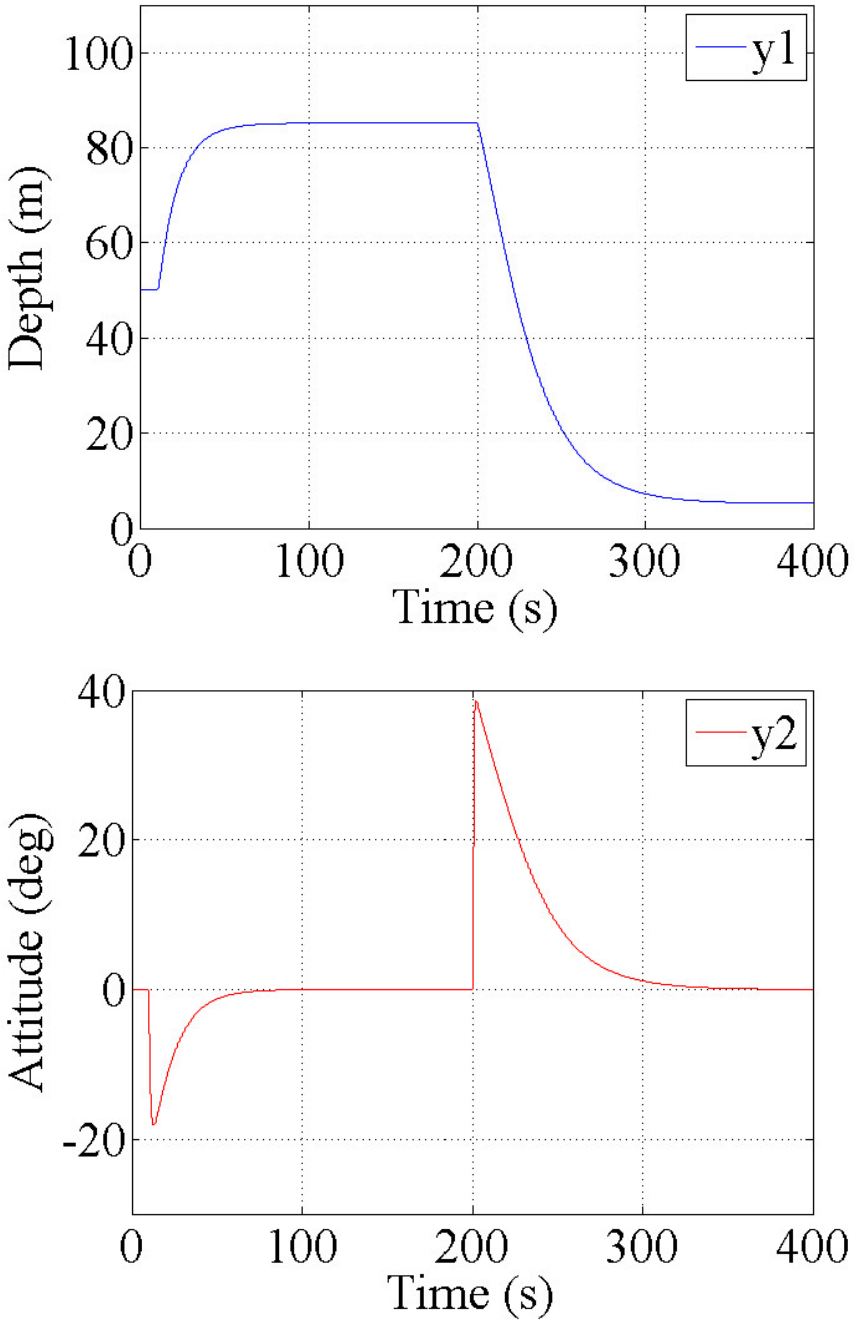

Figure 5.17. Tracking control simulation results of of Pattern 3 by the state-feedback controller.

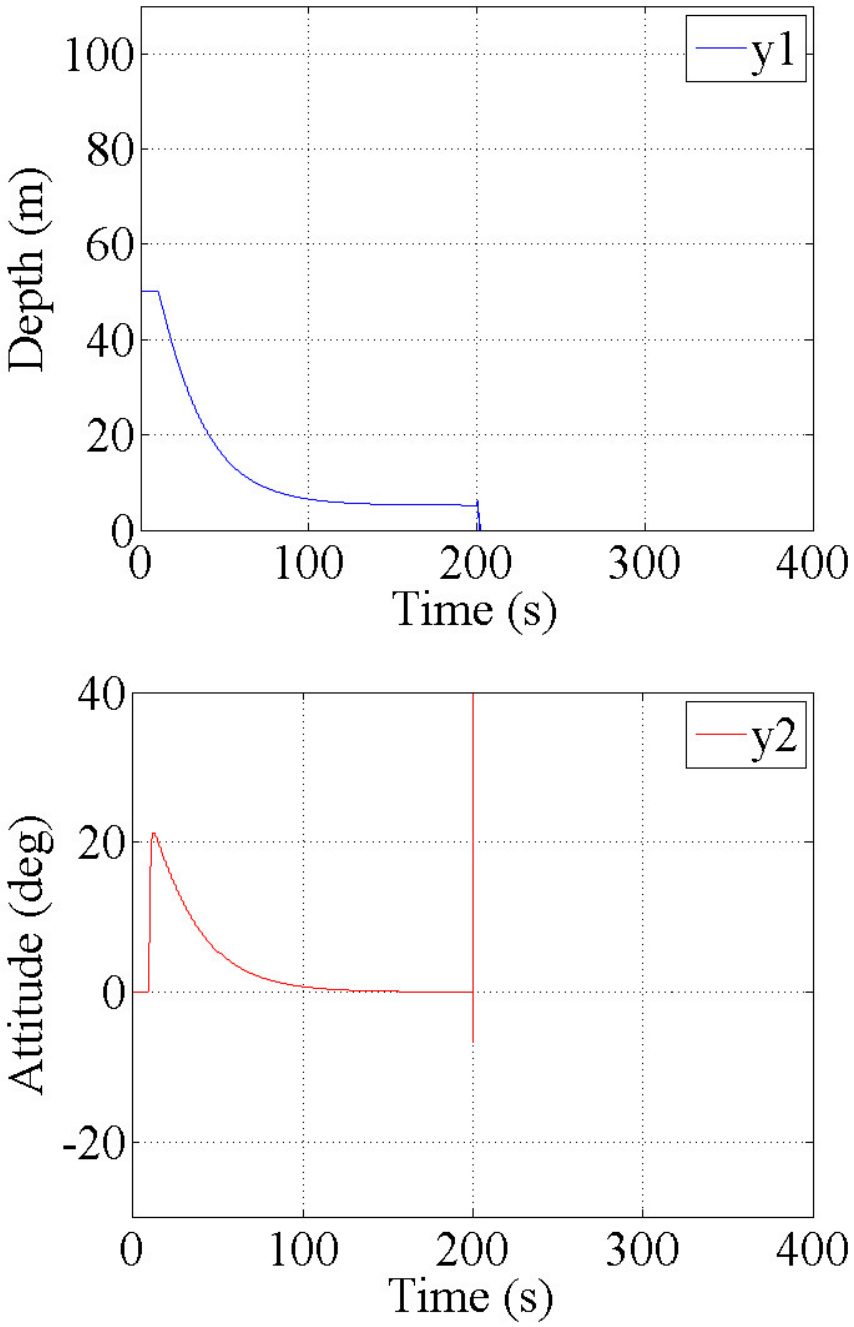

Figure 5.18. Tracking control simulation results of of Pattern 4 by the state-feedback controller.

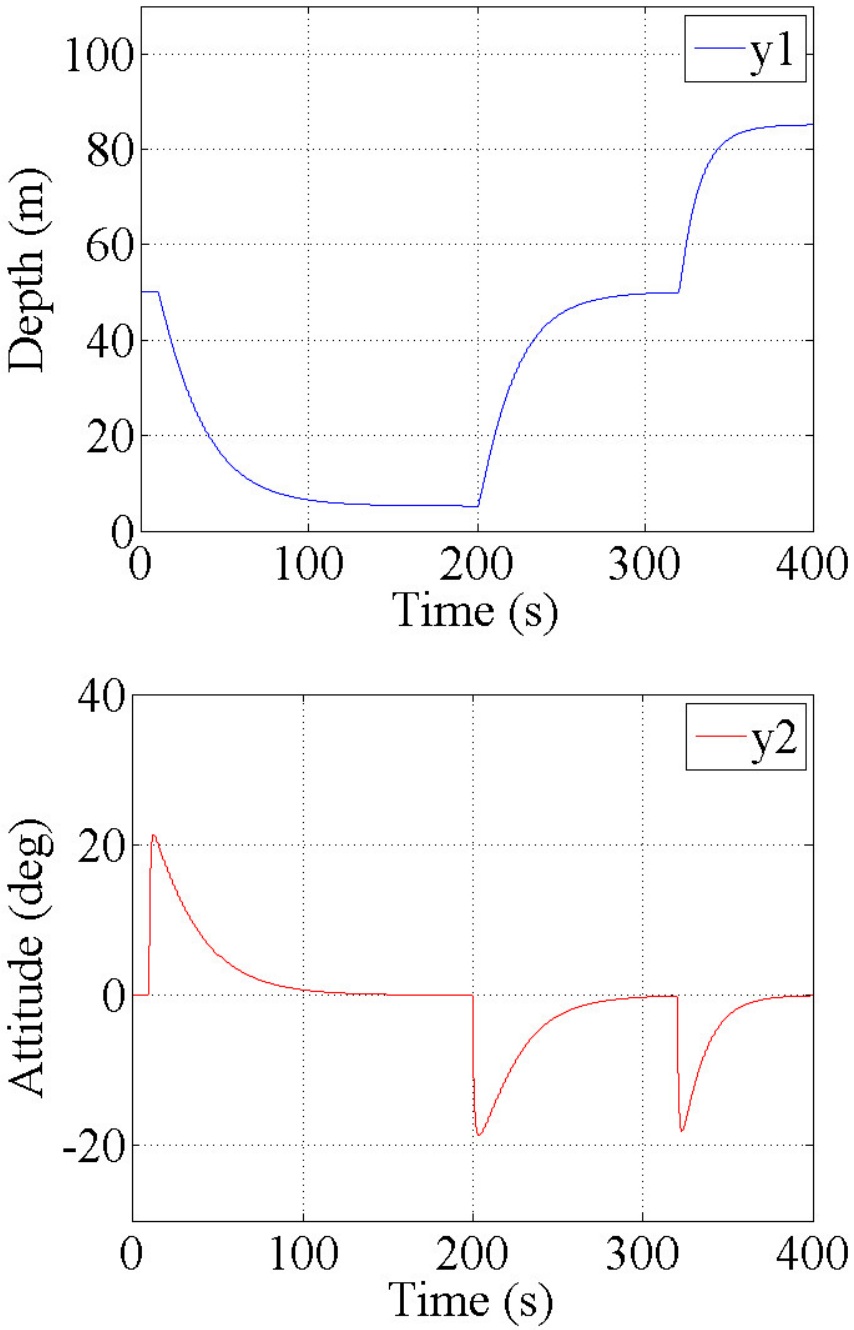

Figure 5.19. Tracking control simulation results of of Pattern 4 with by the state-feedback controller.

6 Robust Motion Control Design Using an LQI-Control-Based Approach

This chapter presents an LQI-control-based approach with the high-gain observer. Theoretically, an LQI control scheme reinforces the robustness of the control system, so that the controller can be expected to regulate not only the lowest-order system with model uncertainties but also higher-order systems. Referring to [44], [53]-[56], a linear Kalman observer-based output-feedback controller is also constructed as a representative of the conventional control system to compare the performance with the proposed approach. Note that all the specific values in this chapter are corresponding to C2.

6.1 Controller Using an LQI State-Feedback Gain

In order to apply an LQI-control-based approach, the expansion of the linear system (3.1) has to be executed by introducing a reference signal for the output as $r = y^* = [50.205, 0]^T$. $\dot{w}_e = (r - y)^T$ extends the state vector w as $w_I = [w^T, w_e^T]^T$ and the augmented system

$$\begin{aligned} \dot{w}_I &= A_I w_I + B_I v \\ A_I &= \begin{bmatrix} A & 0 \\ C & 0 \end{bmatrix} \\ B_I &= \begin{bmatrix} B \\ 0 \end{bmatrix} \end{aligned} \tag{6.1}$$

is derived. Now the LQI state-feedback gain

$$K_I = R_I^{-1} B_I^T P_I \tag{6.2}$$

can be calculated from the positive-definite solution P_I of the Riccati equation

$$A_I^T P_I + P_I A_I - P_I B_I R_I^{-1} B_I^T P_I + Q_I = 0, \tag{6.3}$$

where the weighting matrices are determined after some trial and error as

$$R_I = \begin{bmatrix} 40 & 0 \\ 0 & 1 \end{bmatrix} \tag{6.4}$$

and the identity matrix I_6 for Q_I. The resulting

$$K_I = \begin{bmatrix} -9.0275 & 0.0014 & -1.7780 & 0.0044 & 0.0561 & 0.1478 \\ 112.1885 & -6.5741 & -67.6143 & -1.0255 & -0.9349 & 0.3549 \end{bmatrix} \quad (6.5)$$

minimizes the cost function

$$J_I = \int_0^\infty (w_I^T Q_I w_I + v^T R_I v) dt \quad (6.6)$$

and thereby the control input is represented as

$$v = -K_I w_I. \quad (6.7)$$

6.2 Two-Types of Output-Feedback Controllers

6.2.1 Controller A: High-Gain Observer-Based Output-Feedback Controller

Almost the same as (3.8) in Section 3.2.2. The input

$$v = -K_I \hat{w}_I \quad (6.8)$$

is used with $\hat{w} = \hat{x} - x^* = T^{-1}(\hat{z}) - x^*$ and $\hat{w}_e$ by numerical integration of $\dot{w}_e = (r - y)^T$.

6.2.2 Controller B: Linear Kalman Observer-Based Output-Feedback Controller

For comparison with the proposed control approach, a conventional linear Kalman filter-based controller is also constructed. The Riccati equation

$$P_l A^T + A P_l - P_l C^T R_l^{-1} C P_l + Q_l = 0 \quad (6.9)$$

grounded on the linear system (3.1) is computed, where the identity matrix is applied to the weighting matrices R_l and Q_l. The solution P_l assigns the linear Kalman filter gain

$$L = P_l C^T R_l^{-1} \quad (6.10)$$

as

$$L = \begin{bmatrix} 0.0420 & -0.0232 \\ -2.0053 & 10.8427 \\ 0.0995 & -0.3566 \\ 1.8469 & 60.7922 \end{bmatrix}. \quad (6.11)$$

Eventually the linear Kalman filter

$$\dot{\hat{w}} = A\hat{w} + Bv + L(y - C\hat{w}) \tag{6.12}$$

gives $\hat{w}$, which is utilized in (6.8).

7 Simulation Results for the LQI-Control-Based Approach

This chapter presents control performance evaluation simulations on the LQI-control-based approach presented in Chapter 6. Focusing on C2, demonstrations of three types of control simulations are conducted; the first is regulation simulations with initial deviations from an equilibrium similar to the ones in Section 5.1, the second is regulation simulations with model uncertainties to evaluate the robustness, and the last is a depth tracking. In particular, the LQI-based controllers will be applied not only to the lowest-order ($n = 1$) model but also to the higher-order models. All the evaluations will compare Controller A (the high-gain observer-based controller) with Controller B (the conventional linear Kalman observer-based controller) to show the superiority of the proposed approach.

7.1 Initial Deviation

7.1.1 Settings

First, similarly to Section 5.1, the "maximum allowable initial deviation" id_{max}'s for the both controllers are investigated. In most of previous researches, the towing cable has been approximated by less than five rigid segments, and hence the higher-order models of $n = 2, 3, 5$ are constructed in this study. The procedure is almost the same as in Section 5.1 as follows.

Step1 Set the initial condition $w_n(0) = w_{n+1}(0) = id_1(0) = 0.1^\circ$, $w_i(0) = 0\,(1 \leq i \leq n-1)$ and $\dot{w}_n(0) = \dot{w}_{n+1}(0) = id_2(0) = 0.1^\circ/\mathrm{s}$, $\dot{w}_i(0) = 0\,(1 \leq i \leq n-1)$ for all the cases so that the angles of the cable segment attached to the vehicle and the attitude of the vehicle are shifted from the equilibrium. Simulate taking into account the four patterns of signs, $(\pm id_1, \pm id_2)$ and according to the results, increase (id_1, id_2) by 0.1° and $0.1^\circ/\mathrm{s}$. Repeat the procedure for the purpose of finding the maximal allowable value id_{1max} for id_1 and id_2.

Step2 Set the initial condition id_{1max} for id_1 and id_2 to proceed to the maximal allowable value for id_2. Change only id_2 in a similar manner and find the maximal allowable value id_{2max} for id_2.

Therefore, $id_{max} = (id_{1max}, id_{2max})$ represents the maximum initial deviation of the nth cable segment, the attitude of the vehicle and each angular velocity.

7.1.2 Results

Table 7.1 enumerates the resulting id_{max} and corresponding depth range from the CEP, i.e., 50.205 m, for each case. The comparison of each order of the model reveals that Controller A shows better performance than Controller B from the viewpoint of the larger region of attraction. For example, the id_{max} for controller A with $n = 1$ is (0.7 0.8) while that for controller B with $n = 1$ is (0.5, 0.5). Each corresponding depth range is $[-1.062, 1.054]$ and $[-0.758, 0.754]$, which means that Controller A can regulate the depth range about 0.3 m wider than that with Controller B. Fig. 7.1 illustrates the output of the regulation simulations with the $n = 1$ model, where the initial condition is set as $w(0) = [-0.5, 0.5, 0.5, -0.5]^T$. The top graph depicts the depth of the vehicle and the bottom depicts the attitude. Both controllers eventually regulate the system, but their transient responses are different; the peak of the overshoot with Controller A is less than a half of that with Controller B. This disparity arises from the estimation performance of each observer and Fig 7.2 shows double time scale graphs of the estimation error of x_1 for the both controllers. The top graph is for full time range and the bottom is for the first 1.5 seconds. It is seen that the estimation error for Controller A converges rapidly and this behavior alleviates the overshoot in the output. Thus the superiority of Controller A is ascertained.

However, Table 7.1 also indicates that the difference of id_{max} between the controllers decreases with respect to the order of the system. Moreover, it is opposed to the intuition that the id_{max} for higher-order cases is better than that for lower-order cases. For instance, the id_{max}'s for the both controllers are almost the same with $n = 3$, and that for Controller B with $n = 5$ is the largest value in the table. These results can be interpreted by how to set the initial condition $w(0)$. In the simulations, $w_i(0) = 0\,(1 \leq i \leq n-1)$, so that the impact of the cable segment on the total dynamics relatively reduces proportionately to the number of the point of mass. Considering the corresponding depth range in Table 7.1, the

larger id_{max} for the higher-order models places the initial condition close to the equilibrium compared to those with $n = 1$ model. Recall that Controller B is composed of the linear Kalman observer, whose performance becomes better near the equilibrium point. Fig. 7.3 compares the output of the regulation simulations with $n = 5$ model, where the initial condition is set as $w(0) = [0, 0, 0, 0, -3.1, 3.1, 0, 0, 0, 0, 3.2, 3.2]^T$. As seen from the bottom figure, the attitude of the vehicle with Controller A is slightly over $-45°$, while the attitude with Controller B barely stays within $-45°$. This may be due to the presence of the peaking phenomenon as shown in Chapter 5.1, and the corresponding depth range with $n = 5$ model for the both controllers are substantially identical. Consequently, the results in Table 7.1 are ensuring that Controller A has a larger or at least as large region of attraction as Controller B.

Table 7.1. $id_{max} = (id_{1max}, id_{2max})$ and corresponding depth range from CEP with LQI controller for C2

Controller A	id_{max}	Corresponding depth range (m)
$n = 1$	(0.7, 0.8)	$[-1.062, 1.054]$
$n = 2$	(1.5, 1.6)	$[-1.142, 1.125]$
$n = 3$	(2.1, 2.2)	$[-1.069, 1.046]$
$n = 5$	(3.1, 3.1)	$[-0.952, 0.922]$
Controller B	id_{max}	Corresponding depth range (m)
$n = 1$	(0.5, 0.5)	$[-0.758, 0.754]$
$n = 2$	(1.3, 1.4)	$[-0.989, 0.976]$
$n = 3$	(2.0, 2.1)	$[-1.018, 0.997]$
$n = 5$	(3.1, 3.2)	$[-0.952, 0.922]$

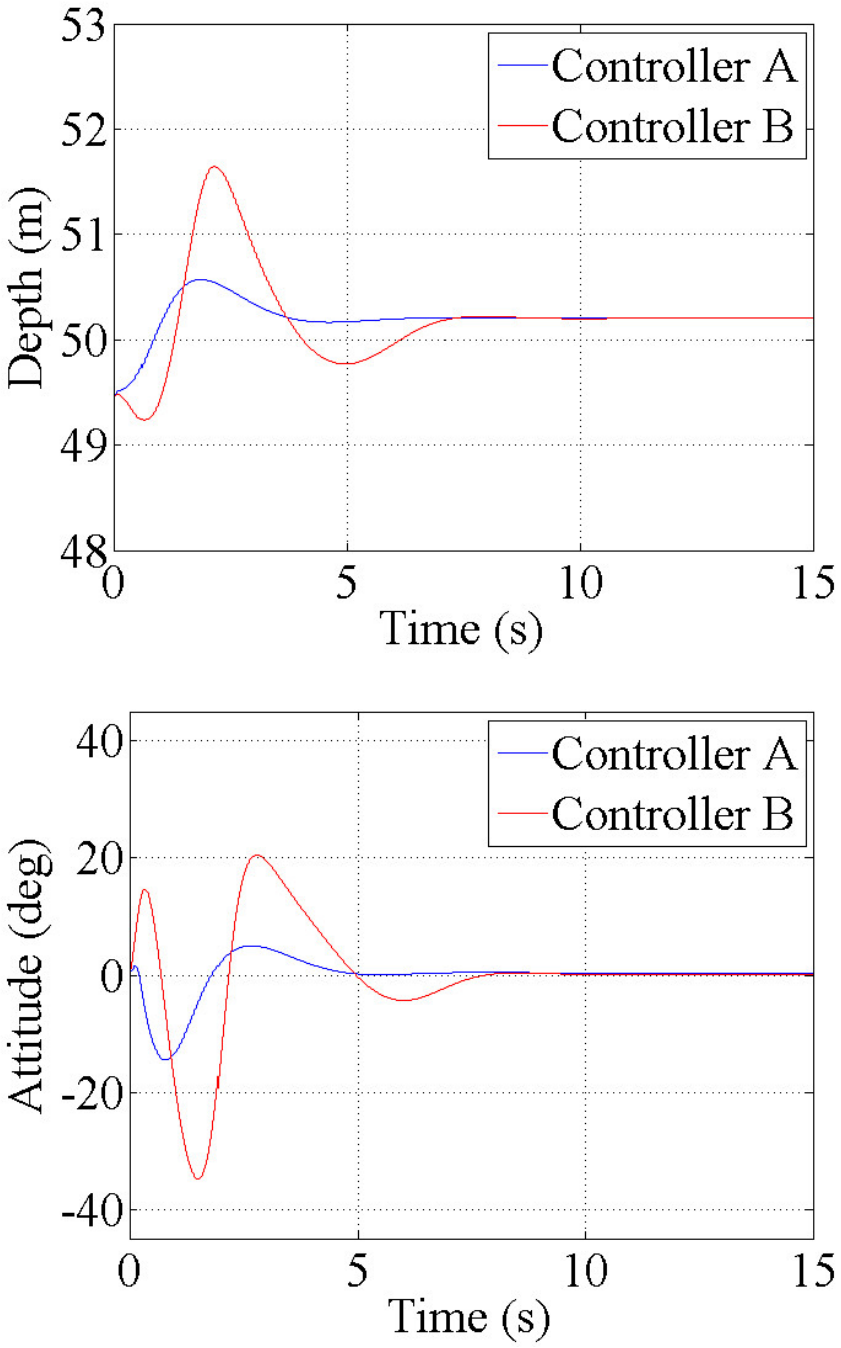

Figure 7.1. Simulation results of depth and attitude regulation with $n = 1$ model and $w(0) = [-0.5, 0.5, 0.5, -0.5]^T$.

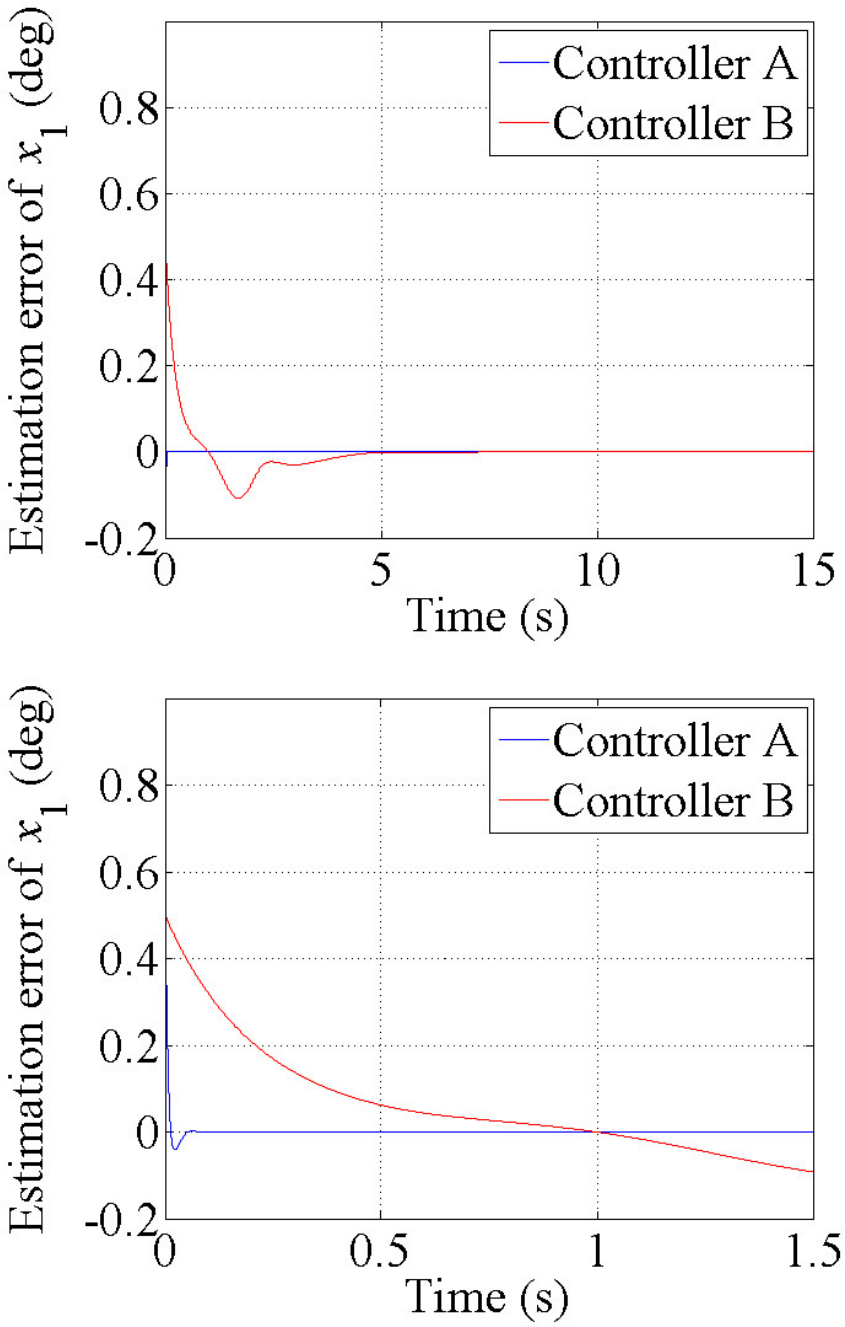

Figure 7.2. Estimation errors of x_1 model with $n = 1$ and $w(0) = [-0.5, 0.5, 0.5, 0.5]^T$; *top* full time range, *bottom* in the first 1.5 seconds.

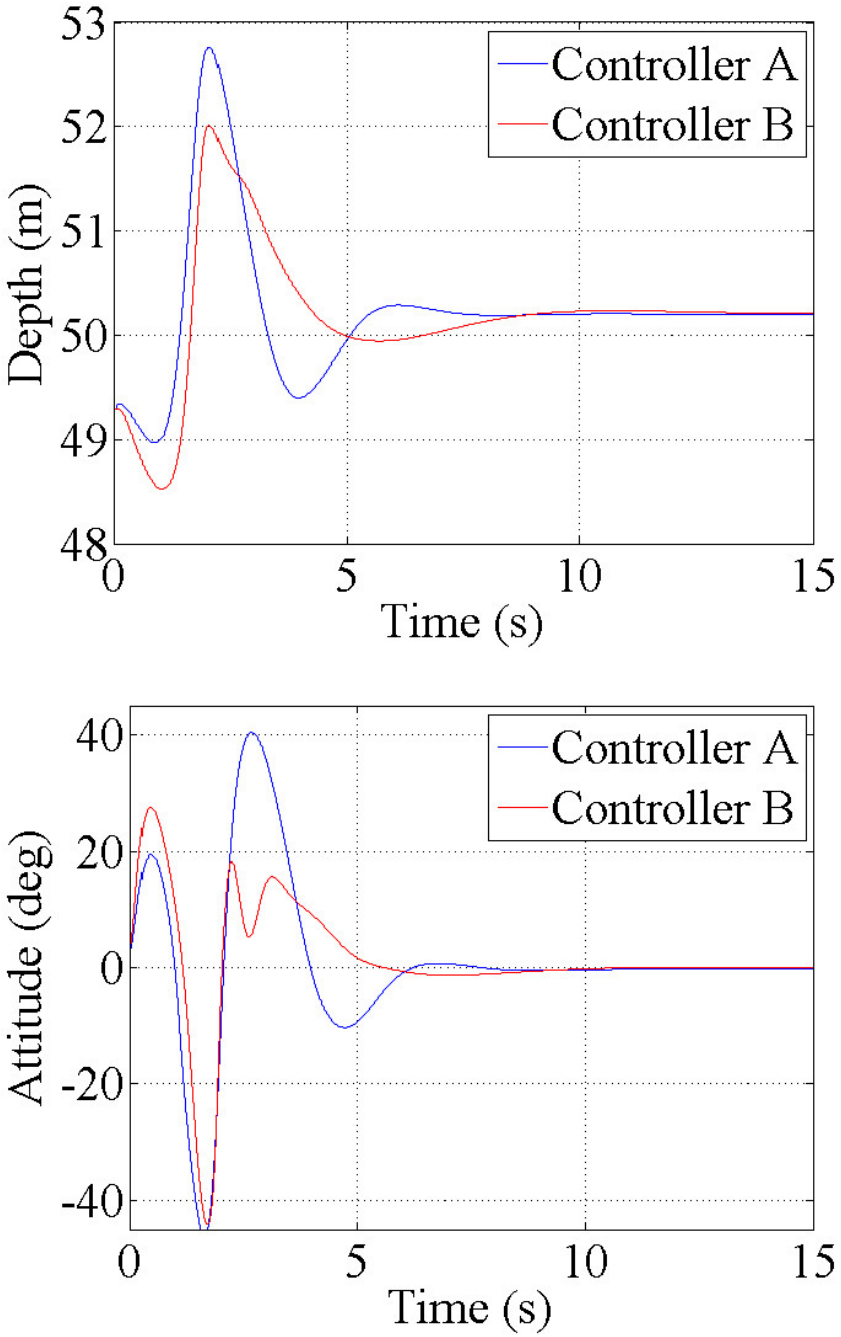

Figure 7.3. Simulation results of depth and attitude regulation with $n = 5$ model and $w(0) = [0, 0, 0, 0, -3.1, 3.1, 0, 0, 0, 0, 3.2, 3.2]^T$.

7.2 Robustness

7.2.1 Settings

Next simulations evaluate robustness of each controller. The both controllers have been already applied to higher-order models, but the previous section has not considered model uncertainties, which have to be taken into account for practical purposes. Therefore, whether the controllers can retain the equilibrium point in the existence of several kinds of model uncertainties or not is evaluated. In order to admit parametric variations, three kinds of perturbations are dealt as in the following;

1. the towing speed v_0 is altered by two patterns as shown in Fig. 7.4, where v_0 gets slow from 4 m/s to 2 m/s (a) and becomes faster from 4 m/s to 6 m/s (b);

2. all the hydrodynamic parameters are perturbed $\pm 20\%$ from their nominal values; and

3. the payload of the vehicle is set to be $+50\%$ from the nominal value.

The towing speed change begins at $t = 20$ s and is terminated at $t = 30$ s. Combining these uncertainty conditions, regulation simulations have been carried out. Table 7.2 summarizes the settings of the conditions for each simulation, where the "hydrodynamic parameters" is abbreviated as "HD". Note that the initial condition $w(0)$ is set at the equilibrium for all the simulations to make the comparison fair.

7.2.2 Results

Figs. 7.5-7.8 and 7.10-7.17 show the time series data of the output. According to the simulation results, Controller A generally demonstrates desirable performances compared to Controller B. To begin with, Figs. 7.5, 7.6, 7.7 and 7.8 are the results with $n = 1$ model for both controllers. It can be seen that the results with Controller B indicate larger overshoot than that with Controller A and chattering-like oscillation in the transient response, particularly in the case with -20% hydrodynamic parameters, i.e., Figs. 7.6 and 7.8. These differences are due to the estimation performance of each controller and Fig. 7.9 presents the estimation

errors of x_1 for the simulation depicted in Fig. 7.6, where the estimation error for Controller A is almost stable even after the towing speed change. By contrast, the estimation error for Controller B fluctuates and does not converge to 0 completely. This can be interpreted from the dynamics of the linear Kalman filter (6.12); the eigenvalues of $(A - LC)$, $\lambda = \{-3.5808, -5.8810+5.2966i, -5.8810-5.2966i, -15.6805\}$, include the stable but oscillatory modes in λ_2 and λ_3. While the convergence of the estimation error of the high-gain observer can be ascertained by the eigenvalues of Hurwitz A_e in (4.3), where $\lambda = \{-70.0000+71.4143i, -70.0000-71.4143i, -70.0000 + 71.4143i, -70.0000 - 71.4143i\}$ with $\epsilon = 0.01$. All the modes are oscillatory and stable, however, the pole is assigned in far left-half plane compared to $(A-LC)$ and hence the estimation error of the high-gain observer converges to 0 smoothly and quickly.

Moreover, the above argument is more conspicuous in the case of higher-order systems. Figs. 7.10, 7.11, 7.12 and 7.13 are the results corresponding to Controller A with $n = 2, 3, 5$ models. For each order case, Controller A can maintain the system at the target depth and attitude with slight deflections in the transient state. By contrast, Figs. 7.14, 7.15, 7.16 and 7.17 are the results corresponding to Controller B with the same conditions, where not all the simulations are successful. Figs. 7.15 and 7.17 reveal that in the highest-order $n = 5$ case with -20% hydrodynamic parameters the control error does not converge, and even in the $n = 3$ case with towing pattern (a) the controller fails to keep their depth and attitude in Fig. 7.15.

Hence, it can be concluded that the linearized system-based observer (Controller B) is not robust to a sufficient degree to model variations and the estimate by the high-gain observer (Controller A) yields desirable control performance under the model uncertainties. This is due to the structural robustness of the high-gain observer itself and thus the robust performance of the whole proposed controller is enhanced.

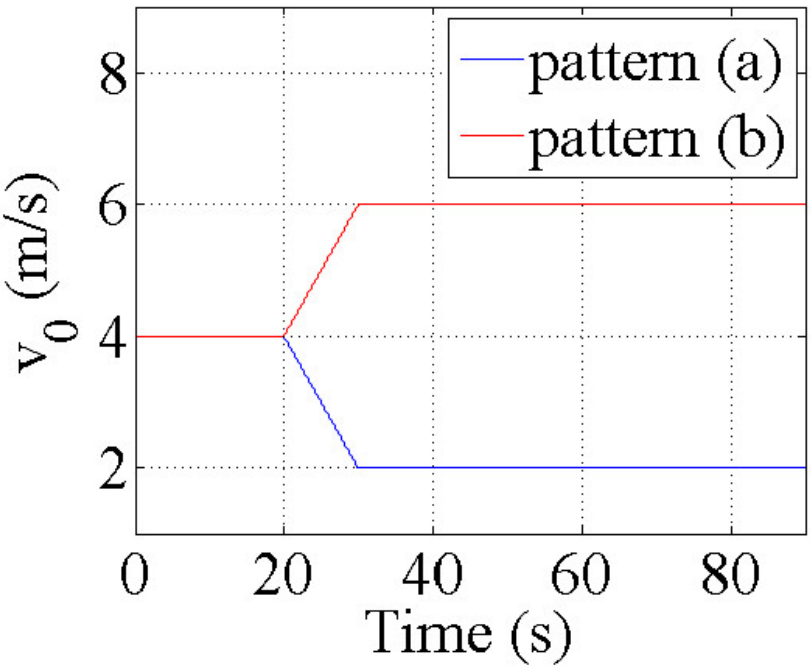

Figure 7.4. Patterns of towing speed change in robust control simulations.

Table 7.2. Settings of each robust control simulation

Figure	7.5	7.6	7.7	7.8
Controller	A and B	A and B	A and B	A and B
n	1	1	1	1
Towing pattern	(a)	(a)	(b)	(b)
HD	+20%	−20%	+20%	−20%
Figure	7.10	7.11	7.12	7.13
Controller	A	A	A	A
n	2, 3, 5	2, 3, 5	2, 3, 5	2, 3, 5
Towing pattern	(a)	(a)	(b)	(b)
HD	+20%	−20%	+20%	−20%
Figure	7.14	7.15	7.16	7.17
Controller	B	B	B	B
n	2, 3, 5	2, 3, 5	2, 3, 5	2, 3, 5
Towing pattern	(a)	(a)	(b)	(b)
HD	+20%	−20%	+20%	−20%

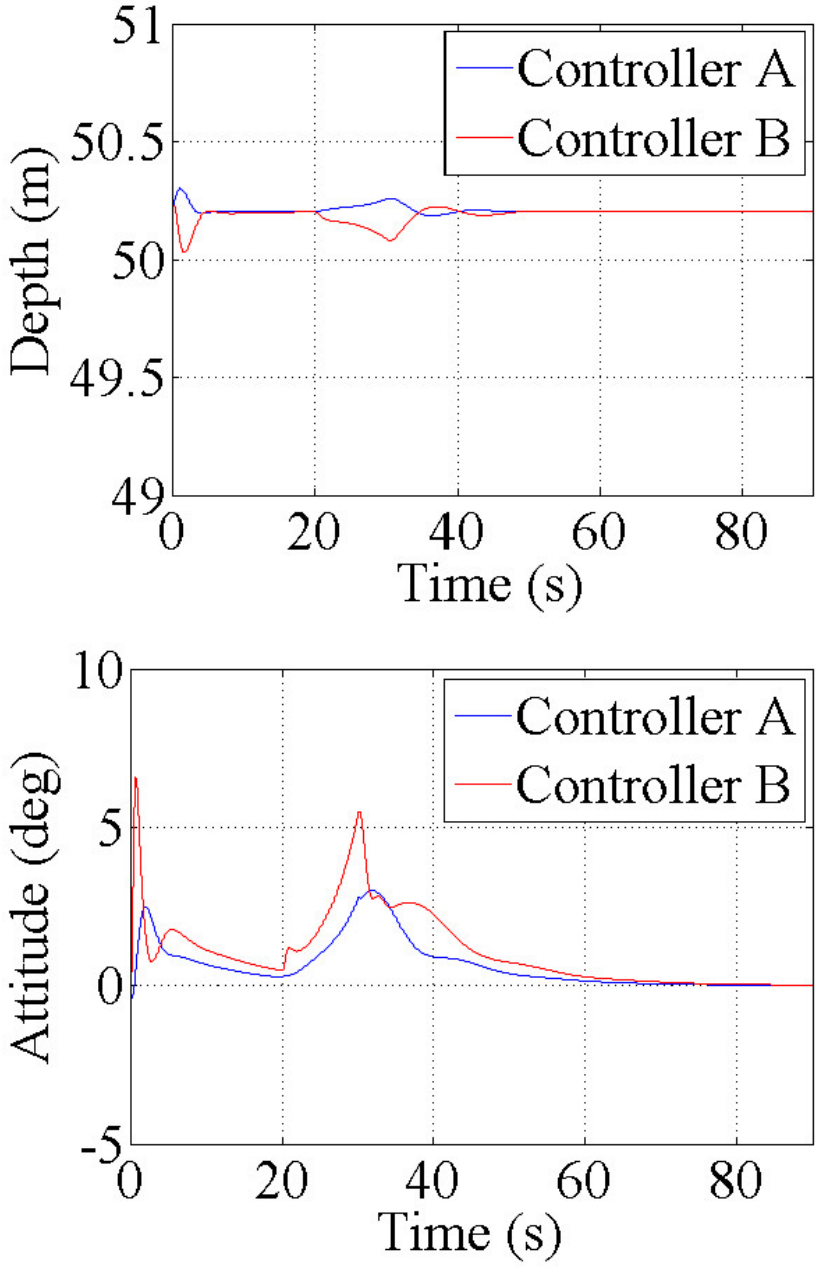

Figure 7.5. Simulation results of robust control performance by both controllers for the lowest-order system with towing pattern (a) and +20% hydrodynamic parameters.

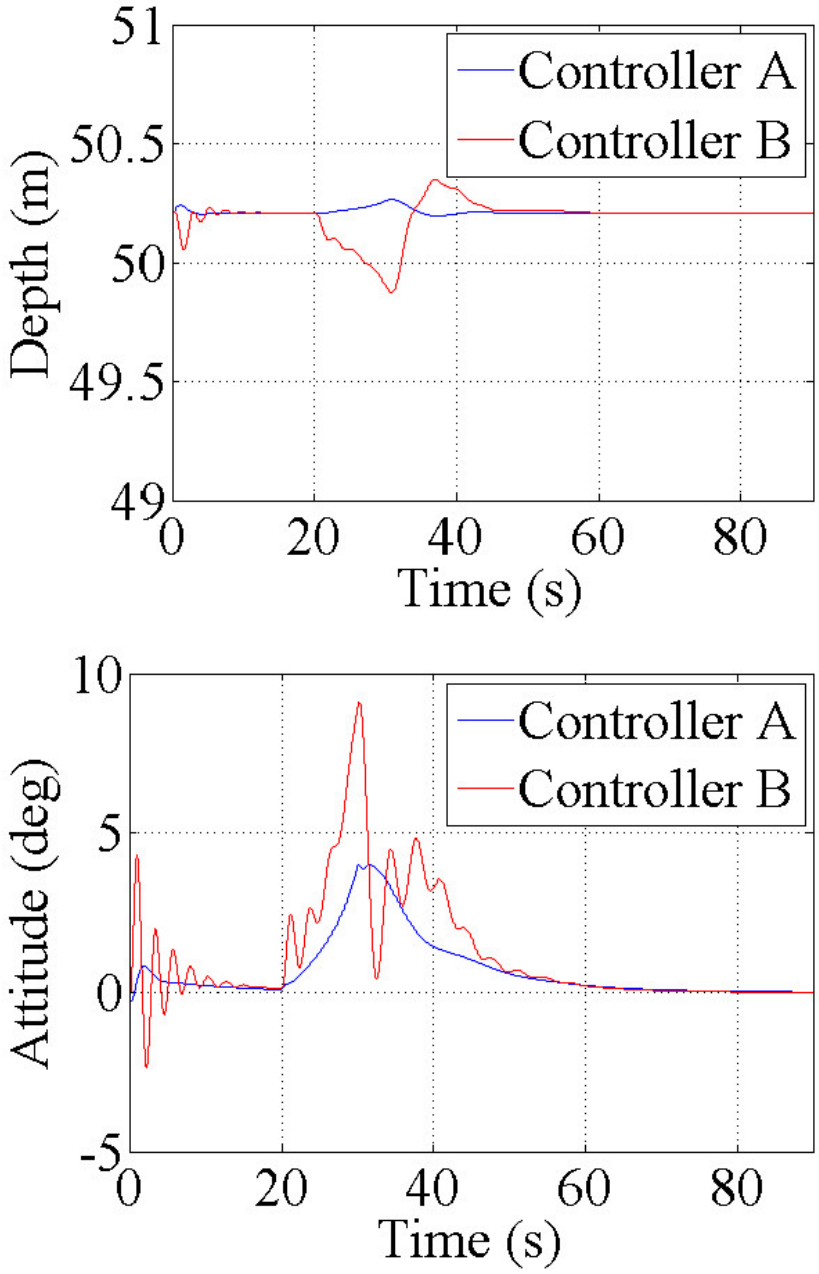

Figure 7.6. Simulation results of robust control performance by both controllers for the lowest-order system with towing pattern (a) and -20% hydrodynamic parameters.

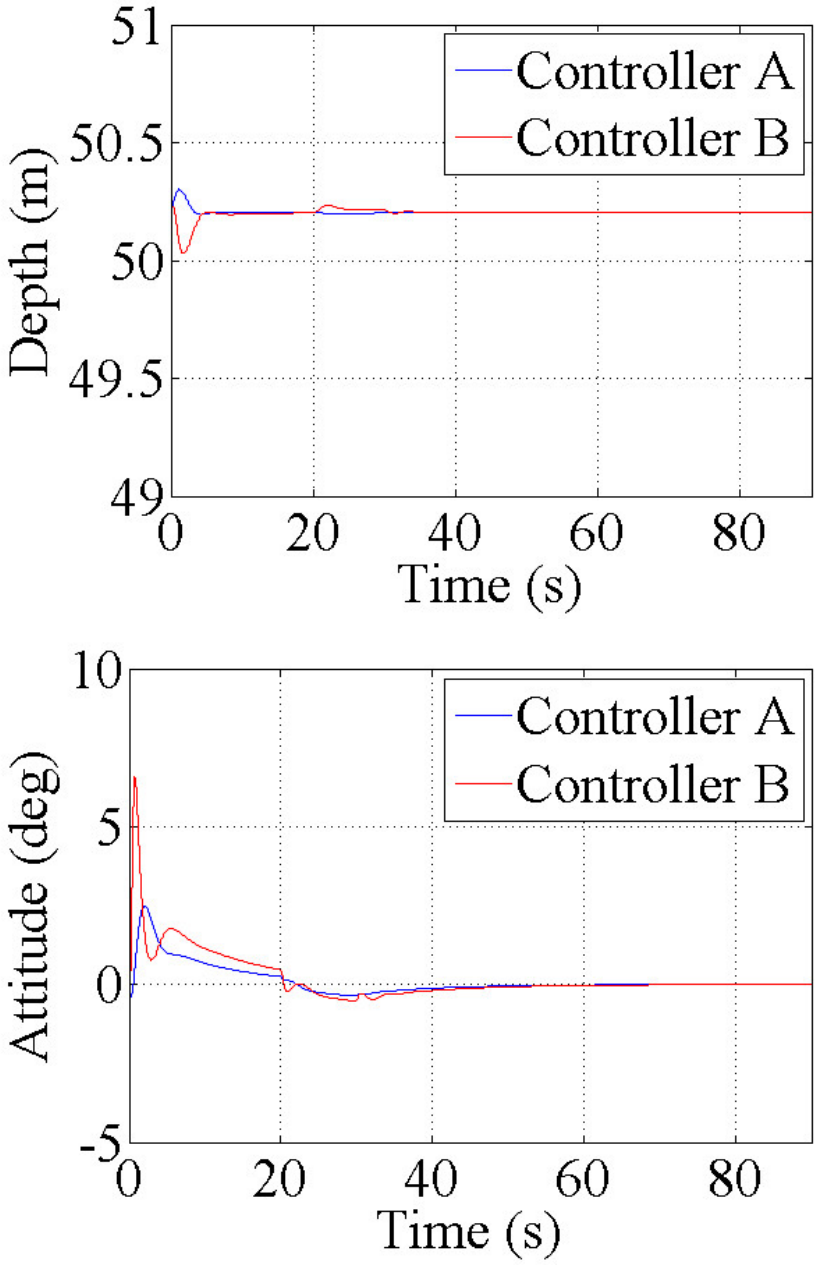

Figure 7.7. Simulation results of robust control performance by both controllers for the lowest-order system with towing pattern (b) and +20% hydrodynamic parameters.

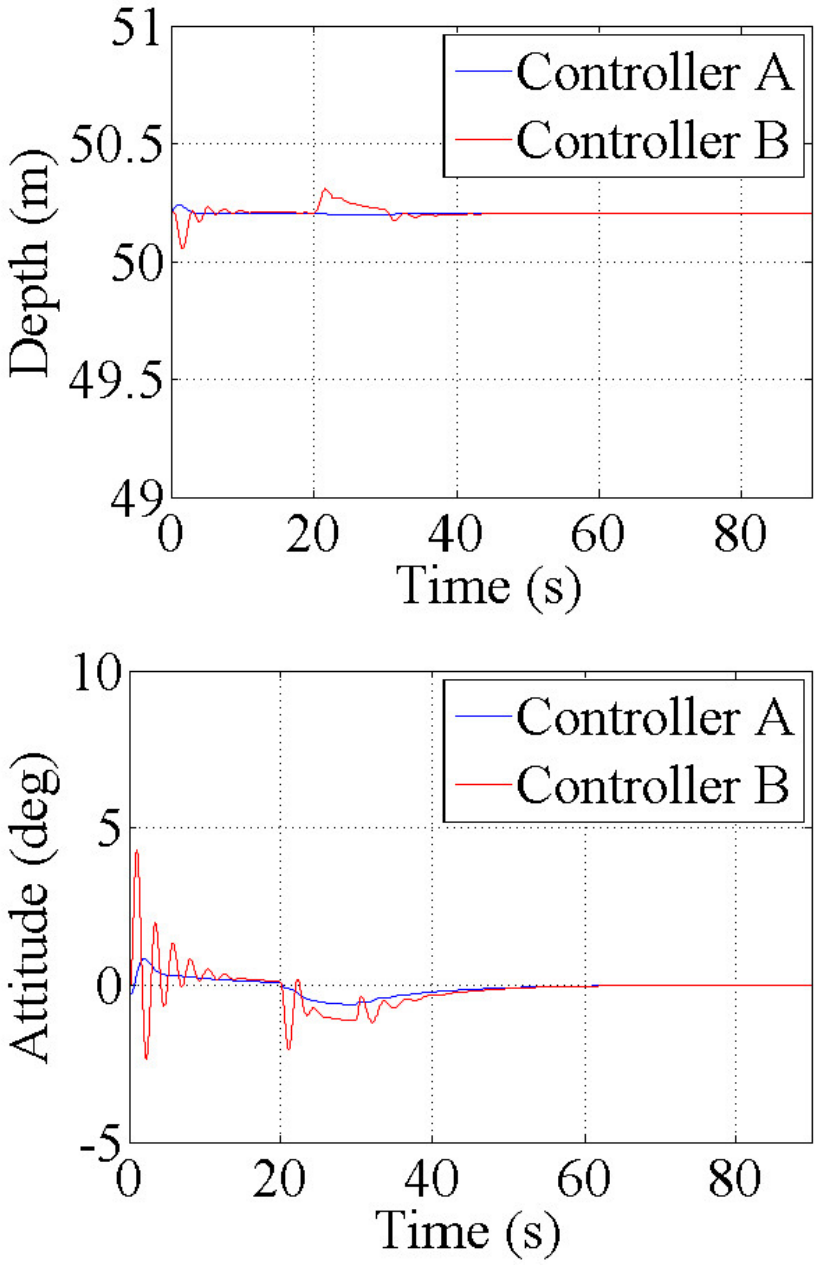

Figure 7.8. Simulation results of robust control performance by both controllers for the lowest-order system with towing pattern (b) and -20% hydrodynamic parameters.

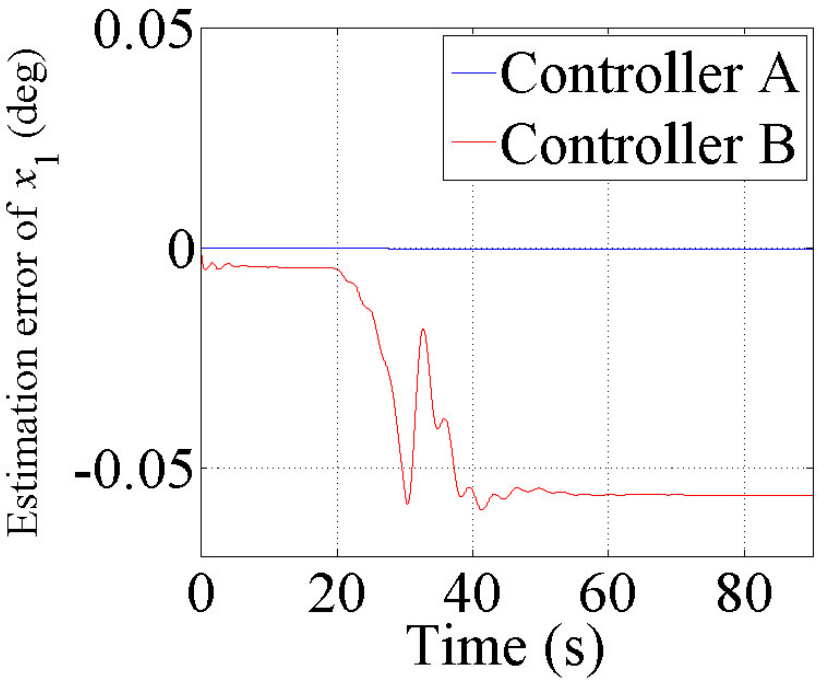

Figure 7.9. Estimation errors of x_1 for the lowest-order system with towing pattern (a) and -20% hydrodynamic parameters.

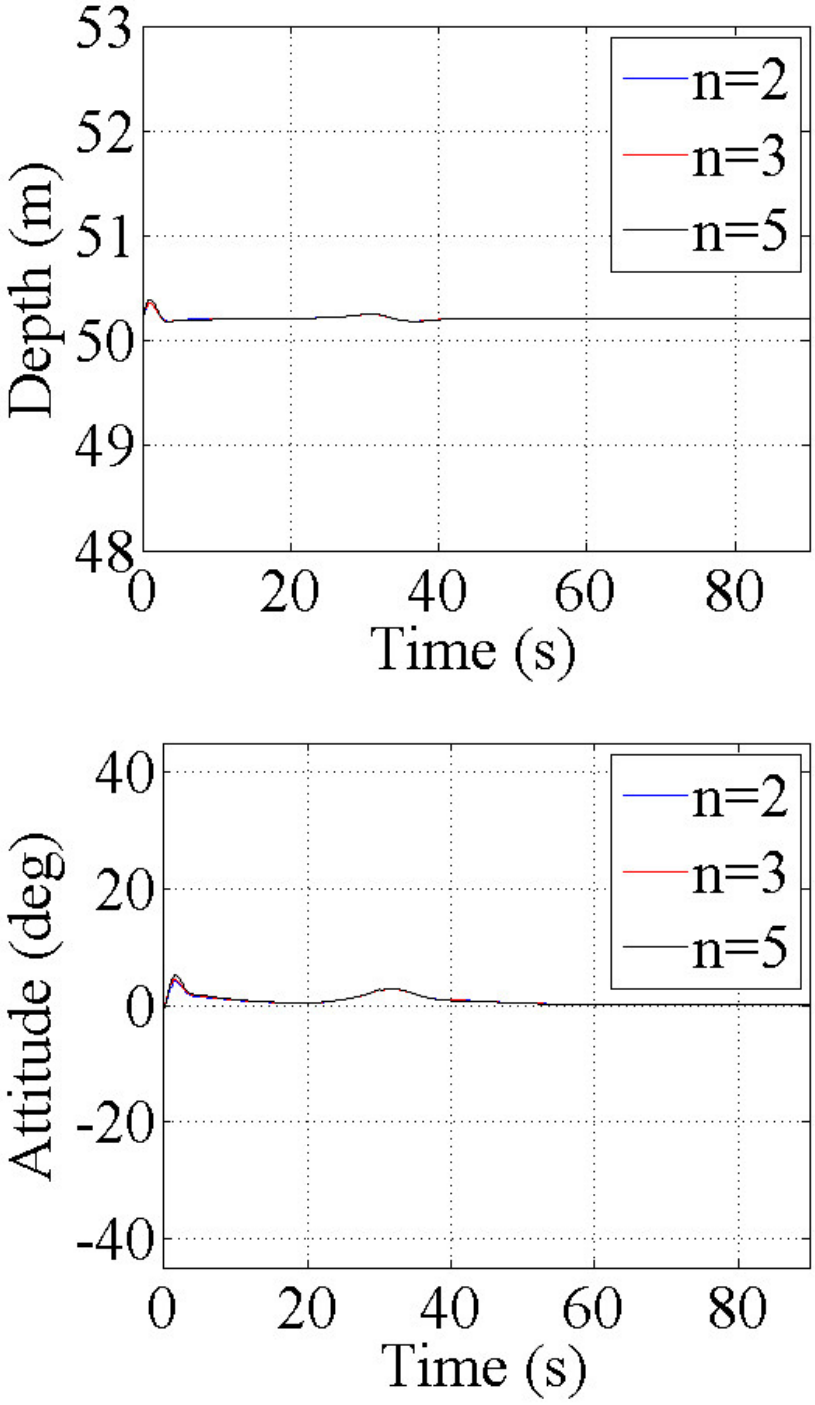

Figure 7.10. Simulation results of robust control performance by Controller A for higher-order systems with towing pattern (a) and +20% hydrodynamic parameters.

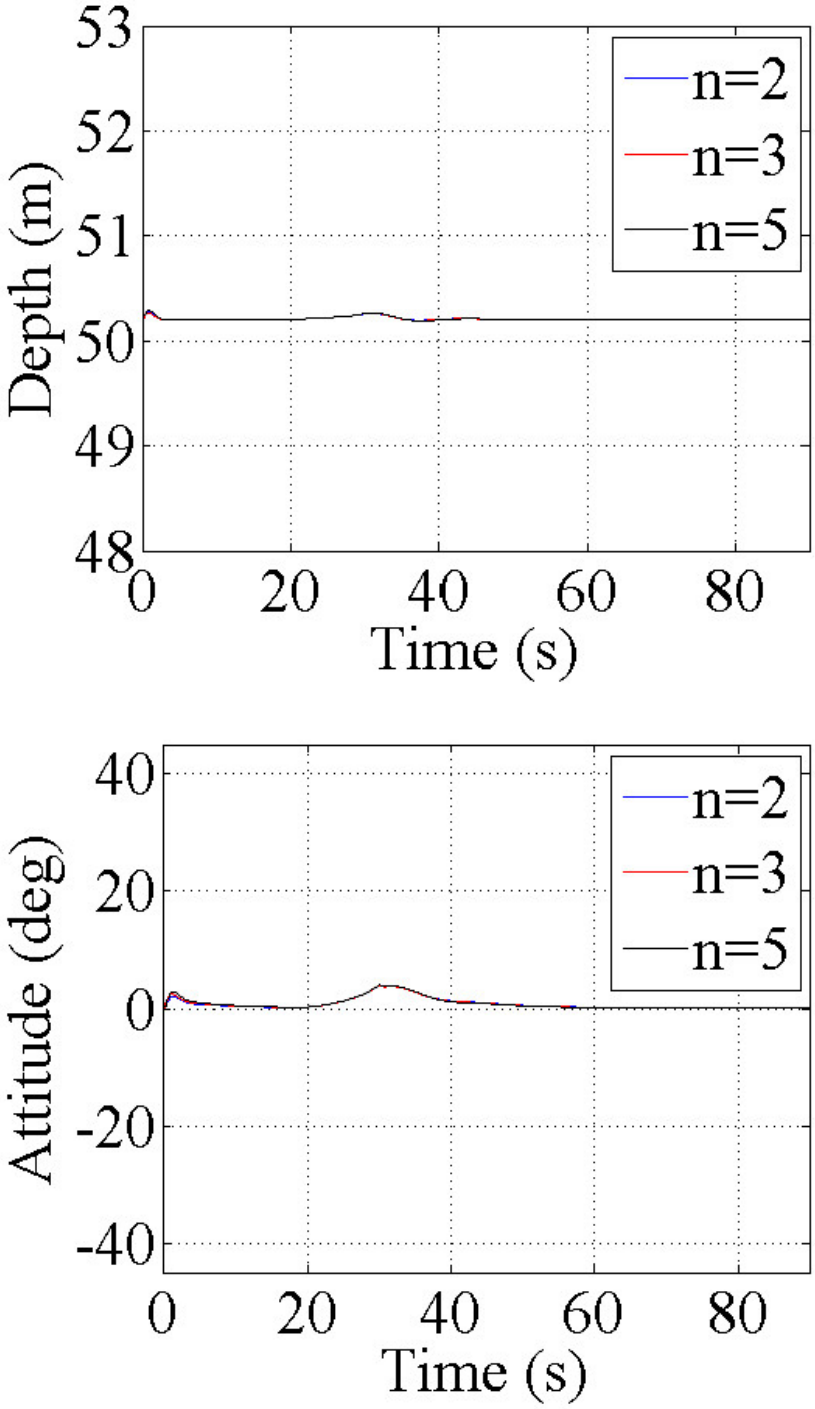

Figure 7.11. Simulation results of robust control performance by Controller A for higher-order systems with towing pattern (a) and −20% hydrodynamic parameters.

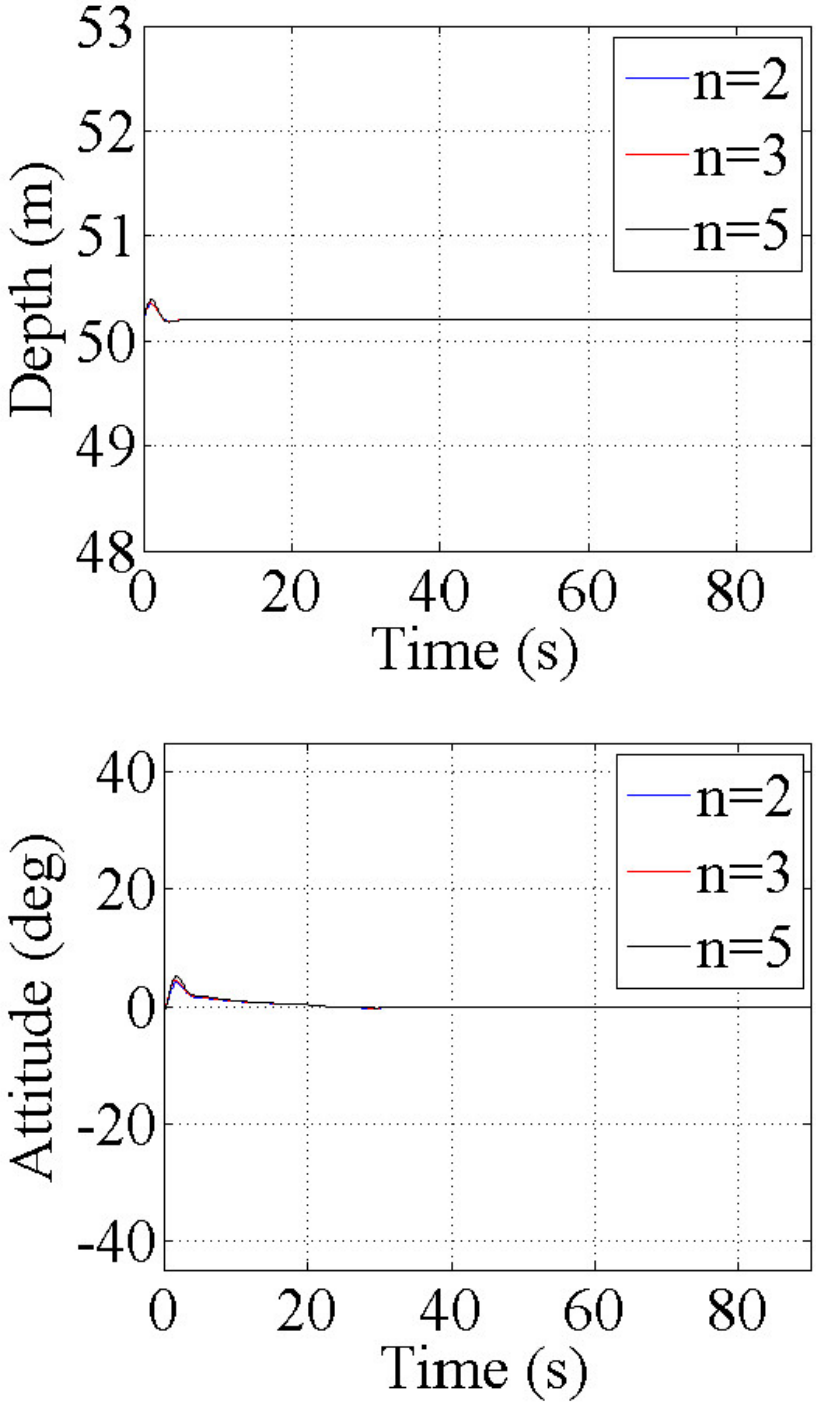

Figure 7.12. Simulation results of robust control performance by Controller A for higher-order systems with towing pattern (b) and +20% hydrodynamic parameters.

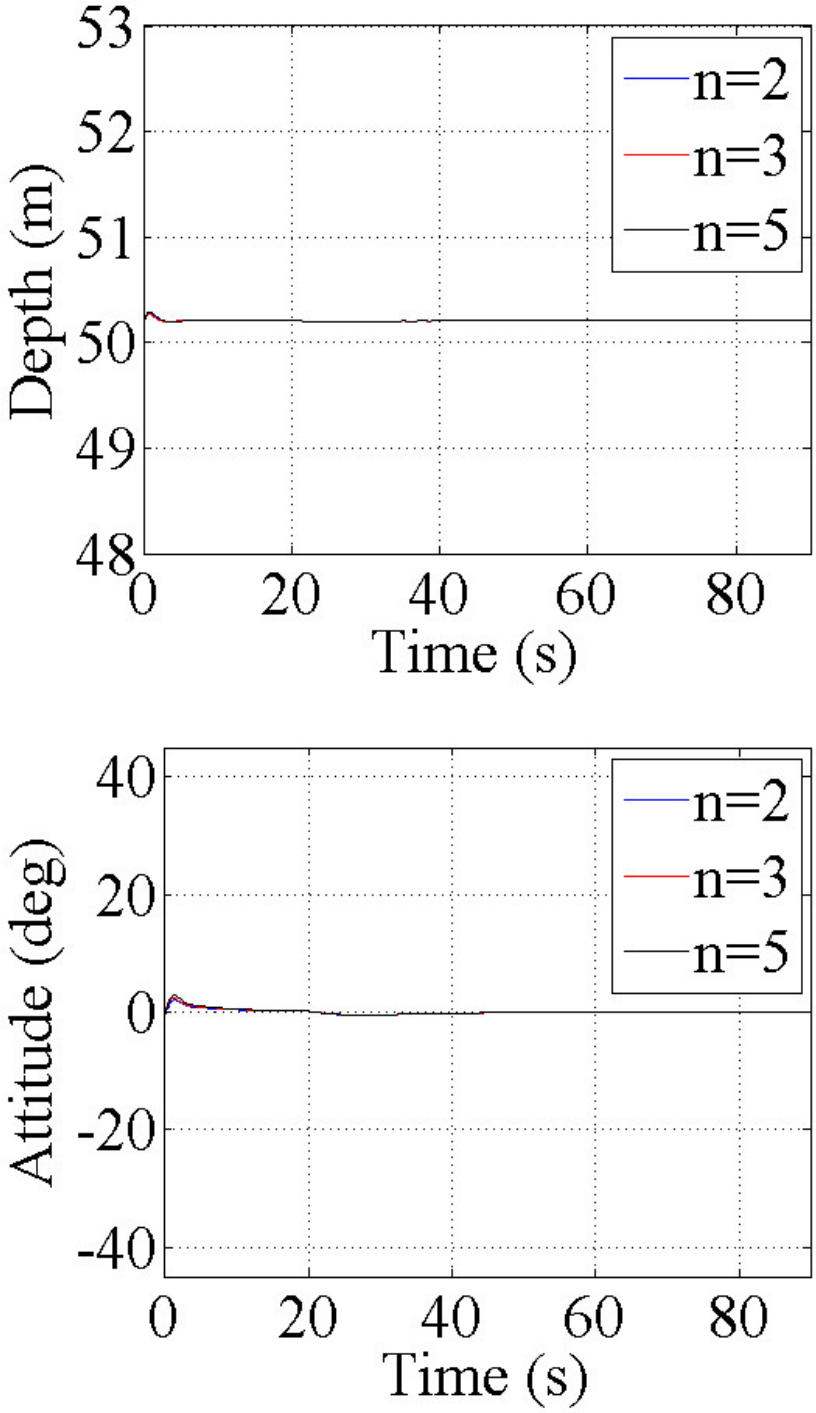

Figure 7.13. Simulation results of robust control performance by Controller A for higher-order systems with towing pattern (b) and +20% hydrodynamic parameters.

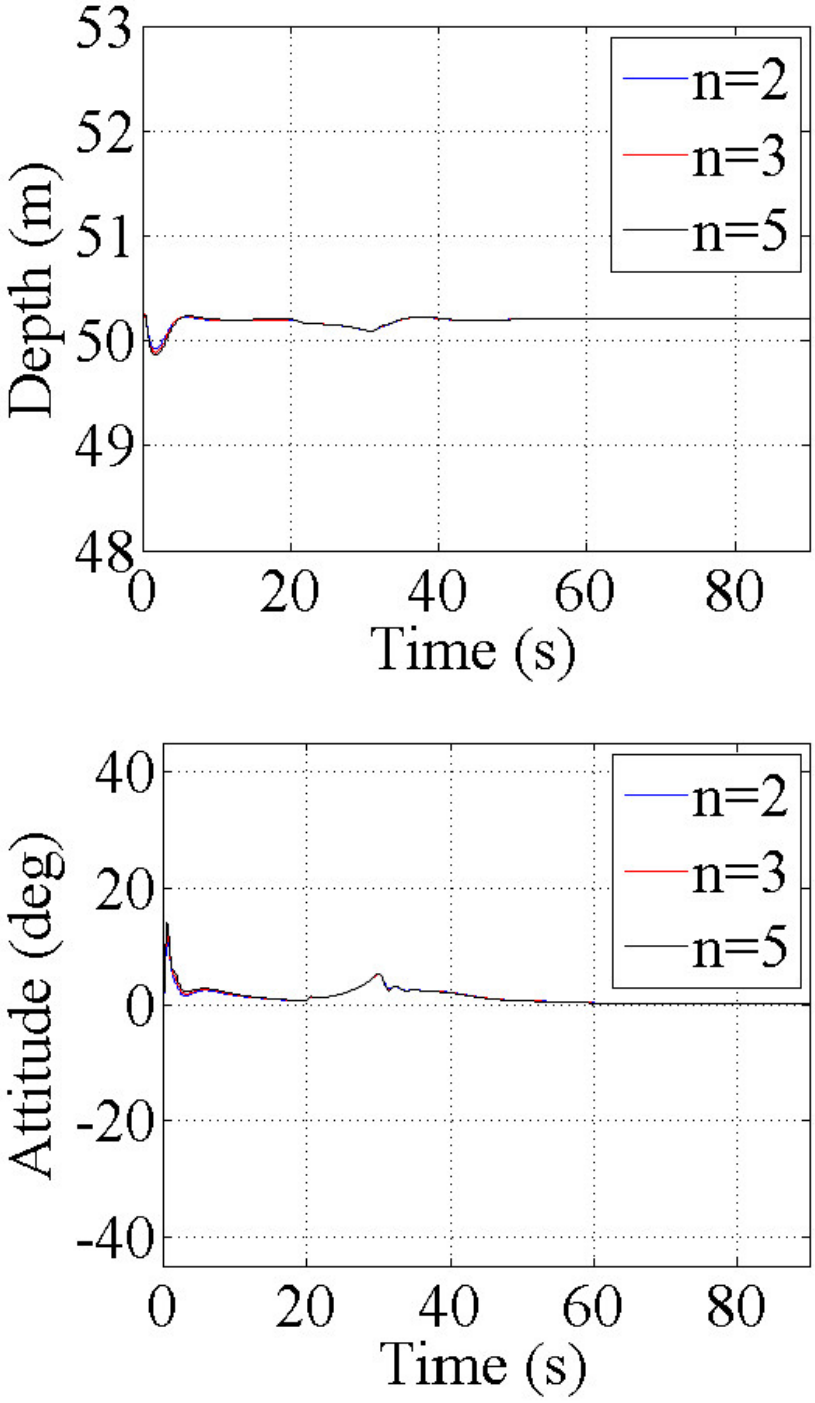

Figure 7.14. Simulation results of robust control performance by Controller B for higher-order systems with towing pattern (a) and +20% hydrodynamic parameters.

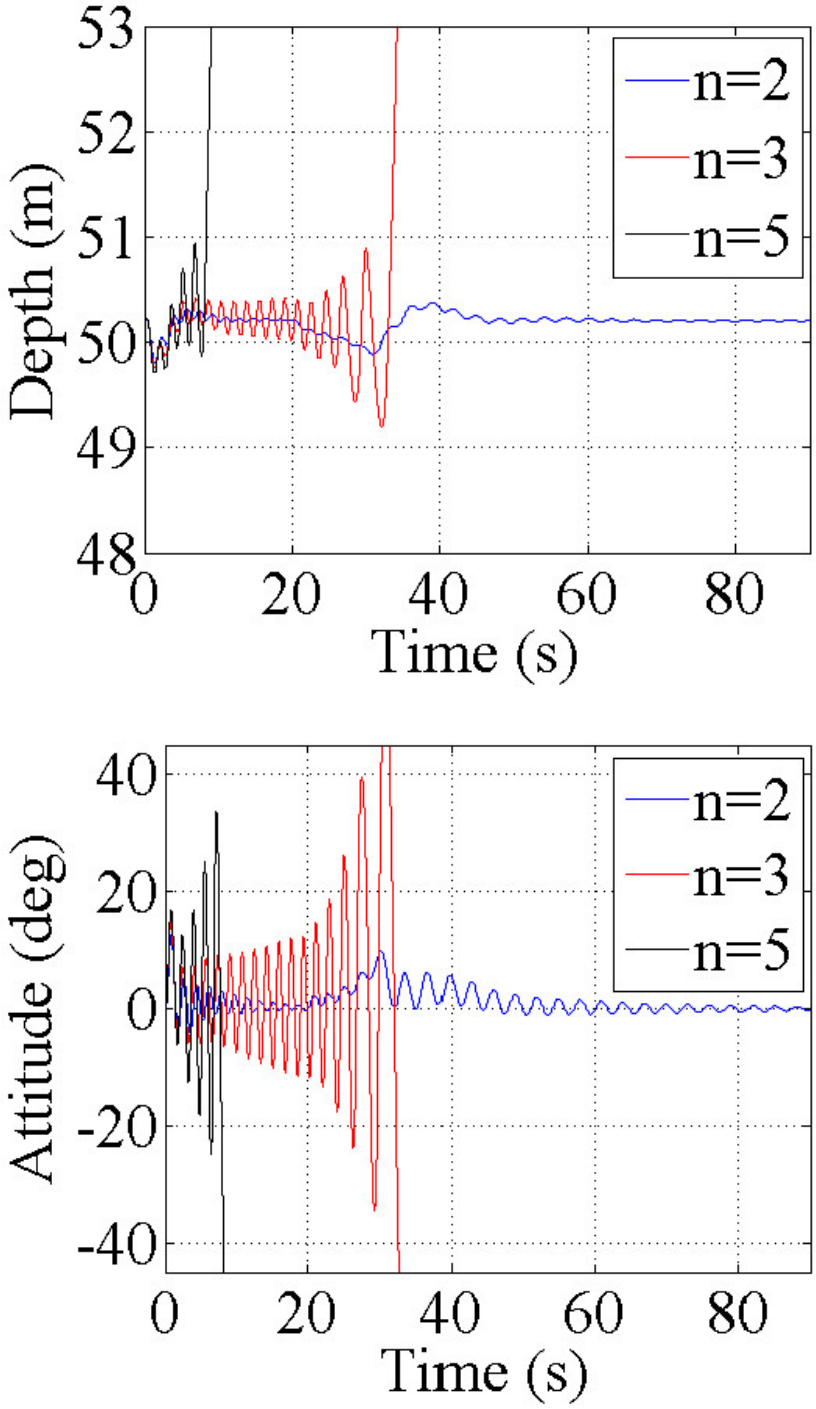

Figure 7.15. Simulation results of robust control performance by Controller B for higher-order systems with towing pattern (a) and −20% hydrodynamic parameters.

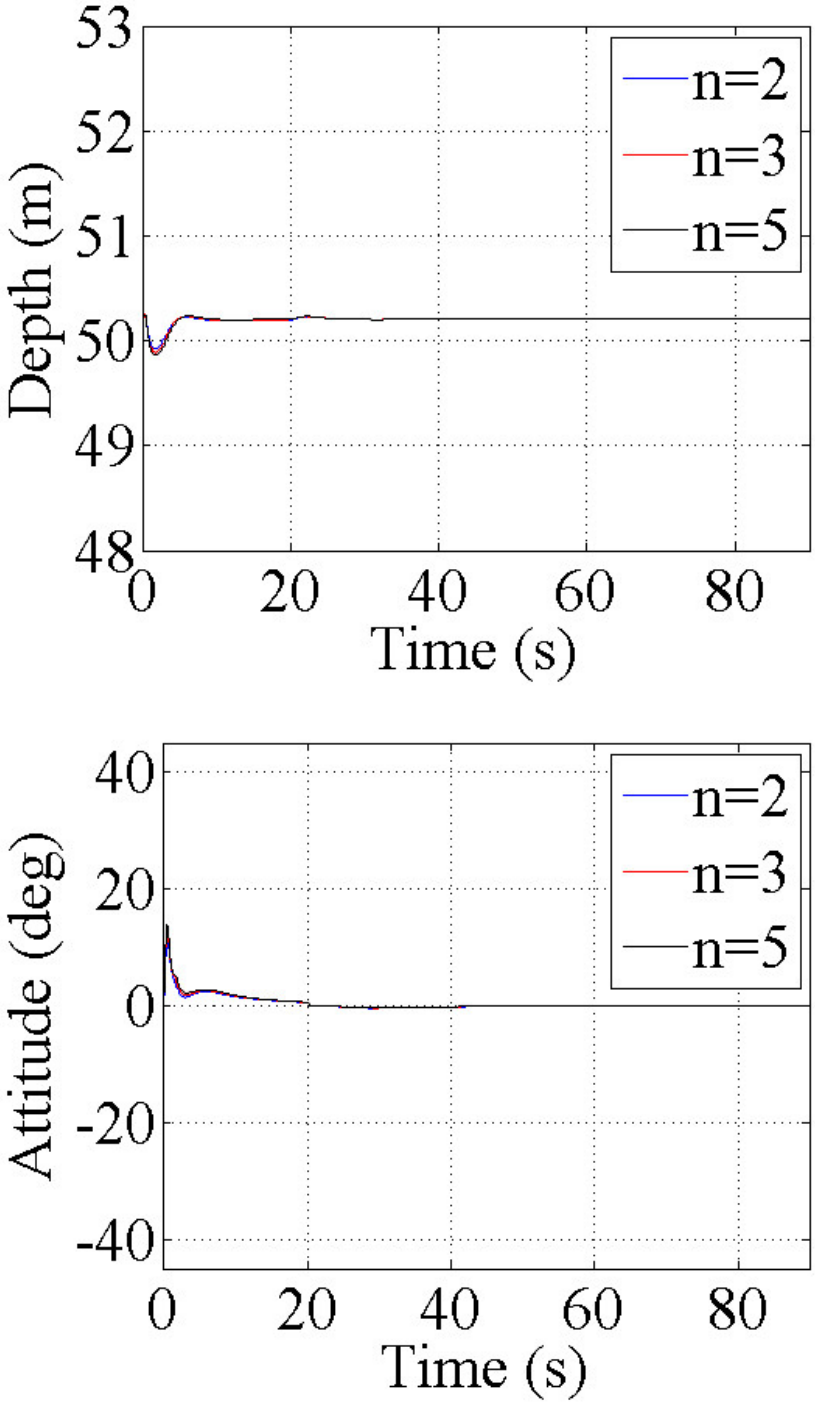

Figure 7.16. Simulation results of robust control performance by Controller B for higher-order systems with towing pattern (b) and +20% hydrodynamic parameters.

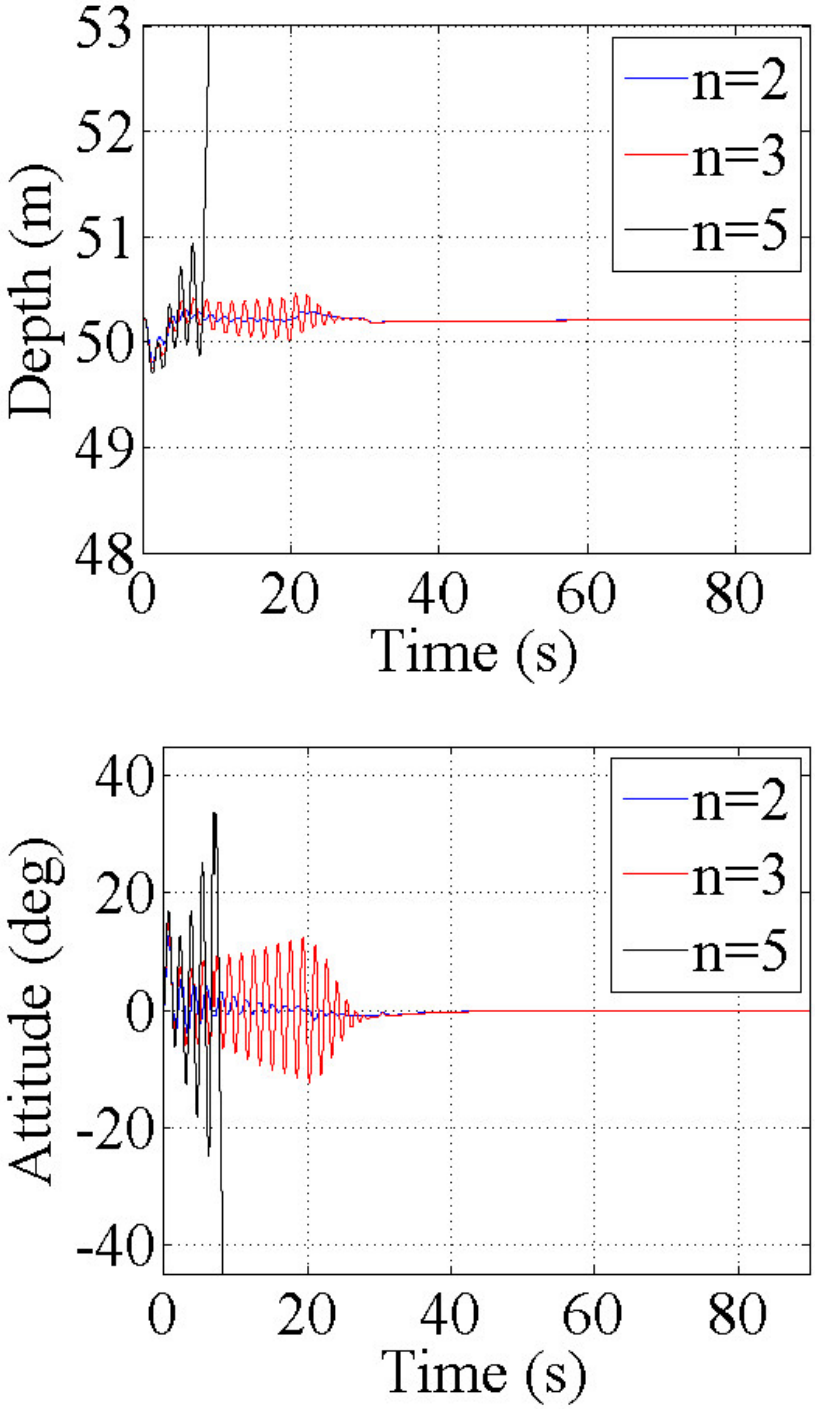

Figure 7.17. Simulation results of robust control performance by Controller B for higher-order systems with towing pattern (b) and −20% hydrodynamic parameters.

7.3 Depth Tracking

7.3.1 Settings

Finally, a depth tracking control and its full operating range are investigated. As demonstrated in Section 5.2, switching controllers is one of the simplest ways to construct the depth tracking control system; however, with LQI-control-based approach, the method is not available at least with no modifications. Fig. 7.18 demonstrates such a result, where Controller A is merely switched at $t = 10$ s to change the depth from 50.205 m to 45.502 m, but the control is lost. Owing to this, another approach to design the depth tracking control system needs to be considered. In Section 6.1, the output reference signal r vector has been introduced as $r_1 = 50.205$ m and $r_2 = 0°$, and the LQI-based controller make the system follow the r. Thus, it can be expected that changing the r_1 gradually will be a facile method to obtain the depth tracking control system. Fig. 7.19 presents the successful result of depth tracking by changing the r_1 as $50.205 \rightarrow 45.502$, where both the depth and attitude are regulated smoothly.

Based on the above observations, the full operating range via changing the reference depth r_1 is examined. The initial state is set at the equilibrium and, in addition to the nominal conditions, the parametric variations are considered as the same combination in the previous section except the towing speed change. Further, as seen from the simulation results in Section 5.2, ascending the vehicle takes longer time but has the wider changeable range than descending the vehicle. In other words, ascending is more likely to keep the system stable compared to descending, and this is immutable in LQI-based-control systems. Therefore, after some trial simulations, it is determined that the change step of r_1 is by 5 m for ascending case and by 2 m for descending case. The timing of the r_1 change is set as every 20 seconds.

7.3.2 Results

With the above conditions, the maximum reachable depth Δd_{max} from the 50.205 m is examined for each direction. Concentrating on the $n = 1$ model, Table 7.3 shows the maximum reachable depth for the both controllers. When ascending the vehicle, only the result of Controller B with -20%

hydrodynamic parameters is $\Delta d_{max} = 20$ m, and the rest of Δd_{max} is 45 m. Fig. 7.20 depicts the outputs for the both controllers with the condition of +50% payload and −20% hydrodynamic parameters, where Controller B fails to regulate the attitude and loses control after $t = 100$ s. While Controller A succeeds to lead the vehicle to 5 m, although the transient attitude shows larger overshoot than that with Controller B. Comparisons have to be also made with the LQ-based control system; the $\Delta d_{max} = 45$ m for ascending is the same reachable depth range with LQ-based controller. In contrast, the Δd_{max} becomes smaller than that with LQ-based control system in case of descending the vehicle. The Δd_{max} for Controller A with nominal condition is 28 m, which is 7 m shorter than the result with LQ-based switching control system in Section 5.2. As for Controller B, even the best Δd_{max} is 16 m. Fig. 7.21 demonstrates the worst case of descending the vehicle (+50% payload and −20% hydrodynamic parameters), where Controller B can not change the depth by just 2 m and Controller A retain the control within 70.205 m.

In order to expand the operating range for descending the vehicle, two types of solutions can be suggested. The one is to reduce the change step of the r_1 from 2 m to 1 m at least after $t = 220$ s. Fig. 7.22 shows such a result by Controller A with blue line and the Δd_{max} becomes 34 m. This value is equal to the result depicted with red line, where the r_1 is changed by 1 m from scratch. In other words, the proposed combination of the step change can change the vehicle depth from 50.205 m to 84.205 m under model uncertainties and can shorten the travelling time about 200 s faster than the case changing the r_1 constantly. Furthermore, $\Delta d_{max} = 34$ m for descending the vehicle is almost the same range as that with LQ-based controller without model uncertainties, $\Delta d_{max} = 35$ m.

The other strategy to expand the operating range is accommodating and constructing the switching control system. Recall the demonstration case in Fig. 7.18, where the switching controller fails to change the depth of the vehicle. This seems to be due to the smallness of the region of attraction compared to the LQ-based controller and to confirm the hypothesis the combination of the r_1 change and the switching controllers are attempted as illustrated in Fig. 7.23; first the r_1 is changed from $50.205 \rightarrow 45.502$ at $t = 10$ s and then the controller is switched from the one for 50.205

m to the one for 45.502 m at $t = 40$ s. Unfortunately, the control is still not succeeded after switching. It can be found from this result that the problem arises not only from the region of attraction, but also from the integral action in the LQI-based control system as indicated in [57]. Thus, the integrator has to be reset in order to realize the switching control system. Fig. 7.24 expressly reveals the effect of resetting the integral error, where the controller is switched successfully with the slight deflection in the attitude around $t = 40$ s. This modification makes it possible to extend the maximum reachable depth in descending the vehicle as shown in Fig. 7.25. The trajectory with blue line is the result of switching control systems, where the controller is switched at $t = 220$ s from the one corresponding to the 50.205 m to the one corresponding to the 70.205 m with resetting the integrator. $\Delta d_{max} = 34$ m is the same range as the previous method and compared to the trajectory with red line, which is the same as Fig. 7.22, i.e., changing the r_1 by 1 m constantly, the switching control system also achieves the curtailment of the traveling time. Note that the change step of the r_1 is set as 1 m after the switching; otherwise, the Δd_{max} almost never improves. However, this depends on the length of the cable and the switching control methodology is rather expected to be available and effective for the TUV system with far longer cables.

In addition, Table 7.4 presents the Δd_{max} for Controller A with higher-order systems. The results for ascending the vehicle are almost changeless, except only the $n = 5$ model with $+50\%$ payload and -20% hydrodynamic parameters; however, this conservative result $\Delta d_{max} = 5$ m is not a serious issue. It can be improved easily as demonstrated in Fig. 7.26, where the timing of the r_1 change for the $n = 5$ case is delayed, every 30 s, so that the depth and attitude are eventually regulated as the results with the $n = 2$ and 3 cases. Consequently, the reachable depth of the ascending control can be regarded as the same for $n = 1, 2, 3, 5$ models for all practical purposes. On the other hand, the Δd_{max}'s for descending the vehicle with $n = 2, 3, 5$ models are also similar to that with the $n = 1$ model. According to Table 7.4, each worst Δd_{max} is 24 m, 26 m, and 28 m for $n = 2, 3, 5$ models respectively when the payload is $+50\%$ and the hydrodynamic parameters are -20%. Fig. 7.27, where the timing of the r_1 change for the higher-order cases is delayed, every 30 s, shows that these values can not be ameliorated

by extending the time step for the alteration of r_1. Therefore, reducing the change step of the r_1 as in Fig. 7.22 and/or the switching controllers as in Fig. 7.25 will be necessary and effectual to improve the operating range of the LQI-based controller.

Hence it can be concluded that the results of depth tracking control assure the superiority of Controller A to Controller B as well, and the proposed LQI-based-control system takes longer time but is able to cover almost the same depth range as the LQ-based switching control system, even under model uncertainties with only one or two controllers.

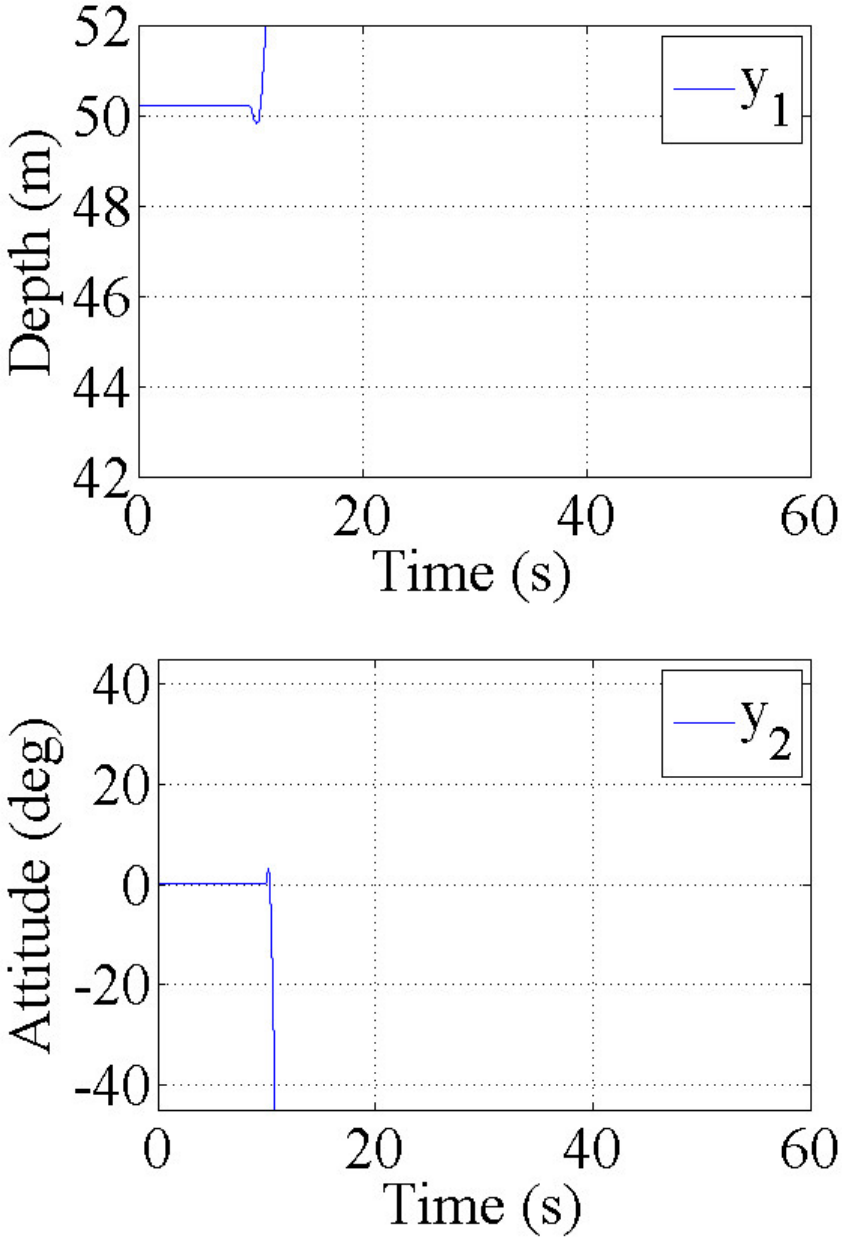

Figure 7.18. Demonstration case of depth tracking by switching controllers.

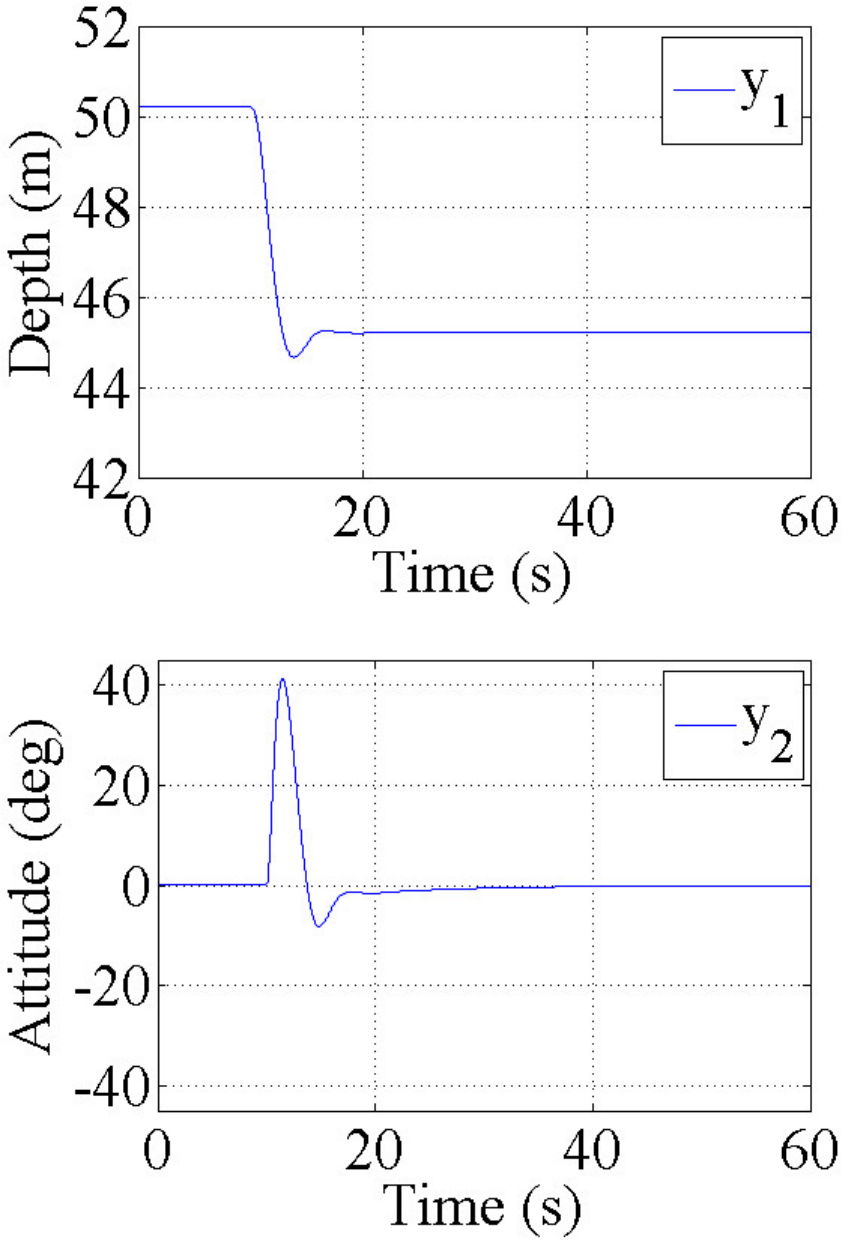

Figure 7.19. Demonstration case of depth tracking by changing the reference depth r_1.

Table 7.3. Reachable depth from CEP for C2 with $n = 1$ model by changing r_1; ascending by each 5 m, descending by each 2 m

Ascending	payload	HD	Δd_{max} (m)
Controller A	nominal	nominal	45
	+50%	+20%	45
	+50%	−20%	45
Controller B	nominal	nominal	45
	+50%	+20%	45
	+50%	−20%	20
Descending	payload	HD	Δd_{max} (m)
Controller A	nominal	nominal	28
	+50%	+20%	32
	+50%	−20%	20
Controller B	nominal	nominal	6
	+50%	+20%	16
	+50%	−20%	0

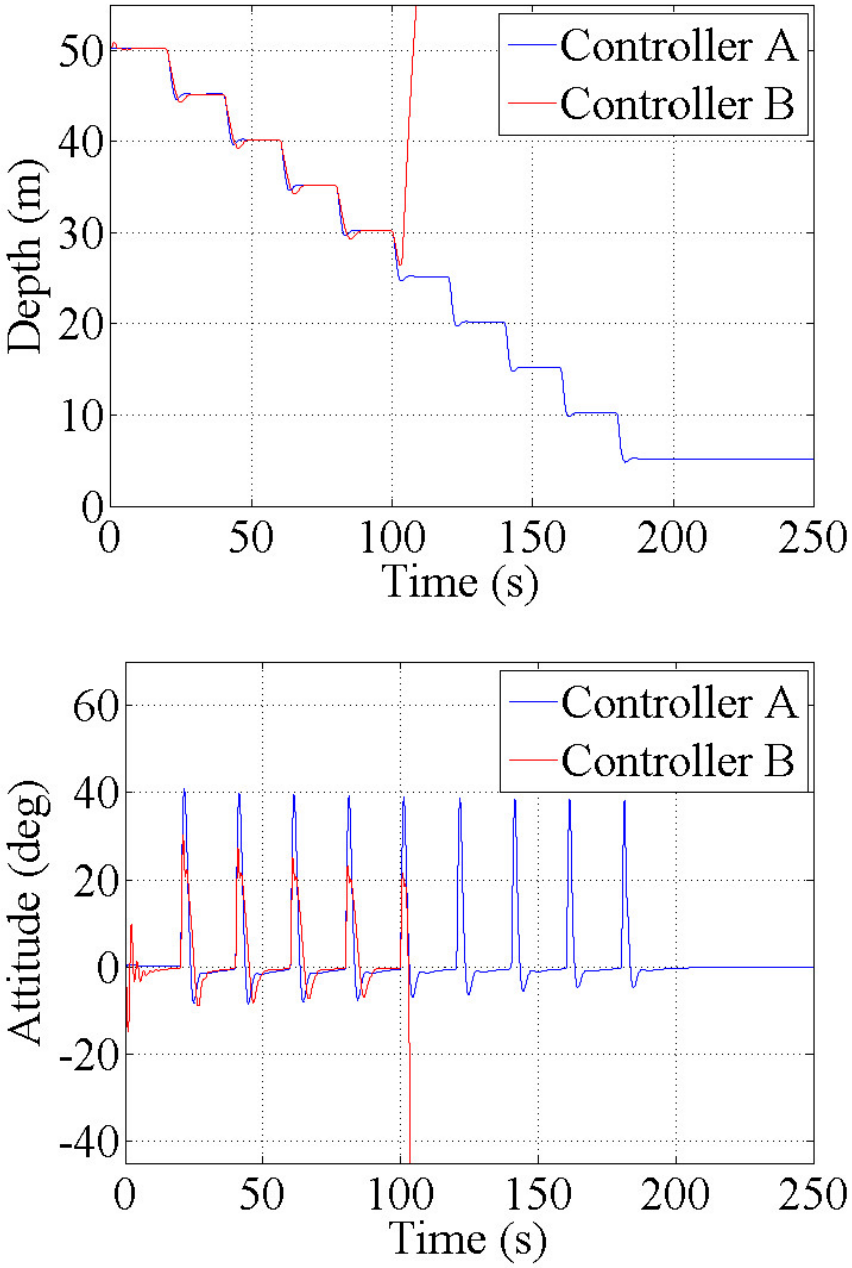

Figure 7.20. Simulation results of ascending depth tracking control for $n = 1$ model by both controllers with $+50\%$ payload and -20% hydrodynamic parameters.

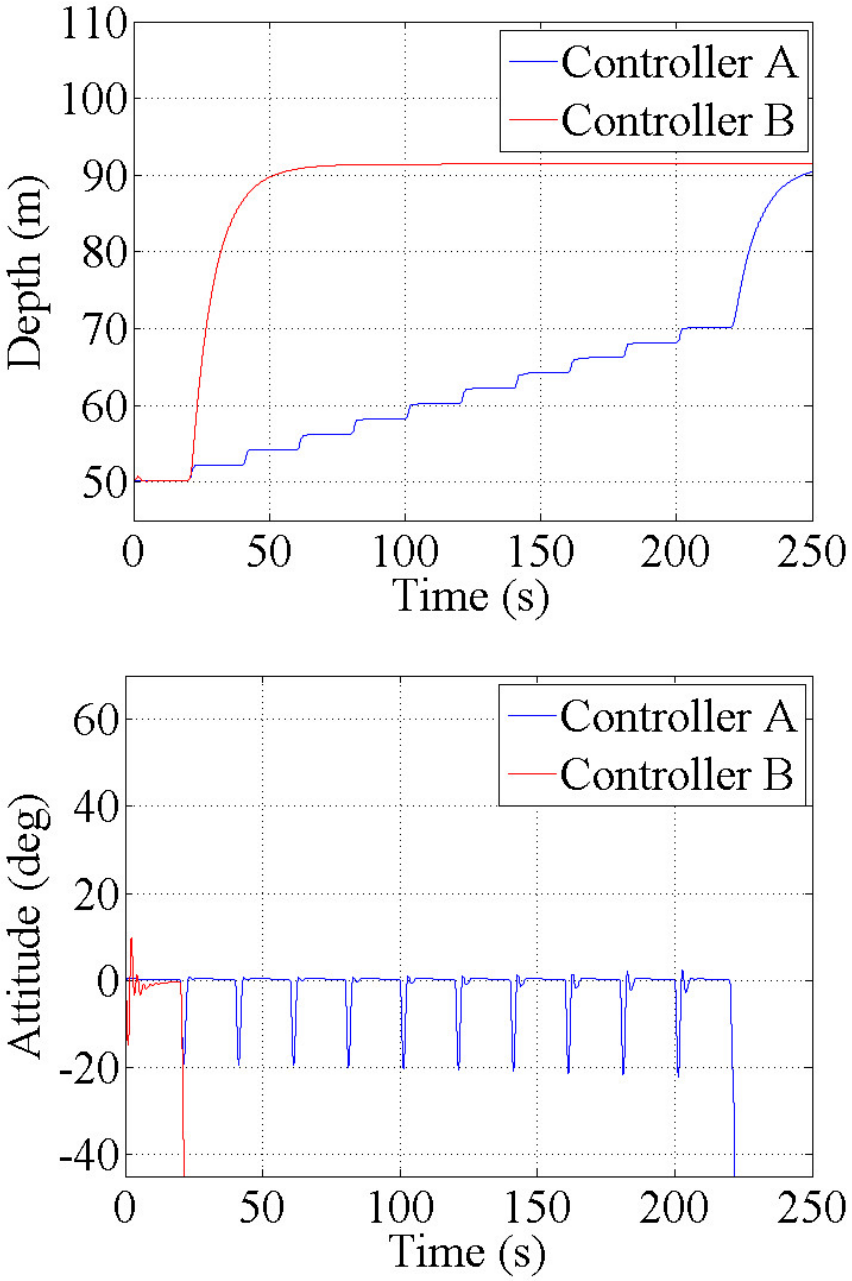

Figure 7.21. Simulation results of descending depth tracking control for $n = 1$ model by both controllers with $+50\%$ payload and -20% hydrodynamic parameters.

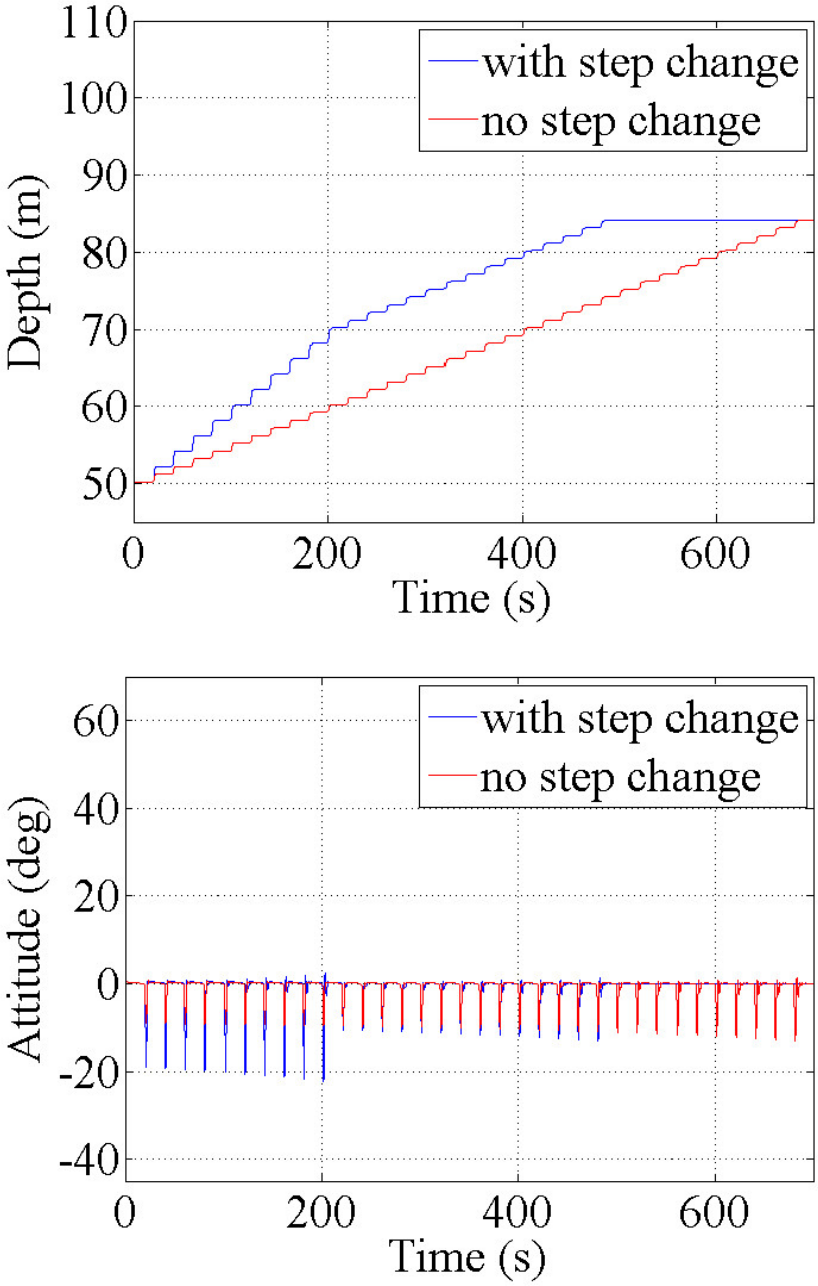

Figure 7.22. Simulation results of descending depth tracking control for $n = 1$ model by Controller A with +50% payload and −20% hydrodynamic parameters; *blue* reduce the change step of r_1 from 2 m to 1 m at $t = 220$ s, *red* the r_1 is changed by 1 m constantly.

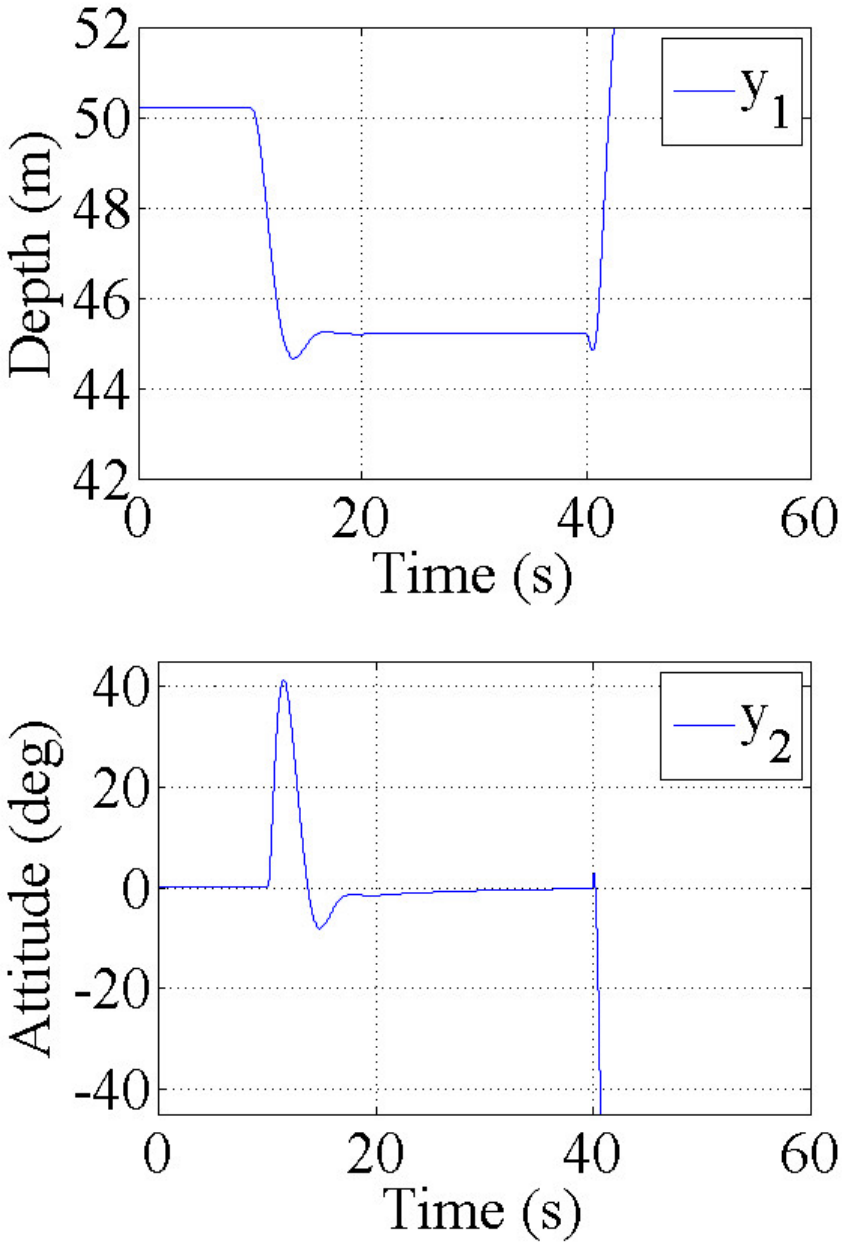

Figure 7.23. Demonstration case of depth tracking by switching controllers with no integrator reset after changing the reference depth r_1.

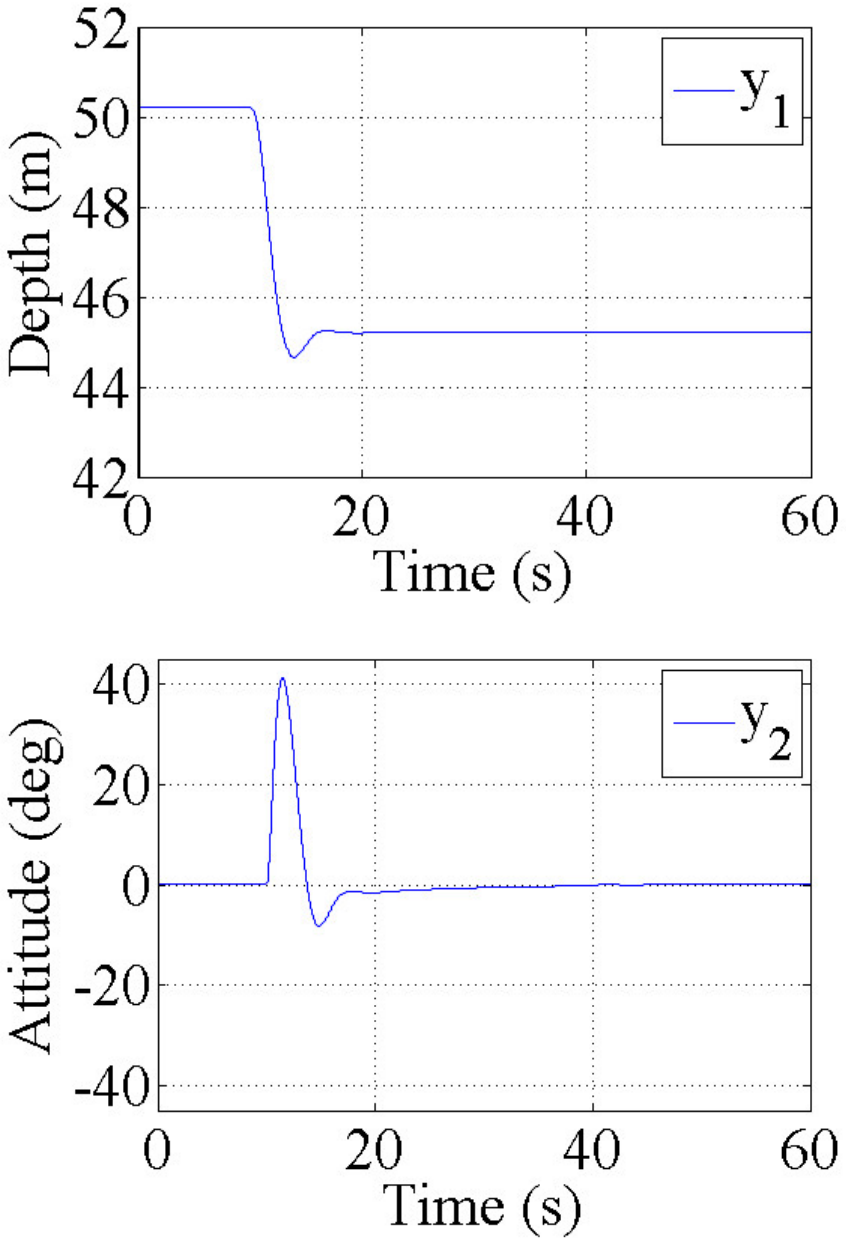

Figure 7.24. Demonstration case of depth tracking by switching controllers with integrator reset after changing the reference depth r_1.

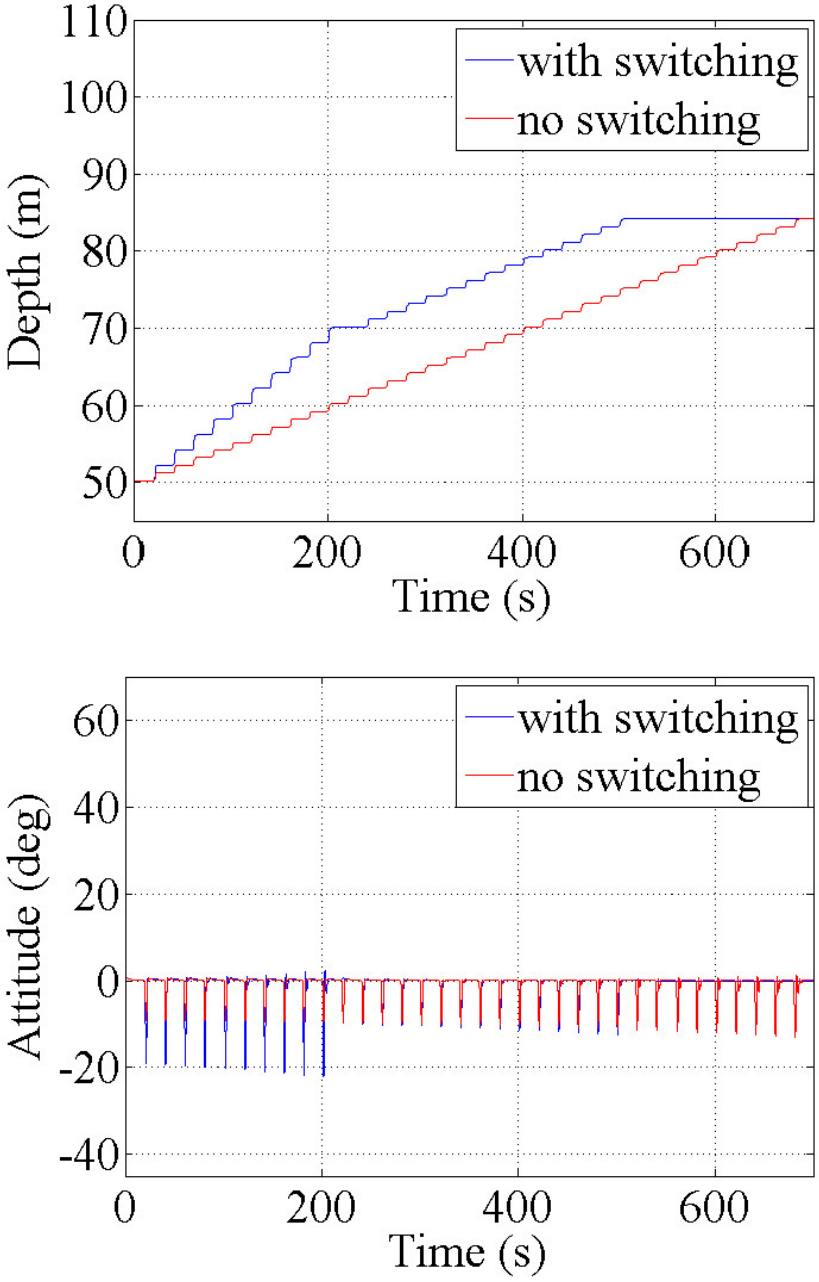

Figure 7.25. Simulation results of descending depth tracking control for $n = 1$ model by Controller A with $+50\%$ payload and -20% hydrodynamic parameters; *blue* switching controllers with integrator reset at $t = 220$ s, *red* the r_1 is changed by 1 m.

Table 7.4. Reachable depth from CEP for C2 with Controller A and higher-order models by changing r_1; ascending by each 5 m, descending by each 2 m

Ascending	Payload	HD	Δd_{max} (m)
$n = 2$	nominal	nominal	45
	+50%	+20%	45
	+50%	−20%	45
$n = 3$	nominal	nominal	45
	+50%	+20%	45
	+50%	−20%	45
$n = 5$	nominal	nominal	45
	+50%	+20%	45
	+50%	−20%	5
Descending	Payload	HD	Δd_{max} (m)
$n = 2$	nominal	nominal	30
	+50%	+20%	34
	+50%	−20%	24
$n = 3$	nominal	nominal	30
	+50%	+20%	34
	+50%	−20%	26
$n = 5$	nominal	nominal	28
	+50%	+20%	32
	+50%	−20%	28

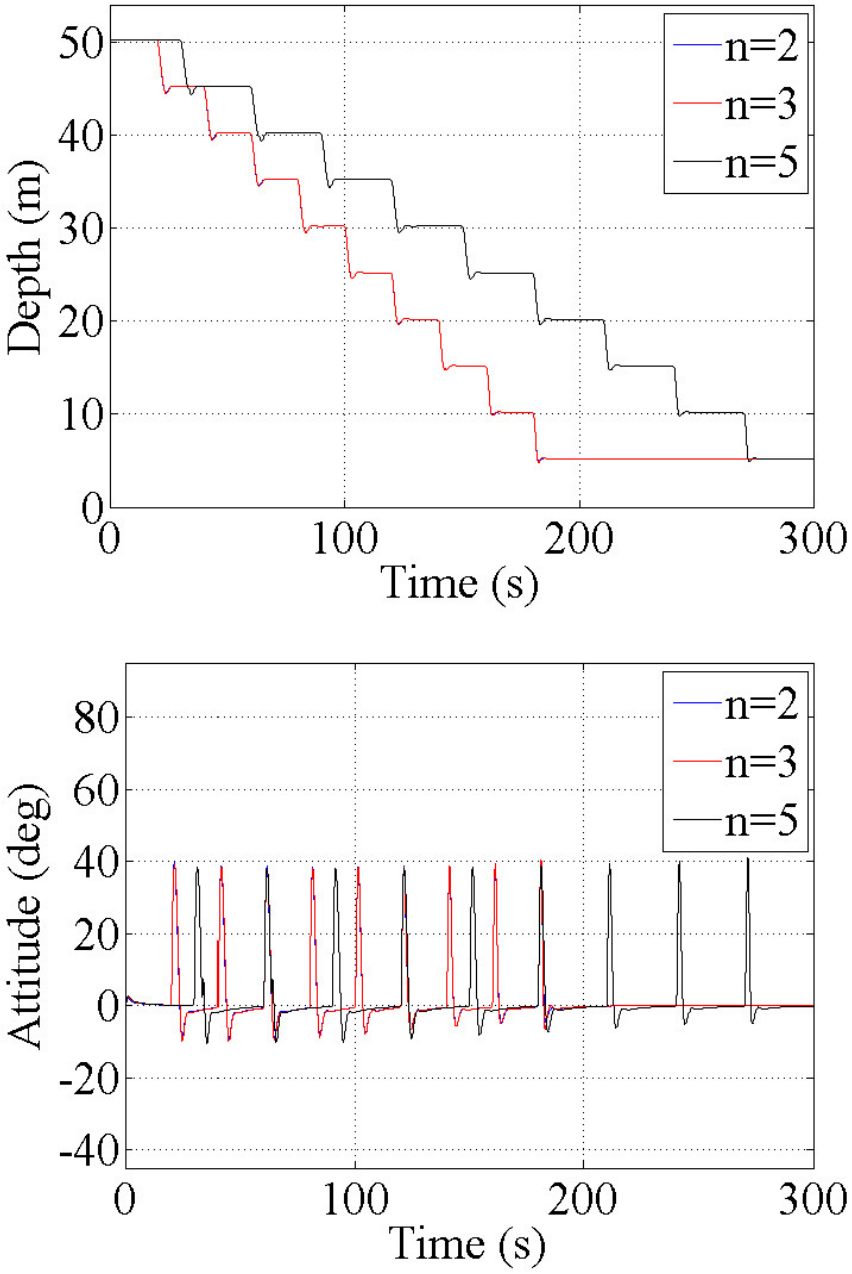

Figure 7.26. Simulation results of ascending depth tracking control for higher-order systems by Controller A with +50% payload and −20% hydrodynamic parameters.

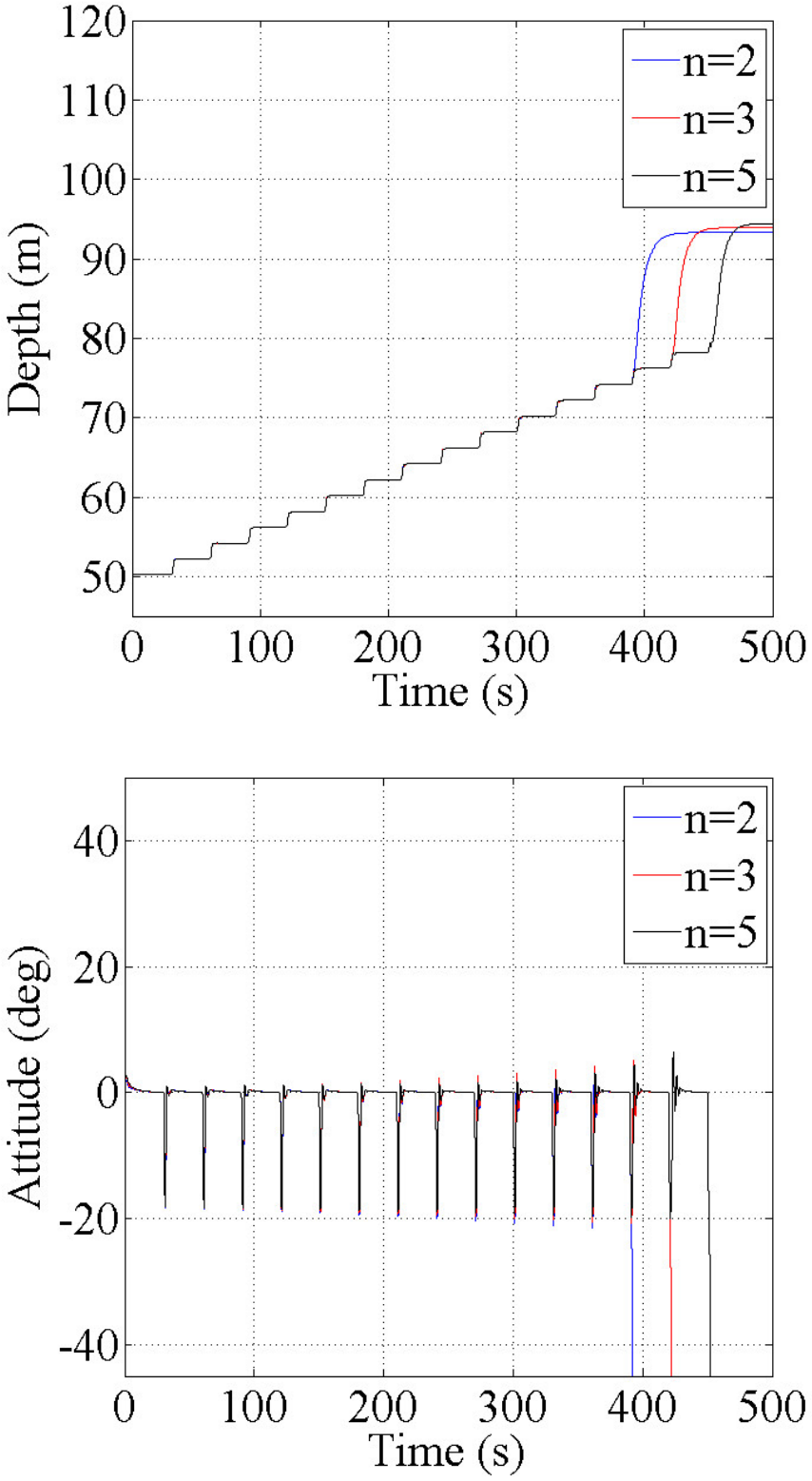

Figure 7.27. Simulation results of descending depth tracking control for higher-order systems by Controller A with +50% payload and −20% hydrodynamic parameters.

8 Conclusions and Scope for Future Work

This dissertation has presented a high-gain observer-based motion control method and stability analysis of a TUV with movable wings. The dynamical models of the TUV with different lengths of the towing cable were given and its explicit state-space representation was derived. Based on the system, two types of control schemes, an LQ-control-based and LQI-control-based approach have been employed and investigated with the high-gain observer so as to estimate the state by fully considering the nonlinear dynamics of the system.

In particular, the most unique contributions of this research are the detailed stability analysis for the LQ-based controller; not only an asymptotic stability of the system has been confirmed but its region of attraction has been estimated. The conservativeness of the conventional estimates has been improved by devising a state-space scaling method, which has high originalities, and this scaling method is extensively available for various kinds of control systems, to say nothing of problems of underwater vehicles.

Some control simulations have also been conducted to evaluate the depth and attitude regulation performances of the LQI-based control systems; regulation simulations with initial deviations from an equilibrium, regulation simulations with model uncertainties and a depth tracking. The proposed controller with the high-gain observer has shown the better robustness especially under model uncertainties compared to the results with the conventional linear Kalman observer. Consequently, the importance of the direct consideration of nonlinearity of the system and the effectiveness of the high-gain observer-based approach in the control system design of TUVs has been confirmed and proved.

Meanwhile, there are remaining works to put the proposed method into practical applications as follows;

Z1 some dynamics ignored in the present study will have to be considered;

Z2 the robustness to environmental water current and other external disturbance factors should be evaluated; and

Z3 the validity of the study need to be verified; especially the experimental

evaluation must be performed.

Z1 indicates the qualifications which are made in section 2.1; that is, the dynamics of the mothership and the wing actuators have been omitted. The latter includes handling of the *dynamic stall*, whose strict modeling requires the consideration of the angles of attack. Besides, the approximation method of the towing cable also has a room for improvement to model the physical characteristics of the cable more precisely. These assumptions will be able to be considered more realistically.

Although the robustness to the model uncertainties of the proposed controller has been examined in this study, the evaluation with disturbance factors like environmental water current and measurement noise has not been done yet. Future work should focus on this aspect and Z2 can be achieved, at least in part, by extending the simulation conditions. For example, towing velocity change might be regarded as a kind of water current and sensor error would be imitated by adding the random noise to the output. To investigate the stability of the control system from the viewpoint is important to apply the proposed approach to existing equipment.

Moreover, Z3 will be the essential subject of future research to implement the proposed motion control method in practice. Since the study in this dissertation is limited to numerical approach and depends on the specific model of a TUV, the confirmation of the validity of the results is an important work. Therefore, experimental data and comparison with simulations are required to demonstrate the effectiveness of the high-gain observer-based controller.

Additionally, the controller utilized in this research is based on the linearized system corresponding to each equilibrium, and hence it may be needed to prepare some controllers with respect to each specific model or situation in advance. This will be inexpedient for real applications. Accordingly, the control system design specification has a room to be improved by, e.g., introducing an adaptive control scheme. It is also desirable to perform the comparison simulations with other existing control design method.

Despite remains of these points of improvement, the proposed control method has a potential for better control of TUVs and will ameliorate TUVs as more accurate and reliable ocean observatories through further investigations.

Acknowledgement

First of all, I would like to express my profound gratitude to my supervisor, associate professor, Masayoshi Toda for the opportunities he has given me throughout this research. His patient guidance and generous support were indispensable for my work.

I would be grateful professor Shigeki Kametani not only for his incisive suggestions but also his vitality, which tells me the importance of experience and practice.

I give great thanks to professor Hisaharu Sakai for his warm encouragement and sincere comments to my effort.

My deep appreciation is given to associate professor Kimihiko Ueno for providing me opportunities of presentation in the periodical session of Japan Society for Mathematical and Physical Fisheries Science.

I would also like to thank all the laboratory members, and special thanks to all the staff in Doctoral Course of Applied Marine Environmental Studies for permitting the chance to complete this study.

Finally, I give great thanks to all of my friends and family for supporting me and always being there for me.

References

[1] J. K. Cochran, "Oceanographic sampling and measurements," *Elsevier Reference Module in Earth Systems and Environmental Sciences*, pp, 1-7, 2014.

[2] T. Ura, and S. Takagawa (Eds.), *Kaichu robot*, Tokyo, Japan: Seizando-Shoten, 1997.

[3] S. Kröger and R. J. Law, "Sensing the sea," *TRENDS in Biotechnology*, vol. 23, no. 5, pp, 250-256, 2005.

[4] D. Roemmich, G. C. Johnson, S. Riser, R. Davis, J. Gilson, W. B. Owens, S. L. Garzoli, C. Schmid and M. Ignaszewski, "The argo program: Observing the global ocean with profiling floats," *Oceanography*, vol. 22, no. 2, pp, 34-43, 2009.

[5] M. Caccia and G. Bruzzone, "Execution control of ROV navigation, guidance and control tasks," *Int. J. Contr.*, vol. 80, no. 7, pp, 1109-1124, 2007.

[6] M. Cavalletti, G. Ippoliti and S. Longhi, "Lyapunov-based switching control using neural networks for a remotely operated vehicle," *Int .J. Contr.*, vol. 80, no. 7, pp, 1077-1091, 2007.

[7] J. P. V. S. Cunha, R. R. Costa and L. Hsu, "Design of a high performance variable structure position control of ROVs," *IEEE J. Ocean. Eng.*, vol. 20, no. 1, pp. 42-55, Jan., 1995.

[8] J. Johnson, G. Madhumitha, N. Yousuf and S. Harikrishnan, "Design, development and fuzzy logic based control of a remotely operated underwater vehicle," in *Proc. IEEE International Conference on Robotics and Automation for Humanitarian Applications*, Kollam, India, Dec., 2016, IEEE Xplore.

[9] N. H. Tehrani, M. Heidari, Y. Zakeri and J. Ghaisari, "Development, depth control and stability analysis of an underwater remotely operated vehicle (ROV)," in *Proc. 8th IEEE International Conference on Control and Automation*, Xiamen, China, Jun., 2010, pp. 814-819.

[10] M. S. Triantafyllou and M. A. Grosenbaugh, "Robust control for underwater vehicle system with time delays," *IEEE J. Ocean. Eng.*, vol. 16, no. 1, pp. 146-151, 1991.

[11] M. T. Vu, H-S. Choi, J. Kang, D-H. Ji and S-K. Jeong, "A study on hovering motion of the underwater vehicle with umbilical cable," *Ocean Eng.*, vol. 135, pp. 137-157, 2017.

[12] J. Yuh and R. Lakshmi, "An intelligent control system for remotely operated vehicles," *IEEE J. Ocean. Eng.*, vol. 18, no. 1, pp. 55-62, Jan., 1993.

[13] Z. Ke-qiang, Z. Hai-yang, Z. Yu-song and G. Jie, "A multi-body space-coupled motion simulation for a deep-sea tethered remotely operated vehicle," *Journal of Hydrodynamics*, vol. 20 no. 2, pp. 210-215, 2008.

[14] K. Alam, T. Ray, and S. G. Anavatti, "A brief taxonomy of autonomous underwater vehicle design literature," *Ocean Eng.*, vol. 88, pp. 627-630, 2014.

[15] E. Bovio, D. Cecchi and F. Baralli, "Autonomous underwater vehicles for scientific and naval operations," *Annual Reviews in Control.*, vol. 30, pp. 117-130, 2006.

[16] G. Griffiths, "Steps towards autonomy: from current measurements to underwater vehicles," *Methods in Oceanography*, vol. 1-2, pp, 22-48, 2012.

[17] L. Paull, S. Saeedi, M. Seto and H. Li, "AUV navigation and localization: a review," *IEEE J. Ocean. Eng.*, vol. 39, no. 1, pp. 131-149, 2014.

[18] R. B. Wynn, V. A. I. Huvenne, T. P. Le Bas, B. J. Murton, D. P. Connelly, B. J. Bett, H. A. Ruhl, K. J. Morris, J. Peakall, D. R. Parsons, E. J. Sumner, S. E. Darby, R. M. Dorrell and J. E. Hunt, "Autonomous underwater vehicles (AUVs): Their past, present and future contributions to the advancement of marine geoscience," *Marine Geology*, vol. 352, pp. 451-468, 2014.

[19] M. R. Benjamin, D. Battle, D. Eickstedt, H. Schmidt and A. Balasuriya, "Autonomous control of an autonomous underwater vehicle towing a vector sensor array," in *Proc. IEEE International Conference on Robotics and Automation*, Roma, Italy, Apr. 2007, pp 4562-4569.

[20] J. D. Holmes, W. M. Carey, J. F. Lynch, A. E. Newhall and A. Kukulya, "An autonomous underwater vehicle towed array for ocean acoustic measurements and inversions," in *Proc. IEEE Europe Oceans 2005*, Brest, France, Jun., 2005 pp. 1058-1061.

[21] J. C. Kinsey, M. A. Tivey, and D. R. Yoerger, "Toward high-spatial resolution gravity surveying of the mid-ocean ridges with autonomous underwater vehicles," in *Proc. IEEE OCEANS 2008*, Quebec City, Canada, Sept., 2008, IEEE Xplore.

[22] T. Knutsen, W. Melle, M. Mjanger, E. Strand, A-L. Fuglestad, C. Broms, E. Bagoien, H. Fitje, O. Ørjansen and T. Vedeler, "MESSOR - A towed underwater vehicle for quantifying and describing the distribution of pelagic organisms and their physical environment," in *Proc. MTS/IEEE OCEANS 2013*, Bergen, Norway, Jun., 2013, pp. 1-12.

[23] L. G. Miller and K. D. Ellenrieder, "Modeling and simulation of an AUV-towfish system," in *Proc. IEEE OCEANS 2013*, San Diego, CA, USA, Sept., 2013, IEEE Xplore.

[24] Jinmo. Prak and N. Kim, "Dynamics modeling of a semi-submersible autonomous underwater vehicle with a towfish towed by a cable," *Int. J. Nav. Archit. Ocean Eng.*, vol. 17, no. 7, pp. 409-425, 2015.

[25] M. A. Tivey, H. P. Jhnson, A. Bradley and D. Yoerger, "Thickness of a submarine lava flow determined from near-bottom magnetic field mapping by autonomous underwater vehicle," *Geophysical Research Letters*, vol. 25, no. 6, pp, 805-808, 1998.

[26] J. D. Geder, R. Ramamurti, J. Palmisano, M. Pruessner, B. Ratna and W. C. Sandberg, 'Four-fin bio-inspired UUV: modeling and control solutions," in *Proc. ASME 2011 International Mechanical Engineering Congress & Exposition*, Denver, Colorado, USA, Nov., 2011.

[27] J. Ghommam and M. Saad, "Backstepping-based cooperative and adaptive tracking control design for a group of underactuated AUVs in horizontal plan," *Int .J. Contr.*, vol. 87, no. 5, pp, 1076-1093, 2014.

[28] E. Y. Hong, H. G. Soon and M. Chitre, "Depth control of an autonomous underwater vehicle, STARFISH," in *Proc. IEEE OCEANS 2010*, Sydney, Australia, May, 2010, IEEE Xplore.

[29] Z. H. Ismail and M. W. Dunnigan, "Nonlinear H∞ optimal control scheme for an underwater vehicle with regional function formulation," *Journal of Applied Mathematics*, vol. 2013, Article ID 732738, Hindawi.

[30] A. Okamoto, J. J. Feeley, D. B. Edwards, R. W. Wall, "Robust Control of a Platoon of Underwater Autonomous Vehicles," in *Proc. OCEANS' 04. MTS/IEEE TECHNO-OCEAN '04*, Kobe, Japan, Nov., 2004, pp 505-510.

[31] P-M. Lee, S-W. Hong, Y-K. Lim, C-M. Lee, B-H. Jeon and J-W. Park, "Discrete-time quasi-sliding mode control of an autonomous underwater vehicle," *IEEE J. Ocean. Eng.*, vol. 24, no. 3, pp. 388-395, 1999.

[32] S. Li, X. Wang and L. Zhang, "Finite-time output feedback tracking control for autonomous underwater vehicles," *IEEE J. Ocean. Eng.*, vol. 40, no. 3, pp. 727-751, 2015.

[33] S. Liu, D. Wang and E. Poh, "Non-linear output feedback tracking control for AUVs in shallow wave disturbance condition," *Int .J. Contr.*, vol. 81, no. 11, pp, 1806-1823, 2008.

[34] A. Manzanilla and R. Lozano, "Nonlinear algorithm with adaptive properties to stabilize an underwater vehicle: real-time experiments," *IFAC PapersOnLine*, vol. 50, issue 1, pp 6857-6862, 2017.

[35] W. Naeem, R. Sutton and S. M. Ahmad, "LQG/LTR Control of an Autonomous Underwater Vehicle Using a Hybrid Guidance Law," *IFAC Proceedings Volumes*, vol. 36, issue. 4, pp, 31-36 2003.

[36] W. Naeem, R. Sutton, J. Chudley, F. R. Dalgleish and S. Tetlow, "An online genetic algorithm based model predictive control autopilot design with experimental verification," *Int .J. Contr.*, vol. 78, no. 14, pp, 1076-1090, 2005.

[37] H. Pan and M. Xin, "Depth control of autonomous underwater vehicles using indirect robust control method," *Int .J. Contr.*, vol. 85, no. 1, pp, 98-113, 2012.

[38] D. E. Sanabria, G. Balas and R. Arndt, "Modeling, control, and experimental validation of a high-speed supercavitating vehicle," *IEEE J. Ocean. Eng.*, vol. 40, no. 2, pp. 362-373, 2015.

[39] J. Han, and W. K. Chung, "Active use of restoring moments for motion control of an underwater vehicle-manipulator system," *IEEE J. Ocean. Eng.*, vol. 39, no. 1, pp. 100-109, 2014.

[40] P. S. Londhe, M. Santhakumar and B. M. Patre, "Task space control of an autonomous underwater vehicle manipulator system by robust single-input fuzzy logic control scheme," *IEEE J. Ocean. Eng.*, vol. 42, no. 1, pp. 13-28, 2017.

[41] Y. Taira, "Robust control for underwater robot manipulators with a time-varying feedback Gain," *Journal of National Fisheries University*, vol. 58 no. 3, pp. 199-205, 2010, in japanese.

[42] B. Lynch and A. Ellery "Efficient control of an AUV-manipulator system: an application for the exploration of europa," *IEEE J. Ocean. Eng.*, vol. 39, no. 3, pp. 552-570, 2014.

[43] X. Wang, J. Shang, Z. Luo, L. Tang, X. Zhang and J. Li "Reviews of power systems and environmental energy conversion for unmanned underwater vehicles," *Renewable and Sustainable Energy Reviews*, vol. 16, pp. 1958-1970, 2012.

[44] W. Koterayama, M. Nakamura, H. Kajiwara and I. Sato, "Development of a towed and self-propulsive vehicle for sea bottom survey," *Journal of the Society of Naval Architects of Japan*, no. 175, pp. 205-218, 1994, in japanese.

[45] B. Buckham, M. Nahon, M. Seto, X. Zhao and C. Lambert, "Dynamics and control of a towed underwater vehicle system, part I: model development," *Ocean Eng.*, vol. 30, pp. 453-470, 2003.

[46] C. Lambert, M. Nahon, B. Buckham and M. Seto "Dynamics and control of a towed underwater vehicle system, part II: model validation and turn maneuver optimization," *Ocean Eng.*, vol. 30, pp. 471-485, 2003.

[47] G. Campa, J. Wilkie and M. Innocenti, "Robust control and analysis of a towed underwater vehicle," *Int. J. Adapt. Control Signal Process*, vol. 12, pp. 689-716, 1998.

[48] J-K. Choi, T. Shiraishi, T. Tanaka and H. Kondo, "Safe operation of an autonomous underwater towed vehicle: towed force monitoring and control," *Automation in Construction*, vol. 20, issue 8, pp. 1012-1019, 2011.

[49] H. Kajiwara, W. Koterayama, S. Yamaguchi and T. Yokobiki, "Robust control system design for a towed underwater vehicle," in *Proc. 2002 Interntional Symposium on Underwater Technology*, Tokyo, Japan, Apr., 2002, pp. 213-216.

[50] N. Kato, "Underwater towed vehicle maneuverable in both vertical and horizontal axis (Part1: Principal configuration and attitude control)," *Journal of the Society of Naval Architects of Japan*, no. 169, pp. 111-122, 1991, in japanese.

[51] N. Kato, "Underwater towed vehicle maneuverable in both vertical and horizontal axis (Part2: Guidance)," *Journal of the Society of Naval Architects of Japan*, no. 171, pp. 571-580, 1992, in japanese.

[52] W. Koterayama, M. Nakamura M. Kashiwagi Y. Kyozuka and M. Ohkusu, "A preliminary design of a depth- and roll-controllable towed vehicle for ocean measurements," *Journal of the Society of Naval Architects of Japan*, no. 163, pp. 130-140, 1988, in japanese.

[53] W. Koterayama, S. Yamaguchi, M. Nakamura and T. Akamatu, "Development of an observation robot 「Flying Fish」 for comprehensive

measurements of ocean environment," *Journal of the Society of Naval Architects of Japan*, no. 179, pp. 193-204, 1996, in japanese.

[54] W. Koterayama, S. Yamaguchi, T. Yokobiki, J.-H. Yoon and H. Hase, "Space-continuous measurements on ocean current and chemical properties with the intelligent towed vehicle "Flying Fish"," *IEEE J. Ocean. Eng.*, vol. 25, no. 1, pp. 130-138, Jan., 2000.

[55] M. Nakamura, H. Kajiwara and W. Koterayama, "Development of an ROV operated both as towed and self-propulsive vehicle," *Ocean Eng.*, vol. 28, pp. 1-43, 2000.

[56] T. Yokobiki, W. Koterayama, S. Yamaguchi and M. Nakamura, "Dynamics and control of a towed vehicle in transient mode," *Int. J. of Offshore and Polar Engineering*, vol. 10, no. 1, pp. 19-25, 2000.

[57] T. Yokobiki, S. Yamaguchi, W. Koterayama and M. Nakamura, "Depth control of towed vehicle "Flying Fish" by H∞ controller," *Engineering Sciences Reports*, Kyushu University, vol.22 no. 3, pp. 323-333, 2000 in japanese.

[58] D. Hopkin, M. Davies and I. Gartshore, "The aerodynamics and control of a remotely-piloted underwater towed vehicle," *Canadian Aeronautics and Space Journal*, vol. 36, no. 3, pp. 122-129, Sep., 1990.

[59] P. N. Jithin and M. N. Senthil Prakash, "Numerical investigation of the hydrodynamic behavior of the depressor," *Int. J. Mech. Eng.*, vol. 3, no. 1, pp, 256-264, 2014.

[60] P. P. Lalu, "Numerical simulation of two-part underwater towing system," D.Ph. Thesis, Cochin University of Science and Technology, Department of Ship Technology, 2013.

[61] A. Linklater, "Design and simulation of a towed underwater vehicle," M.Sc. Thesis, Virginia State University, Department of Aerospace Engineering, 2005.

[62] M. Nakamura, J. Noda, T. Ishimaru, K. Nakamura and K. Matuoka, "Study on deep tow system -Part 1 model experiment and motion

simulations-," *Journal of the Japan Society of Naval Architects and Ocean Engineers*, no. 24, pp. 227-240, 2017, in japanese.

[63] J. M. Preston, "Stability of towfish used as sonar platforms," in *Proc. OCEANS '92. Mastering the Oceans Through Technology*, Newport, RI, USA, Oct., 1992, pp 888-893.

[64] E. M. Schuch, "Towfish design, simulation and control," M.Sc. Thesis, Virginia State University, Department of Aerospace Engineering, 2004.

[65] E. M. Schuch, A. C. Linklater, N. W. Lambeth and C. A. Woolsey, "Design and simulation of a two stage towing system," in *Proc. OCEANS 2005 MTS/IEEE*, vol. 2, Washington DC, USA, Sep., 2005, pp. 1705-1712.

[66] F. C. Teixeira, A. P. Aguiar and A. M. Pascoal, "Nonlinear control of an underwater towed vehicle," in *Proc. 7th IFAC Conference on Manoeuvring and Control of Marine Craft*, Lisbon, Portugal, 2006.

[67] F. C. Teixeira, A. P. Aguiar and A. Pascoal, "Nonlinear adaptive depth tracking and attitude control of an underwater towed vehicle," in *Proc. 8th IFAC Conference on Manoeuvring and Control of Marine Craft*, Guaruja, SP, Brazil, 2009, pp. 211-216.

[68] F. C. Teixeira, A. P. Aguiar and A. Pascoal, "Nonlinear adaptive control of an underwater towed vehicle," *Ocean Eng.*, vol. 37, pp. 1193-1220, 2010.

[69] A. Cammarata and R. Sinatra, "Parametric study for the steady-State equilibrium of a towfish," *Journal of Intelligent & Robotic Systems*, vol. 81, issue 2, pp. 231-240, 2016.

[70] S. K. Srivastava and C. Ganapathy, "Dynamic behavior of underwater towed-cable in linear profile," *Int. J. of Scientific & Engineering Research*, vol. 2, issue 7, pp. 1-10, 2011.

[71] J. I. Gobat and M. A. Grosenbaugh, "Time-domain numerical simulation of ocean cable structures," *Ocean Eng.*, vol. 33, pp. 1373-1400, 2006.

[72] M. A. Grosenbaugh, "Transient behavior of towed cable systems during ship turning maneuvers," *Ocean Eng.*, vol. 34, pp. 152-1542, 2007.

[73] F. S. Hover, M. A. Grosenbaugh and M. S. Triantafyllou , "Calculation of dynamic motions and tensions in towed underwater cables," *IEEE J. Ocean. Eng.*, vol. 19, no. 3, pp. 449-457, 1994.

[74] Z. Ke-qiang, Z. Dao-chang, C. Ying, Y. Chun-ling, W. Rong, L. Yonglin and Z. Feng, "Nonlinear hydrodynamic response of marine cable-body system under random dynamic excitations," *Journal of Hydrodynamics*, vol. 21, issue 6, pp. 851-855, 2009.

[75] I. C. Matulea, A. Năstase, N. Tălmaciu, G. Slămnoiu and A. M. Goncalves-Coelho, "On the equilibrium configuration of mooring and towing cables," *Applied Ocean Research*, vol. 30, pp. 81-91, 2008.

[76] H. I. Parka, D.H. Jungb, and W. Koterayama, "A numerical and experimental study on dynamics of a towed low tension cable," *Applied Ocean Research*, vol. 25, pp. 289-299, 2003.

[77] R. K. Vandana, "Finite element analysis of underwater towed cables," in *Proc. 2013 International Conference on Energy and Environment*, Kerala, India, 2013, pp. 116-124.

[78] M. A. Vaz and M. H. Pate, "Transient behaviour of towed marine cables in two dimensions," *Applied Ocean Research*, vol. 17, pp. 143-153, 1995.

[79] J. Biao, Z. Qiang and Z. Yang, "Analysis on transient behavior of cable-towed acoustic array," in *Proc. 2015 International Conference on Intelligent Systems Research and Mechatronics Engineering*, Zhengzhou, China, 2015, pp. 2084-2089.

[80] Y. Bing-ka, Z. Ke-qiang, Z. Yan-jie and Q. Dao-wu, "Dynamic response of towed line array," *Journal of Hydrodynamics*, vol. 25, issue 4, pp. 616-619, 2013.

[81] D. E. Calkins, "A metamodel-based towed system simulation," *Ocean Eng.*, vol. 26, pp. 1183-1247, 1998.

[82] H. K. Shin, J. S. Ryue, H-T. Ahn, H. S. Seo and O-C. Kwon, "Study on dynamic behavior analysis of towed line array sensor," *Int. J. Nav. Oc. Engng.*, vol. 4, issue 1, pp. 9-19, 2012.

[83] S. K. Srivastava and C. Ganapathy, "Experimental investigations on loop manoeuvre of underwater towed cable array system," *Ocean Eng.*, vol. 25, no 1, pp. 85-102, 1998.

[84] J. X. Yang, C. G. Shuai, L. He, S. K. Zhang and S. T. Zhou, "The dynamic research and position estimation of the towed array during the U-turn process," *Journal of Physics: Conference Series*, vol. 744, no 1, 2016, IOP Publishing.

[85] O. Blintsov, "Development of the mathematical modeling method for dynamics of the flexible tether as an element of the underwater complex," *Eastern-European Journal of Enterprise Technologies*, vol. 1, no. 7 (85) pp. 4-14, 2017.

[86] Z. Feng, and R. Allen, "Evaluation of the effects of the communication cable on the dynamics of an underwater flight vehicle," *Ocean Eng.*, vol. 31, pp. 1019-1035, 2004.

[87] J. W. Kamman and T. C. Nguyen, "Depth enhancement of an underwater towed system using hydrodynamic depressor," *Naval Coastal Systems Center*, Paman City, Florida, Technocal Memorandum 492-88, 1990.

[88] C. Liu, Y. Zhang and X. Yuan, "Simulation of recycling cable in underwater towed system," in *Proc. 2012 International Conference on Mechanical Engineering and Material Science*, Paris, France, 2012, pp. 70-72.

[89] P. Vinod, R. Francis, P. Prabhasuthan and O. R. Nandagopan, "Depth enhancement of an underwater towed system using hydrodynamic depressor," *Defence Science Journal*, vol. 66, no. 5, pp. 546-551, 2016.

[90] J. Wu and A. T. Chwang, "A hydrodynamic model of a two-part underwater towed system," *Ocean Eng.*, vol. 27, pp. 455-472, 2000.

[91] J. Wu and A. T. Chwang, "Experimental investigation on a two-part underwater towed system," *Ocean Eng.*, vol. 28, pp. 735-750, 2001.

[92] J. Wu and A. T. Chwang, "Investigation on a two-part underwater manoeuvrable towed system," *Ocean Eng.*, vol. 28, pp. 1079-1096, 2001.

[93] J. Wu, J. Ye, C. Yang, Y. Chen, H. Tian and X. Xiong, "Experimental study on a controllable underwater towed system," *Ocean Eng.*, vol. 32, pp. 1803-1817, 2005.

[94] Z-J. Yuan, L-A. Jin, W. Chi, X-G. Jiang and Z. Zhi-Lin, "The underwater towed system behavior during ship turning maneuvers," *Journal of Marine Science and Technology*, vol. 25 no. 4, pp. 464-474, 2017.

[95] T. S. Walton and H. Polachek, "Calculation of transient motion of submerged cables," *Mathematics of computation*, vol. 14, pp. 27-46, 1960.

[96] M. Toda, "A theoretic analysis of control system structure of towed underwater vehicles," in *Proc. 44th IEEE Conference on Decision and Control & European Control Conference*, Seville, Spain, Dec., 2005, pp. 7526-7533.

[97] A. Minowa, "System analyses and motion control of a towed underwater vehicle," M.Eng. Thesis, Tokyo University of Marine Science and Technology, Department of Marine System Engineering, 2005.

[98] A. Minowa and M. Toda, "Motion control of towed underwater vehicles with movable wings using a high-gain observer based approach," in *Proc. IEEE 10th Conference on Industrial Electronics and Applications*, Auckland, New Zealand, Jun., 2015, pp. 1893-1898.

[99] H. K. Khalil, *Nonlinear Systems*, 3rd ed., New Jersey, USA: Prentice-Hall, 2002.

[100] A. Saberi and H. K. Khalil, "An initial value theorem for nonlinear singularly perturbed systems," *Systems & Control Letters*, vol. 4, no. 5, pp, 301-305, 1984.

[101] F. Esfandiari and H. K. Khalil, "Output feedback stabilization of fully linearizable systems," *Int. J. Contr.*, vol. 56, no. 5, pp, 1007-1037, 1992.

[102] H. K. Khalil and Esfandiari, "Semiglobal stabilization of a class of nonlinear systems using output feedback," *IEEE Transactions on Automatic Control*, vol. 38, no. 9, pp, 1412-1415, 1993.

[103] N. A. Mahmoud and H. K. Khalil, "Asymptotic stabilization of minimum phase nonlinear systems using output feedback," in *Proc. IEEE 32nd Conference on Decision and Control*, San Antonio, TX, USA, Dec., 1993, pp. 1960-1965.

[104] S. Oh and H. K. Khalil, "Nonlinear output-feedback tracking using high-gain observer and variable structure control," *Automatica*, vol. 33, no. 10, pp, 1845-1856, 1997.

[105] A. N. Atassi and H. K. Khalil, "A separation principle for the control of a class of nonlinear systems," *IEEE Transactions on Automatic Control*, vol. 44, no. 9, pp, 1672-1687, 1999.

[106] H. K. Khalil, "High-gain observers in nonlinear feedback control," in *Proc. IEEE 2008 International Conference on Control, Automation and Systems*, Seoul, Korea, Oct., 2008, IEEE Xplore.

[107] H. K. Khalil and L. Praly, "High-gain observers in nonlinear feedback control," *Int. J. Robust Nonlinear Control*, vol. 24, pp, 993-1015, 2014.

Appendix

A Coefficient Matrix and LQ State-Feedback Gain

C1

$$A = \begin{bmatrix} 0 & 0 & 1 & 0 \\ 0 & 0 & 0 & 1 \\ -0.1215 & -1.8432 & -12.8184 & -0.1147 \\ 2.3757 & 142.2780 & 947.059 & -3.3922 \end{bmatrix}$$

$$B = \begin{bmatrix} 0 & 0 \\ 0 & 0 \\ -1.3484 & -0.0752 \\ 27.412 & -30.5795 \end{bmatrix}$$

$$C = \begin{bmatrix} 25.9766 & 0 & 0 & 0 \\ 0 & 1 & 0 & 0 \end{bmatrix}$$

$$K = \begin{bmatrix} -0.2167 & -2.0583 & -13.195 & -0.0137 \\ 0.9590 & -4.2853 & -20.506 & -0.9572 \end{bmatrix} \tag{A.1}$$

C2

$$A = \begin{bmatrix} 0 & 0 & 1 & 0 \\ 0 & 0 & 0 & 1 \\ -0.1058 & -0.4796 & -12.7549 & -0.0284 \\ 6.8972 & 136.15 & 3123.9 & -3.7899 \end{bmatrix}$$

$$B = \begin{bmatrix} 0 & 0 \\ 0 & 0 \\ -0.3516 & -0.0199 \\ 27.0915 & -30.738 \end{bmatrix}$$

$$C = \begin{bmatrix} 86.6025 & 0 & 0 & 0 \\ 0 & 1 & 0 & 0 \end{bmatrix}$$

$$K = \begin{bmatrix} -0.1579 & -1.8100 & -37.3134 & 0.0588 \\ 0.9782 & -4.3394 & -70.6158 & -0.9557 \end{bmatrix} \tag{A.2}$$

C3

$$A = \begin{bmatrix} 0 & 0 & 1 & 0 \\ 0 & 0 & 0 & 1 \\ -0.0913 & -0.19995 & -12.7148 & -0.0109 \\ 11.9006 & 128.945 & 6155.62 & -4.2322 \end{bmatrix}$$

$$B = \begin{bmatrix} 0 & 0 \\ 0 & 0 \\ -0.1471 & -0.0085 \\ 27.8936 & -30.8774 \end{bmatrix}$$

$$C = \begin{bmatrix} 173.2050 & 0 & 0 & 0 \\ 0 & 1 & 0 & 0 \end{bmatrix}$$

$$K = \begin{bmatrix} -0.1383 & -1.2947 & -51.7839 & 0.1766 \\ 1.0828 & -4.5994 & -145.9590 & -0.9492 \end{bmatrix} \tag{A.3}$$

C4

$$A = \begin{bmatrix} 0 & 0 & 1 & 0 \\ 0 & 0 & 0 & 1 \\ -0.0806 & -0.1133 & -12.7168 & -0.0057 \\ 15.7717 & 122.901 & 9095.73 & -4.5824 \end{bmatrix}$$

$$B = \begin{bmatrix} 0 & 0 \\ 0 & 0 \\ -0.0836 & -0.0049 \\ 29.6943 & -30.9358 \end{bmatrix}$$

$$C = \begin{bmatrix} 259.8080 & 0 & 0 & 0 \\ 0 & 1 & 0 & 0 \end{bmatrix}$$

$$K = \begin{bmatrix} -0.2031 & -0.5841 & -37.4782 & 0.3046 \\ 1.2487 & -4.8329 & -218.8875 & -0.9276 \end{bmatrix} \tag{A.4}$$

C5

$$A = \begin{bmatrix} 0 & 0 & 1 & 0 \\ 0 & 0 & 0 & 1 \\ -0.3641 & -1.4467 & -39.2573 & -0.0243 \\ 47.4748 & 472.696 & 11290.4 & -19.4075 \end{bmatrix}$$

$$B = \begin{bmatrix} 0 & 0 \\ 0 & 0 \\ -1.2017 & -0.0683 \\ 195.5130 & -247.3660 \end{bmatrix}$$

$$C = \begin{bmatrix} 173.2050 & 0 & 0 & 0 \\ 0 & 1 & 0 & 0 \end{bmatrix}$$

$$K = \begin{bmatrix} -0.6891 & 0.3656 & -0.8502 & 0.4688 \\ 0.3821 & -2.5392 & -36.3883 & -0.8165 \end{bmatrix} \tag{A.5}$$

C6

$$A = \begin{bmatrix} 0 & 0 & 1 & 0 \\ 0 & 0 & 0 & 1 \\ -0.3197 & -0.8299 & -37.3954 & -0.0126 \\ 62.5326 & 437.687 & 16289.5 & -20.1454 \end{bmatrix}$$

$$B = \begin{bmatrix} 0 & 0 \\ 0 & 0 \\ -0.6920 & -0.0398 \\ 193.8790 & -248.2880 \end{bmatrix}$$

$$C = \begin{bmatrix} 259.8080 & 0 & 0 & 0 \\ 0 & 1 & 0 & 0 \end{bmatrix}$$

$$K = \begin{bmatrix} -0.6272 & 0.4805 & 2.8132 & 0.4864 \\ 0.3172 & -2.4004 & -50.8155 & -0.8049 \end{bmatrix} \tag{A.6}$$

B Proof

B.1 Proof of Lemma 1

Suppose $w \notin D$ for $\exists w \neq 0 \in \Omega_w$. Then, due to $w \in \Re^n \setminus D$ and the origin in the interior of D, there exists $w_0 = tw \in \partial D$ $(0 < t < 1)$. Since $w_0 \in \partial D$ with (4.25),

$$\begin{aligned} r_{w\min} &\leq \|w_0\| \\ &= t\|w\|. \end{aligned}$$

Thus, $\|w\| \geq r_{w\min}/t > r_{w\min}$. In contrast, $w \in \Omega_w$ with (4.26) and (4.27) means

$$0 < \lambda_{\min}(P)\|w\|^2 \leq w^T P w \leq \lambda_{\min}(P) r_{w\min}^2.$$

because P is positive definite, and hence

$$\|w\| \leq r_{w\min},$$

which is a contradiction. Therefore, $\Omega_w \subseteq D$. The proof is completed.

B.2 Proof of Theorem 2

Since P is positive definite, $P^{1/2}$ is also positive definite and nonsingular. Then, the linear map $\mathcal{T}_P$ is continuous and bijective with continuous inverse, hence is a homeomorphism, which implies that the topological structures of D and $D_{w'}$ are equivalent. In particular, not only (4.34) and $\mathcal{T}_P^{-1}(D_{w'}) = D$, but also $\mathcal{T}_P(\text{Int } D) = \text{Int } D_{w'}$ and $\mathcal{T}_P(\partial D) = \partial D_{w'}$, and *vice versa* with the inverse, where $\text{Int}(\cdot)$ denotes the interior of the set.

Therefore, with (4.35) and (4.36)

$$\begin{aligned} \sigma_{w'} &= \left(\min_{w' \in \partial D_{w'}} \|w'\|\right)^2 \\ &= \left(\min_{w \in \partial D} \|P^{1/2} w\|\right)^2 \\ &\geq \left(\lambda_{\min}(P^{1/2}) \min_{w \in \partial D} \|w\|\right)^2 \\ &= \lambda_{\min}(P) r_{w\min}^2 \\ &= \sigma_w, \end{aligned}$$

and thus $\Omega_w \subseteq \Omega_{w'}$.

Next, consider $\Omega'_{w'} = \{w' \mid w'^T I_n w' \leq \sigma_{w'}, w' \in \Re^n\}$, then $\Omega'_{w'} \subseteq D_{w'}$ from Lemma 1. Further, for $\forall w \in \Omega_{w'}$, using $w' = \mathcal{T}_P(w)$ with (4.33) and (4.37)

$$\begin{aligned} w'^T I_n w' &= \mathcal{T}_P(w)^T \mathcal{T}_P(w) \\ &= (P^{1/2} w)^T (P^{1/2} w) \\ &= w^T P w \\ &\leq \sigma_{w'}, \end{aligned}$$

which implies $\mathcal{T}_P(\Omega_{w'}) \subseteq \Omega'_{w'} \subseteq D_{w'}$. Moreover, since $\mathcal{T}_P^{-1}(D_{w'}) = D$, $\mathcal{T}_P(w) \in D_{w'}$ for $\forall w \in \Re^n$ implies $w \in D$. Therefore, $\Omega_{w'} \subseteq D$. The proof is completed.